Ultra-High Speed Signal Generation Combining OTDM and High-Order Modulation Formats

Luca Ferrari

Danmarks Tekniske Universitet - Fotonik

Università degli Studi di Padova - Dipartimento di Ingegneria dell'Informazione

A thesis submitted for the double degree of:

Master of Science (MSc) in Telecommunication

Laurea Specialistica in Ingegneria Elettronica

August 2010

Supervised by:

C. Peucheret, M. Galili, H. C. Hansen Mulvad, and M. E. Valcher

Abstract

This thesis is focused on high-order modulation formats as a means to increase spectral efficiency and in turn reduce the cost per bit of an optical transmission system. Special attention is devoted to DQPSK and 16QAM, together with optical time-division multiplexing, with the aim of maximizing the exploitation of a single wavelength on a single fiber.

A numerical model for simulating an optical communication system is described, and most of the effort is spent on transmitter and fiber link. By means of the mentioned model, we develop a study of the IQ modulator non-idealities, amongst which the limitedness of the phase modulators bandwidth. On top of this, we analyze the behavior and the applicability of a pulse source based on the phase modulation of a CW source and on the following propagation of the light through a dispersive element. The simulation and comparison of NRZ-DQPSK, NRZ-16QAM, 4-channel OTDM DQPSK, and 4-channel OTDM 16QAM are carried out basing on a number of typical impairments like laser linewidth, chromatic dispersion, and fiber nonlinearities. Minor attention is also devoted to different techniques to numerically simulate light propagation over nonlinear fiber.

The results of an extensive laboratory experience are reported. An 8-channel OTDM QPSK system with clock recovery, coherent receiver and DSP is realized at a symbol rate of 10 GBd/s, corresponding to 160 Gb/s on a single wavelength and on a single fiber. The demodulation is shown successful and paths for improvement are depicted.

To my parents, everlasting roots of my happiness.

Ai miei genitori, radici perenni della mia felicità.

Acknowledgements

I would hereby like to deeply thank you, Christophe, for being an enormous teacher, for following me devotedly and with dedication over a whole year of work, for having a great balance between being understanding and motivating. You will always have a special place in my heart of student.

Also great is the gratitude towards you, Michael, for spending a big deal of your time playing around with us in the lab. It was especially thanks to your skills and your brightness if we could obtain such exciting results down there.

Darko, Leif, thanks to both of you for all the help and the advice.

Checco, a big hug to you. No words need to be spent, by now you know my heart.

Never could I forget Daizzi, for the hours spent playing video games when I needed a break. And thanks to you, Mat, for being such an incredible flatmate. Pap, you are a surprise, and thank you so much for having the fastest PC on earth.

Michelle, you are a sun shining in my sky.

Grazie anche a voi, mamma e papà, per avermi sempre fatto sentire il vostro amore. Sono orgoglioso di voi, e spero voi lo siate di me.

Thanks to you, Daniele, for being like a brother to me. And thanks to all of you, my dear friends, I would be nobody without your love.

And thanks to You, God, for letting me breathe this wonderful life.

Contents

List of Figures

List of Tables

1

Introduction

Welcome, dear reader, let us introduce you to this thesis with a brief overview. The first section retains the main motivations for the interest in high-speed multi-level modulation with OTDM. We will also suggest a few references of the state of the art within this field. The second section constitutes a summary of the chapters of this thesis. The final section is just a discussion of the prerequisites for understanding the treated topics. Please, note that we will not explain the concepts touched in this first chapter right away, for this Chapter 2 will do.

1.1 Motivations and State of the Art

In this day and age, a fast and convenient access to information of all sorts is becoming more and more desirable. We utilize internet more than ever, and the way we do it has been shifting from mere browsing to heavy downloading, file sharing, online video gaming, etc. The usage of e-mails as means of communication has peaked in the recent years, as simple everyday experience suggests us.

The common communication technology user expects not only a consistent quality of service, but even an improve of this year after year, while the providers struggle to allow for increasingly bandwidth consuming applications. The internet traffic was estimated to be growing at a rate of about 115% in 2005 [6], and this trend does not seem to slow down, especially considering that more and more services are now delivered through the internet. Let us think of digital television, video calls, etc.

Optical communications already play a major role in carrying and redistributing all this information. Long-haul connections are today built by means of fiber optics systems, since they are by far superior to the other electrical wireline and wireless links for bandwidth and attenuation (about 0.2 dB/km across a bandwidth of several THz [6]). However, today's commercial systems only employ OOK modulation, which consists in having two light intensity levels, generally on and off, corresponding to the bits 1 and 0. This is an extremely simple modulation format, especially because it allows for directly detecting the light transforming it into electrical power by means of a photodetector. So far it has been enough to meet the needs of the market, and new fibers have been deployed to expand the capacity of any links.

Nonetheless, the fierce increase in demand suggests research in other ways of transmitting information over fiber. Every time a fiber is deployed, trenches are dug, labor is needed, and then maintenance will follow. These are just some of the costs related to the installation of optical fibers. Clearly, one would like to exploit a fiber as much as possible, so to need fewer of them. The answer to this comes from high-order modulation formats and multiplexing techniques.

By modulating the signal in advanced ways, we achieve a variety of advantages. If we maintain the same symbol rate, more bits are mapped in one symbol, so that the actual bit rate is increased. If we decide to reduce the symbol rate, then we can transmit the same amount of information with slower electronics. In both cases the cost per bit is reduced, or the the spectral efficiency[1] is enhanced. This is true as long as we do not consider the added costs due to the higher complexity of such modulation formats. Transmitter and receiver get more and more sophisticated with increasing modulation orders. Increased complexity is generally also cause of higher tendency to failures and breakdowns.

On top of this, interest for novel optical modulation formats arises form the fact that they show different transmission properties. As an example, M-PSK modulations are quite robust against self-phase modulation, since the power is constant for all the symbols of the constellation. This allows to transmit over longer distances without need for optical-to-electrical conversion to regenerate the signal, helping cutting on costs.

[1] In telecommunications, the spectral efficiency is defined as the bit rate that can be transmitted over a given bandwidth.

A second way to exploit a single fiber to transmit more data is multiplexing. Wavelength-division multiplexing (WDM) is a promising path, but the one of major focus in this work is optical time-division multiplexing (OTDM). It consists in dividing the symbol slot into sub-slots assigned to different channels. Each channel will be represented by a sequence of modulated pulses, so that the overall bit rate will be multiplied by the number of channels. Of course, high-order modulations with multiplexing schemes are generally less resilient to channel noise and system non-idealities, and their behavior in this respect is to be studied and estimated before any commercial system is devised.

The complexity of such systems had made them difficult to implement for many years, until digital signal processing was introduced for optical communications together with coherent detection. The potential of digital elaboration of signal samples allows today to avoid some of the optical complexity necessary to receive high-order modulation formats, and also enables for the compensation of some of the system impairments, opening up a whole new set of possibilities.

A lot of research has been going on in the last years about higher-order modulation formats and multiplexing techniques. In [7], the transmission of 5.1 Tb/s on a single wavelength channel was demonstrated with OTDM 16QAM. Also in [8] and [9] similar experiments are reported. By employing WDM and RZ-DQPSK, a record fiber capacity of 25.6 Tb/s was set in [10]. In this department, some of my esteemed supervisors achieved a single wavelength data signal capacity of 5.1 Tb/s utilizing DQPSK, OTDM, PolMux, and direct detection. This was done with a record OTDM channel symbol rate of 1.28 GBd/s [11].

1.2 Goals and Thesis Overview

The goal of this project was to investigate high-order modulation formats together with OTDM. The work was carried out together with my dear friend Francesco Patarnello. The present document is mostly focused on signal generation and fiber transmission, while the complementary part [12] delves into the details of coherent detection with DSP. The two theses should be read together in order to have a complete picture of the discussed system, nevertheless we tried to make them as self-sufficient as possible, so that they can be consulted separately.

This thesis is segmented into four main chapters, plus this introduction and a conclusion regrouping major findings and potential future work for improvement. We have tried to apply a strong and deep structure of sections, so that finding a specific piece of information should not be too difficult when flipping through the index.

Chapter 2 presents a vast introduction to most of the issues treated in this work. The aim is not to provide a strong theoretical background, for which plenty of books exist, the best example probably being [4], but to bring justifications for all the choices made when modeling the system[1]. We also provide a large amount of definitions for parameters we need later on. We can consequently see this chapter as a funding basis for our work.

Chapter 3 is a thorough description of our Matlab® model. This was the work of many months, together with gathering the understanding and theoretical basis necessary to realize it. We try to give detailed descriptions of how we implemented the several different blocks of an optical communication system, often reporting short chunks of code as clarifying examples.

Chapter 4 contains a selection of some of the simulations we performed with our numerical model, hopefully most of which are novel and interesting. We tried to look for a small number of well reported results, instead of applying an all-covering brute force approach. This is due to the limitedness of the time at our disposal and to the fact that such sources already exist (see [6]).

Chapter 5 is a report of a long and exciting laboratory experience during which we implemented a 160 Gb/s 8-channel OTDM QPSK optical communication system with clock recovery, coherent detection, and DSP. This is an unexpectedly awesome result of which we are proud and for which, as for the rest of the thesis, we have to thank quite a few people.

1.3 Prerequisites for the Reading and Conventions

In Section 2.1 we will try to give some information about basic principles of optical communications and of engineering in general. This does not make this thesis, as probably any thesis, fully understandable for everybody. The goal we set for ourselves

[1] This is an ambitious goal. We hope we have managed to justify at least the vast majority of them.

when writing it was to make it as clear, simple, and pleasant to read as possible. We doubt we fulfilled this difficult task[1], but we hope we got quite close.

Nonetheless, for a complete comprehension of the topics, one needs basics of electromagnetism, Fourier theory, communications theory, probability theory, a little bit of quantum mechanics, and some salt on top. We ourselves are far from mastering these subjects, but a shallow knowledge about them would definitely help enjoy this work.

During the course of the various sections, we try to disseminate a lot of figures. There are two reasons for this. The first (and we are afraid to admit, very influencing) is that they look extremely nice if well done, the second is that they tremendously help understand concepts and results. In general, the captions of the figures will not be too long, and all the related details will be found in the text. Let us also remark that, when we show schematics of optical communication systems or of their sub-parts (and this will be quite often), the optical connections (fibers, couplers, etc.) will be green, the electrical ones black. This will be true only in the cases in which both are present, if we show a coupler alone, we will draw it black.

We hope the reader will appreciate, and we wish him/her a cozy and nice time with this thesis.

[1]Making things appear easy is by far more challenging than making them look complicated, we believe.

2

Theoretical Background and Conventions

This chapter aims at providing the reader with a theoretical basis for later understanding both our model of an optical communication system and its actual implementation. We do not aspire to be thorough to the finest details, but we will just try to provide the necessary elements with clarity and simplicity.

The first section gives a brief introduction to some of the very basics required to handle the following topics with confidence. Then, the description of the several parts of an optical communication system starts. We begin by discussing optical transmitters, to then move to the optical channel. Finally, we delve into the theory of optical receivers.

2.1 Preliminary Knowledge

We hereby provide some elements of engineering knowledge that many readers might lack. This section exists and is so extensive because we were asked by a very dear person to make this thesis a bit more understandable for people belonging to other fields of study. Without the necessary and painfully acquired background of most engineers, a confident and complete understanding of the subject treated is probably impossible. Nonetheless, we sincerely hope that the following pages will help any interested reader to appreciate at least the taste of this work a bit better.

Any engineer with some experience in telecommunications could (and probably should) skip this section, paying attention maybe just at our definitions of optical signal

(borrowed from Christophe Peucheret, precious supervisor of ours, and found in Section 2.1.1) and of OSNR (see Section 2.1.11). The experienced reader will hopefully forgive us for being here and there a little naive and not extremely rigorous in this section, but that is exactly the style we wanted. Where needed, like in the aforementioned two sections, we will be as precise as possible.

2.1.1 Optical Signal Description

In this section we will develop a simple expression for the electric field of our optical signal. This requires some background knowledge about Maxwell's equations and electromagnetic theory. In the end we will explain the concept of modulation and highlight the different ways in which light can be modulated.

From electromagnetic theory, it is known that a plane wave can be described as (please note the phase convention, i.e. phase increasing with time)

$$\mathbf{E}(\mathbf{r},t) = \mathrm{Re}\left\{\mathbf{A}(\mathbf{r},t)\, e^{j(\omega_0 t - \mathbf{k}\cdot\mathbf{r})}\right\}, \tag{2.1}$$

in which $\mathbf{E}(\mathbf{r},t)$ is the electric field, depending on both space and time. Trivially, ω_0 and $\mathbf{k}$ are respectively the angular frequency and the wave vector characterizing the light, while $\mathbf{A}(\mathbf{r},t)$ is a complex vector that will be shown closely related to the complex envelope of the field. Note that ω_0 is related to the frequency (measured in Hz) through

$$\omega_0 = 2\pi f_0. \tag{2.2}$$

The wave is a transverse one, so, assuming that the direction of propagation be z, in a system where $\mathbf{r} = r_{\mathrm{x}}\widehat{\mathbf{x}} + r_{\mathrm{y}}\widehat{\mathbf{y}} + r_{\mathrm{z}}\widehat{\mathbf{z}}$, (2.1) takes the form

$$\mathbf{E}(z,t) = \mathrm{Re}\left\{\mathbf{A}(z,t)\, e^{j(\omega_0 t - \beta z)}\right\}, \tag{2.3}$$

where β is the component of $\mathbf{k}$ along z. $\mathbf{A}(z,t)$ can be written as

$$\mathbf{A}(z,t) = \kappa\left[u_{\mathrm{x}}(z,t)\,\widehat{\mathbf{x}} + u_{\mathrm{y}}(z,t)\,\widehat{\mathbf{y}}\right], \tag{2.4}$$

where κ is a normalization factor and u_{x} and u_{y} are complex functions. Calculating the magnitude of the vector $\mathbf{A}(z,t)$

$$|\mathbf{A}|^2 = \mathbf{A}\cdot\mathbf{A}^* = \kappa^2\left[|u_{\mathrm{x}}(z,t)|^2 + |u_{\mathrm{y}}(z,t)|^2\right], \tag{2.5}$$

where * is the operation of conjugation and we have dropped the dependence on space and time for simplicity. Applying the Poynting theorem we derive the light intensity as

$$I(z,t) = \frac{1}{2}\epsilon_0 cn\kappa^2 \left[|u_{\mathrm{x}}(z,t)|^2 + |u_{\mathrm{y}}(z,t)|^2 \right], \tag{2.6}$$

in which ϵ_0 is the vacuum permittivity, c the speed of light and n the refractive index of the medium. Since the optical power is obtained multiplying the intensity by an area A_{eff}, sometimes referred to as effective area (i.e. the area over which the intensity is integrated), if we set

$$\kappa = \sqrt{\frac{2}{\epsilon_0 cn A_{eff}}}, \tag{2.7}$$

then we can have a convenient representation of the optical power,

$$P(z,t) = |u_{\mathrm{x}}(z,t)|^2 + |u_{\mathrm{y}}(z,t)|^2. \tag{2.8}$$

If we now decompose u_{x} and u_{y} into their phase and magnitude components, we get

$$\mathbf{A}(z,t) = \kappa \left[A_{\mathrm{x}}(z,t)\, e^{-j\phi_{\mathrm{x}}(z,t)} \widehat{\mathbf{x}} + A_{\mathrm{y}}(z,t)\, e^{-j\phi_{\mathrm{y}}(z,t)} \widehat{\mathbf{y}} \right]. \tag{2.9}$$

Defining common and differential phases as

$$\phi(z,t) = \frac{\phi_{\mathrm{x}}(z,t) + \phi_{\mathrm{y}}(z,t)}{2} \tag{2.10}$$

and

$$\delta = \phi_{\mathrm{x}}(z,t) - \phi_{\mathrm{y}}(z,t), \tag{2.11}$$

one can write

$$\mathbf{A}(z,t) = \kappa e^{-j\phi(z,t)} \left[A_{\mathrm{x}}(z,t)\, e^{-j\frac{\delta(z,t)}{2}} \widehat{\mathbf{x}} + A_{\mathrm{y}}(z,t)\, e^{j\frac{\delta(z,t)}{2}} \widehat{\mathbf{y}} \right]. \tag{2.12}$$

We now introduce the normalized Jones vector

$$\mathbf{e}(z,t) = \frac{1}{\sqrt{A_{\mathrm{x}}^2(z,t) + A_{\mathrm{y}}^2(z,t)}} \left[A_{\mathrm{x}}(z,t)\, e^{-j\frac{\delta(z,t)}{2}} \widehat{\mathbf{x}} + A_{\mathrm{y}}(z,t)\, e^{j\frac{\delta(z,t)}{2}} \widehat{\mathbf{y}} \right], \tag{2.13}$$

which yields

$$\mathbf{A}(z,t) = \kappa e^{-j\phi(z,t)} \sqrt{A_{\mathrm{x}}^2(z,t) + A_{\mathrm{y}}^2(z,t)}\, \mathbf{e}(z,t) = \kappa \sqrt{P(z,t)}\, e^{-j\phi(z,t)} \mathbf{e}(z,t). \tag{2.14}$$

Interestingly, the magnitude of $\mathbf{A}(z,t)$ is the complex envelope of the electric field, while its polarization is defined by the normalized Jones vector $\mathbf{e}(z,t)$.

We can finally go back to a more suitable expression for the electric field,

$$\mathbf{E}(t) = \mathrm{Re}\left\{\sqrt{P(t)}e^{-j\phi(t)}e^{j\omega_0 t}\mathbf{e}(t)\right\}, \tag{2.15}$$

where, for simplicity, we have set $\kappa = 1\ \mathrm{m}^{-1}(\mathrm{s/F})^{1/2}$. We have also dropped the dependence on the spatial coordinate, which is of little interest for us, since we will always observe the behavior of light in a fixed position and over a time window, in order to monitor the flow of information carried by the modulated electrical field.

Modulating the optical signal means varying some of its properties according to another signal (generally called driving or modulating signal). This is done in most cases to transfer information to the optical signal, to then transmit it over a desired distance. (2.15) makes it clearly visible that we have various degrees of freedom when modulating light. Within this work, we will concentrate our efforts on modulation formats that act on power, $P(t)$, and phase, $\phi(t)$, even though also angular frequency, ω_0, and polarization, $\mathbf{e}(t)$, can be modulated.

Let us conclude by clarifying that, in most cases, we will omit the polarization term when referring to our optical signals. Moreover, we will refer to the complex electric field, forgetting about taking the real part, ending up with the following very simple definition,

$$E(t) = \sqrt{P(t)}e^{-j\phi(t)}e^{j\omega_0 t} = A(t)\,e^{j\omega_0 t}. \tag{2.16}$$

2.1.2 Fourier Transform and Spectral Density

Here we define the Fourier transform as we will calculate it in this work, moreover we will remind the reader of the concept of spectral density. In this thesis the frequency will be denoted with f when meaning actual frequency (measured in Hz), and ω when meaning angular frequency (measured in rad/s). Clearly, $\omega = 2\pi f$.

Signals have a time domain description (let us call it $g(t)$), as one should readily understand. It is also possible to provide a description of the signal in the frequency domain, and this is obtained by Fourier transforming $g(t)$,

$$G(f) = \mathcal{F}(g(t)) = \int_{-\infty}^{\infty} g(t)\,\mathrm{e}^{-j2\pi ft}dt. \tag{2.17}$$

Equation 2.17 will stand as definition of the Fourier transform we use in this thesis. The inverse Fourier transform will thus be

$$g(t) = \mathcal{F}^{-1}(G(f)) = \int_{-\infty}^{\infty} G(f)\,\mathrm{e}^{j2\pi ft}df. \tag{2.18}$$

Note that other definitions have opposite signs at the exponential. We are not going to provide any further insight of Fourier theory since the basics of this subjects are a prerequisite for this thesis.

The *autocorrelation* of a signal is defined as the convolution of the signal with the conjugated version of itself (which for real signals coincides with the signal), denoted with *,

$$R_g(t) = g * g^*(t) = \int_{-\infty}^{\infty} g(\tau)\, g^*(t-\tau)\, d\tau. \tag{2.19}$$

If we now Fourier transform $R_g(t)$, we will obtain something called *Power Spectral Density* (PSD),

$$S_g(f) = \mathcal{F}(R_g(t)) = \int_{-\infty}^{\infty} R_g(t)\, \mathrm{e}^{-j2\pi ft} dt. \tag{2.20}$$

$S_g(f)$ is measured in W/Hz and tells us how much of the overall signal power is concentrated in a certain frequency bandwidth, if we integrate it over the desired frequencies. This is what we commonly call the *power spectrum* of the signal and is shown by spectrum analyzers. In practice, the power of the signal is measured with a certain frequency resolution Δf, and what is actually shown is $\int_{\Delta f} S_g(f)\, df$[1], which is measured in W. The modeling of optical and electrical spectrum analyzers is described in Section 3.5.3. An example of time domain and frequency domain representations of a signal is shown in Figure 2.1.

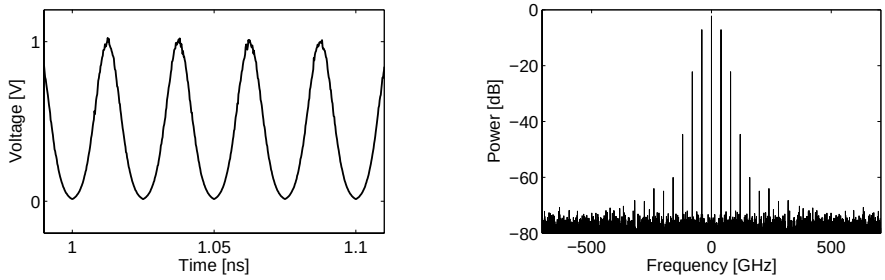

(a) (b)

Figure 2.1: (a) Time domain representation and (b) spectrum of a pulse train.

It can be proved that the squared modulus of the Fourier transform of a signal coincides with its PSD. This means that the power spectrum can be obtained in two

[1]Here we have neglected to consider the shape of the filtering window utilized by the spectrum analyzer. For simplicity, we have assumed it was a rectangular window of width Δf and height 1. The concept of filtering will be explained in Section 2.1.4.

different ways, either by measuring the autocorrelation of the signal, or by calculating the Fourier transform.

2.1.3 Elements of Probability Theory and Noise Sources

The goal of this section is to give a simple and intuitive introduction to the concept of noise, providing basic elements of probability theory which will be then taken for granted. We also list the most common sources of noise in an optical communication system, without delving into detail, since all of them will have a dedicated section before or later within this work. It is anyway important that their primitive idea be understood from the beginning, for we will need to name them here and there in early stages.

In telecommunications and electronics, noise is a word that refers to undesired signals overlapping to the one carrying the information. It is normally due to fundamental properties of the matter (like its being quantized) and is in no way eliminable, even though there are techniques to reduce it. Noise signals never have an analytically describable time domain representation and they are characterized statistically. Noise can indeed be seen as a random process, which collapses into the concept of random variable if we consider a specific instant in time. We will here recall some very basic concepts of probability theory, without the ambition of being extremely rigorous but with the aim of providing the reader with some tools for a better understanding of a few statements later on in this thesis.

A random variable can assume values in a certain set, which can be continuous or discrete. A continuous random variable is described through its *probability density function* (pdf), which we will denote as $f(x)$. $f(x)$ gives the relative likelihood that the variable assume the value x. The probability that a continuous random variable occur in a given set is simply the integral of its pdf over the set. Clearly the integral over the whole set has to yield 1 as result. The random variables we will treat are continuous and have values in the set of real numbers. When numerically simulate noise the continuity will obviously become discreteness.

The *mean* of a continuous random variable is given by

$$\mu = \int_{-\infty}^{\infty} x f(x)\, dx, \tag{2.21}$$

whereas its *variance* is obtained as

$$\sigma^2 = \int_{-\infty}^{\infty} (x-\mu)^2 f(x)\, dx. \tag{2.22}$$

While the concept of mean should be intuitive, the variance gives a measure of the spreading of $f(x)$ with respect to μ. The square root of the variance is called *standard deviation* and is most often preferred to the variance because it is expressed in the same units as the variable itself.

Discrete random variables are characterized by having a discrete set of values they can assume. They are described by their *probability distribution*, which gives the probability of the variable assuming a specific value. We will call this function $p(x_i)$, where the subscript i denotes that we are considering a specific value in the set of possible ones. The sum of $p(x_i)$ over the whole set of possible values has to give 1. Note that, while $p(x_i)$ gives the actual probability of the event x_i to occur, the pdf $f(x)$ needs to be integrated over a certain set to give a probability.

The mean of a discrete random variable is defined as

$$\mu = \sum_i x_i p(x_i), \tag{2.23}$$

and the variance becomes trivially

$$\sigma^2 = \sum_i (x_i - \mu)^2 p(x_i). \tag{2.24}$$

In both equations the sum is performed over the whole set of values.

One of the most famous and useful probability density functions is surely the *Gaussian* (or *Normal*) one. The characteristic bell-shaped pdf is expressed as

$$f(x) = \frac{1}{\sqrt{2\pi\sigma^2}} \mathrm{e}^{-\frac{(x-\mu)^2}{2\sigma^2}}. \tag{2.25}$$

In nature, most random phenomena have been observed to behave like Gaussian noise. As we will see in Chapter 3, we will use the assumption of Gaussian noise extensively. In particular, noise in engineering has been historically most often treated as AWGN, which stands for additive white Gaussian noise. *Additive* means that the noise is linearly added on top of the signal amplitude, whereas *white* requires the noise spectral density to be constant and *Gaussian* the pdf to be Gaussian, as explained above. This is not applicable to all kinds of noise sources, of course, nor we will use it blindly. On the

contrary, we will try to justify our choices. Generally the aforementioned assumptions regarding noise allow for simpler analysis and modeling.

Some of the most important sources of noise in an optical communication system are:

- Intensity noise,
- Amplified spontaneous emission (ASE) noise,
- Phase noise,
- Shot noise,
- Thermal noise.

Intensity noise is typically observed due to optical transmitters (i.e. lasers, see Section 2.2.1.3) and consists in oscillations of the emitted power. ASE noise is produced in optical amplifiers and affects both real and imaginary parts of the electrical field, as described in Section 2.3.5. Phase noise means noise influencing the phase of the signal, and under this definition ASE noise brings also phase noise (the phase of a complex number depends on both real and imaginary parts). More specifically, we tend to talk about the phase noise introduced by oscillators, for example lasers (see Section 2.2.1.2). Shot noise and thermal noise are well-known fluctuations in the current in any electrical circuit (we will discuss them in our receiver, see Sections 2.4.2 and 2.4.3).

We will model most of these as AWGN, while phase noise will require some more complexity and will be characterized as a so-called *Wiener process*. Explanations and justifications are left to the specific sections.

2.1.4 Filtering

Here we define the concepts of filtering, and bandwidth. This will help some readers understand later discussions and hopefully remove any doubts concerning the definitions of filter shape and bandwidth employed throughout this thesis.

The operation of *filtering* a signal consists in removing its undesired frequency components. Practically, this corresponds to shaping the signal spectrum according to a well defined filter transfer function. Ideally, filters are passive components (i.e. they do not need power supply) and for this reason they do not amplify the signal, but just

remove energy from it at the desired frequencies. There is a massive amount of different filters for several engineering fields, but the ones that we will use are electrical filters (both analog and digital) and optical filters. We are not going of discuss the physical implementation of filters, because of the ampleness of this subject and in consideration of the fact that our model of filters will be purely mathematical and will not take into account the non-idealities related to the real devices.

A filter is characterized by an *impulse response*, which we will call $h(t)$. By definition, this is the output of the filter when the input is an ideal impulse $\delta(t - t_0)$, where δ is a Dirac's delta function centered in t_0. For an input signal $g(t)$, the output of the filter is given by the convolution of signal and filter impulse response (assumed purely real),

$$g_{out}(t) = g * h(t) = \int_{-\infty}^{\infty} g(\tau)\, h(t - \tau)\, d\tau. \tag{2.26}$$

Note that, according to this definition, when setting an impulse as input one gets the impulse response as output, as stated above,

$$g_{out}(t) = \delta * h(t) = \int_{-\infty}^{\infty} \delta(\tau)\, h(t - \tau)\, d\tau = h(t) \int_{-\infty}^{\infty} \delta(\tau)\, d\tau = h(t), \tag{2.27}$$

in which the properties $g(x)\,\delta(x) = g(0)\,\delta(x)$ and $\int_{-\infty}^{\infty} \delta(x)\, dx = 1$ have been used.

The Fourier transform of the filter impulse response is called *frequency response*, and within this analysis it will be denoted with $H(f)$. By Fourier transforming (2.26), and exploiting the property of convolutions becoming products when transformed, one gets

$$G_{out}(f) = \mathcal{F}(g(t)) = G(f)\, H(f). \tag{2.28}$$

Generally filters are described by means of their frequency response, since this gives right away an idea of which frequencies will be suppressed during the process. For example, when we talk about a *Gaussian filter*, we will mean that the frequency response of the filter is Gaussian.

The analog electrical filters we will use are *low-pass* filters. This means they suppress frequencies from a certain cut-off frequency on, letting the lower frequencies pass. Optical filters are instead *band-pass* filters, since they allow only the frequencies set around a certain central frequency (generally the optical carrier f_0) to pass. Optical signals spectra show all the power concentrated around a high-frequency carrier, and low-pass filtering them would not make much sense.

We define the *bandwidth* of a filter as the breadth in frequency of $|H(f)|^2$. To be able to measure it we need to fix lower and upper cut-off frequencies. In this work we will define the cut-off frequency as the frequency at which $|H(f)|^2$ is half of its maximum value. Since a decrease of 3 dB corresponds to dividing by two, the bandwidth defined in this way is called *3-dB bandwidth*. It is also customary to measure the bandwidth where $|H(f)|^2$ reaches $1/e$ of its maximum value. For low-pass filters the lower cut-off frequency is set to 0, while band-pass filters have both lower and higher cut-off frequencies determined with the aforementioned 3-dB rule.

We would just like to remark that our definition of bandwidth considers only the positive frequencies, while the so-called *full bandwidth* will be twice as much, comprising also the negative ones.

2.1.5 Bit Error Rate

In telecommunications, the final goal is generally to transmit as much information as possible, as fast as possible, in as reliable and robust a way as possible. When it comes to measuring the tendency of the system to wrongly detect the signal, i.e. to return errors in the detected bit sequence, it is customary to talk about *bit error rate* (BER). The BER is simply the number of wrong bits over the total number of transmitted bits. Normally errors are not systematic (for a correctly implemented communication system) and are due to noise. Therefore the BER cannot be calculated from an analytical expression[1] and statistical methods are required.

2.1.6 Multilevel Signaling

In telecommunications, utilizing multilevel modulation means mapping a certain amount of bits (the smallest pieces of information, namely 1s and 0s) in one comprehensive symbol. Let us introduce some of the notation that will be used throughout this thesis and explain a few elementary concepts.

We define the *modulation order* as the number of possible symbols in a specific modulation, and we will label it with M. If one symbol stands for m bits, then $M = 2^m$. The rate at which we transmit symbols is called *symbol rate* and will be denoted with R_S. Trivially, if in one symbol there are m bits, then we can also define the *bit rate* as

[1] Under very strong assumptions and for a simple receiver this can be done, see [4].

$R_b = m \cdot R_S$. From this the concepts of *symbol slot* and *bit slot* should come naturally. We will call them T_S and T_b respectively, and they will be

$$T_S = \frac{1}{R_S}, \tag{2.29}$$

$$T_b = \frac{1}{R_b} = \frac{T_S}{m}. \tag{2.30}$$

Note that practically all the m bits within a symbol are transmitted together, so it is not possible to receive one single bit by looking at the signal for a time as long as T_b. We need to detect the whole symbol and then we will be able to retrieve the m bits.

This leads to the concept of *bit mapping*. Mapping means assigning a different symbol S_k to each possible selection of m bits $\{b_{1_k}, b_{2_k}, ..., b_{m_k}\}$. For this to be possible an alphabet of at least 2^M symbols is needed. In the case of optical communications the signal will be characterized by amplitude and phase (together with frequency and polarization) and this makes it very convenient to define the symbols as complex numbers,

$$S_k = S_k^i + jS_k^q, \tag{2.31}$$

where S_k^i is the real part of S_k and i stands for *in-phase*, while S_k^q is the imaginary part of S_k and q stands for *quadrature*.

This allows for the representation of symbols on the complex plane, obtaining something called *constellation*. Each modulation format is characterized by a specific constellation[1]. In this work we will concentrate only on the modulation formats which were studied within this thesis. These are:

- OOK,
- BPSK,
- QPSK,
- 16QAM.

[1]Each constellation can assume all possible positions given by a rotation around the center of the complex plane. This is because the phases can only be measured relatively to each other, and not in an absolute fashion.

OOK stands for on-off keying and is the simplest modulation format. The signal is intensity modulated so that the amplitude can assume just two different values, while the phase is untouched. The modulation order is 2 and the concept of symbol collapses into the one of bit. Obviously this is not a high-level modulation format, but it will be used more than once in this work, for example in Section REF4.1 to check the correctness of our model by comparing with the quantum limit.

BPSK (binary phase-shift keying) is a binary modulation as well (meaning that there are only two symbols in the alphabet). They have the same amplitude but opposite phases. If differentially encoded (see Section 2.1.10) the signal can be directly detected (see Section 3.4.4.2).

QPSK (quadrature phase-shift keying) is a form of MPSK. In these modulations the intensity of the transmitted signal is constant, whereas the phase takes M different values, equally spaced (in the case of QPSK they are spaced of $\pi/2$). For QPSK the modulation order is clearly 4, so that two bits are contained in each symbol. This is a largely studied modulation format, and together with differential encoding it is possible to use it in combination with direct detection. The constellations of OOK, BPSK, QPSK and 16QAM are shown in Figure 2.2.

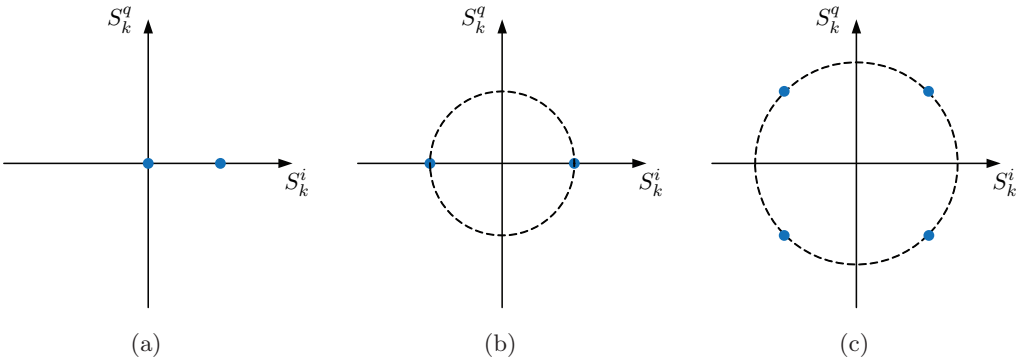

Figure 2.2: Constellations for (a) OOK, (b) BPSK, and (c) QPSK modulations.

16QAM (16 quadrature amplitude modulation) is relatively recent in the field of optical communications. The modulation order is 16, and therefore each symbol carries 4 bits of information. There are two different ways of performing this modulation, which lead to two constellations. They are called *star*- and *square*-16QAM, but we will exclusively treat the latter. In it, the intensity can assume four values, while there are as many as twelve possible phases in the constellation. In Figure 2.3 the constellations

of the two versions of 16QAM modulation are showed. The reason why 16QAM is sometimes preferable is that the distance between two neighboring symbols on the complex plane is more homogeneous than in the case of the star version. This turns into a better OSNR performance, i.e. for the same amount of noise an equal BER is obtained for less signal power. On the other hand, it is not possible to employ direct detection for the square-16QAM, while it is for a differentially encoded star-16QAM. From now on we will neglect to specify *square* in front of 16QAM, it will be implicit.

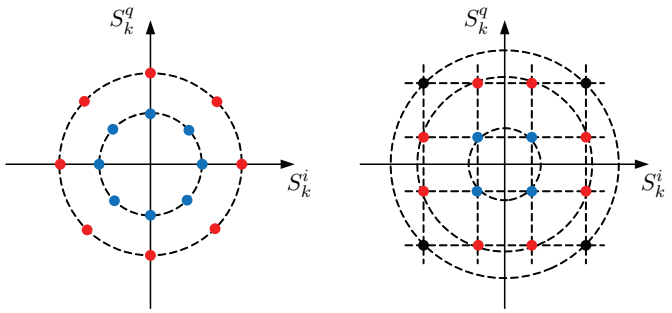

Figure 2.3: Constellations for (a) star- and (b) square-16QAM modulations.

A question should have hopefully arisen by now: why do we use high-level modulation instead of the much simpler OOK? As one will see in Section 3.2, the transmitter gets more complicated for high-order modulations. This is undeniably cause for increased costs and difficulty of implementation. And most engineers know that higher complexity in most cases turns into lower reliability. But there are at least two very good reasons for being interested in high-level optical modulation,

- Increased spectral efficiency,
- Decreased bandwidth requirements for the electrical components.

Let us start by discussing the first bullet. Spectral efficiency is generally defined as the amount of information that can be transmitted within a certain bandwidth, and it is measured in bit/s/Hz. If B is the bandwidth occupied by the signal (defined in the same way as the filter bandwidth described in Section 2.1.4), the spectral efficiency can be calculated as

$$SE = \frac{R_b}{B} = \frac{M \cdot R_S}{B} \tag{2.32}$$

Since the width of the spectrum of the signal depends on the symbol rate, and not on the bit rate (one should look at Figure 2.4 for being convinced of this statement), by means of an increased M we can increase SE.

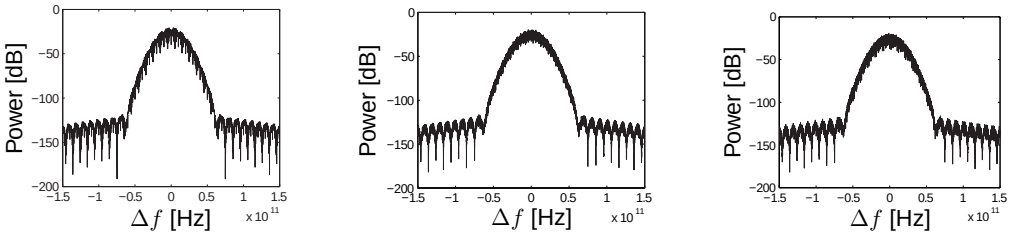

Figure 2.4: Spectra of the signal for (a) BPSK, (b) QPSK, and (c) 16QAM modulations, with $R_S = 10$ GBd/s. On the x-axis we have the frequency difference with respect to the optical carrier frequency.

Having a more confined spectrum (for the same bit rate) turns into a lower impact of chromatic dispersion (if this concept is unknown, please see Section 2.3.3). Therefore, exploiting multi-level modulation we can transmit at higher data rates while chromatic dispersion keeps impairing the system in the same way. Moreover, squeezing the spectrum of our signal allows to pack a larger number of channels in a WDM[1] system. WDM is however not treated in this work.

The second advantage of employing multi-level signaling is that we decrease the requirements for bandwidth in the electronics driving the modulators (or we increase the bit rate while keeping the same requirements. Let us make a simple example. We want to transmit 40 Gb/s over an optical fiber. OOK would require electronic circuitry generating a driving signal at 40 Gb/s, while QPSK would necessitate two signals at 20 Gb/s each (see how the modulator is actually implemented in Section 3.2.6.3).

All in all, thanks to high-order modulation we can transmit more data on the same fiber, saving on the costs of additional fibers. Of course, high-level signaling requires more components to be implemented. A cost optimization should be carried out in practical applications.

[1]Wavelength Division Multiplexing is a technique consisting in transmitting several channels (i.e. distinct streams of information) over the same fiber. Each channel is characterized by a different optical carrier wavelength.

2.1.7 NRZ and RZ

All modulation formats can exist in two formats: *non-return-to-zero* (NRZ) and *return-to-zero* (RZ). In the former we will modulate the output of a CW laser, so that a pulse occupying the whole symbol slot will be transmitted if the symbol has non-zero power. The latter format requires the power to go to zero at the symbol slot borders. This is typically achieved by modulating pulses instead of a CW signal. Figure 2.5 should clarify this concept.

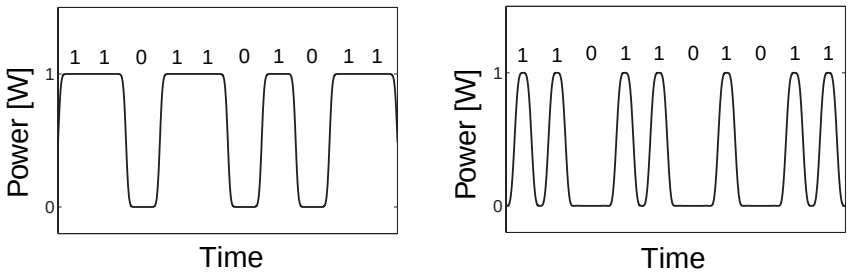

(a) (b)

Figure 2.5: Example of OOK with (a) NRZ format and (b) RZ format.

RZ formats are especially interesting because they allow for OTDM (see Section 2.1.9). A lot of work has been done on comparing RZ and NRZ formats. We do not want to start this discussion here, the eager reader can begin its journey from [13].

There are several ways to make a pulse source. One is the direct modulation of a laser (lasers are discussed in Section 2.2.1), which is rarely suitable for baud rates higher than 10 GBd/s due to the bandwidth limitations of lasers operated in this way [4]. A second option is to exploit pulse carvers, which are treated in Section 2.2.4. Finally we can employ a mode-locked laser (see Section Section 2.2.1.4), which is a most common, and very expensive, solution. In this work, we will consider the second and the third options.

Let us conclude by giving two important definitions. When assessing the width of a pulse, we will always mean its *full width at half maximum* (FWHM), that is simply the difference between the time instants at which the pulse power equals half of the peak value (see Figure 2.6). Sometimes we might need to use a different definition (and we will make it clear when the case presents itself). According to this, the pulse width is

measured at $1/e$ of the peak value. The second concept we should keep in mind is the one of *extinction ratio* (ER). In a pulse, it is the ratio between the peak power and the lowest power (see Figure 2.6). It is generally measured in dB.

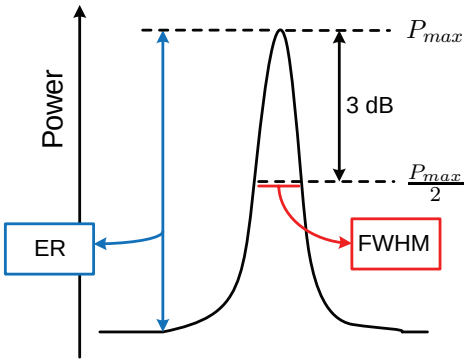

Figure 2.6: Definition of FWHM and ER.

We also need to introduce the concept of *root mean square* (rms). It is a measure of how much the pulse is spread in time with respect to the middle point, and can be defined as

$$T_{rms} = \sqrt{\frac{\int_{t_0-T_S/2}^{t_0+T_S/2} (t-t_0)^2 P(t)\, dt}{\int_{t_0-T_S/2}^{t_0+T_S/2} P(t)\, dt}}, \tag{2.33}$$

where $P(t)$ is the pulse power, t_0 the time corresponding to the pulse peak, and we have supposed to have a train of pulses, therefore limiting the integral over a symbol slot. Such a definition will be very useful in Section 4.2. Note that the pulse rms will be measured in s and labeled as T_{rms}. The smaller T_{rms}, the more the energy of the pulse is confined close to the peak.

2.1.8 Relation Frequency-Phase and Chirp

We need now to introduce the relation existing between phase and instantaneous frequency of a signal,

$$\Delta f(t) = \frac{1}{2\pi}\frac{d\phi(t)}{dt}. \tag{2.34}$$

As one can see, the frequency undergoes instantaneous shifts depending on the time derivative of the phase (i.e. depending on how fast the phase changes in time). This phenomenon is known as *chirp*. Let us give some useful definitions in the case chirp occurs in a pulse. We have positive chirp when the frequency shift is such that the

trailing part of the pulse has a higher frequency (the so-called "blue shift") and the leading part a lower one ("red shift"). A negative chirp is simply the other way around.

2.1.9 OTDM and PolMux

Let us first clarify the concept of *multiplexing*. It is a process through which multiple streams of information (called *channels*) are put together and transmitted over the same medium. In our case, we will employ two kinds of multiplexing, *optical time-division multiplexing* (OTDM) and *polarization multiplexing* (PolMux).

OTDM consists in packing several channels so that each of them has a fraction of the symbol slot dedicated. The simplest way to grasp the concept right away is to look at Figure 2.7. It should be clear that this is realizable only if we use an RZ format. Clearly, if we have N channels to which we equally allocate time-resources, every channel will have a dedicated time slot $T_S^{ch} = T_S/N$.

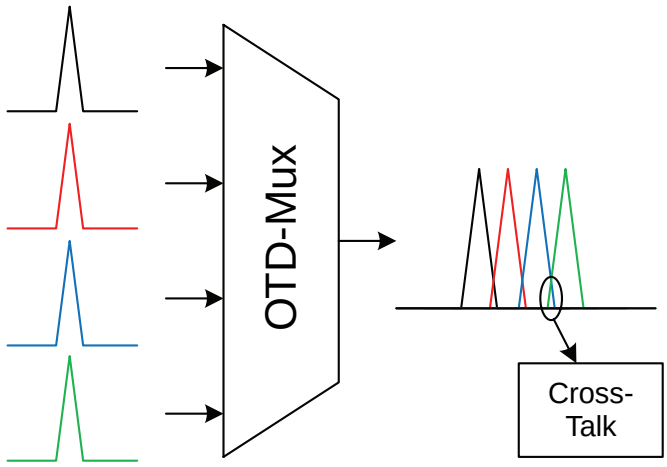

Figure 2.7: Concept of OTDM with highlighting of cross-talk.

OTDM systems are interested by a phenomenon called *cross-talk*, and illustrated in Figure 2.7. When multiplexing different channels, some of the energy of one channel will end up in the other ones, unless the pulses are totally confined within T_S^{ch}. In practice this is never realized, since the pulse tails will always extend outside of the allocated time slot. This superposition of electric fields brings interference, and the pulses are unavoidably distorted. One should intuitively understand that cross-talk degrades the quality of transmission causing errors in the message we want to convey. Normally, to minimize cross-talk (more precisely to equalize the performance of all the

channels), channels should be equally spaced in time. Notice that cross-talk assumes also other forms in different contexts[1], but this is all we will need in this work. OTDM cross-talk will be object of study in Section 4.2.3.

The other multiplexing technique we applied in our study, even though less extensively than OTDM, is PolMux. We have seen in Section 2.1.1 that the optical signal is characterized by a polarization state, which is described by a vector $\mathbf{e}$. This means that two fields orthogonally polarized with respect to each other would not interfere when co-propagating. This clearly results from the observation that their field vectors would be linearly independent. If we multiplex two orthogonally polarized optical channels onto the same fiber, we will double the transmitted bit rate. The drawbacks of this reside in the increased complexity of transmitter and especially receiver, and in polarization-related impairments such as polarization rotation and polarization mode dispersion. PolMux has been treated in detail in [12], so we do not discuss it further here.

2.1.10 Encoding and Decoding

Coding (or encoding) and decoding are topics that have attracted enormous interest within the field of telecommunications. For the purpose of this thesis, we will need just the very basics of this subject (with the risk of awakening the rage of the experts).

Encoding consists in mapping groups of bits into other groups of bits (or symbols into other symbols). Most often, also the operation of mapping groups of bits into symbols is denoted as coding. Decoding is basically the inverse operation, which supposedly restitutes the original bit stream. This can be done in a variety of ways, and for several reasons. The encoding will be discussed in detail for each of the modulation formats we use in Section 3.2, here we just want to introduce important concepts that will be then taken for granted in the remainder of the thesis. Among the numerous applications and varieties of encoding, the ones we are interested in are:

- Forward error correction (FEC),
- Grey coding,
- Differential encoding.

[1] For example, in WDM systems cross-talk takes place between channels at different frequencies because their spectra are not neatly separated.

FEC is a method employed to make the system more resilient to errors due to the noise introduced by the system, especially the optical channel (see Section 2.3.5). Before transmission, the bit stream is separated in chunks of equal length and extra bits are added, so to create redundancy of information. At the receiver the decoder is then able to detect part of the errors (very primitively, we could say that the more redundancy we add, the more errors we can detect within a certain number of received bits), and maybe correct some of them. If the correction cannot take place, then a retransmission is requested. This technique has allowed engineers to consider a optical communication system *error free* not anymore when the BER is lower than 10^{-9}, but now between 10^{-3} and 10^{-4} [14]. This justifies our choice of targeting almost all of our simulations to values of the BER within this interval.

Grey coding is used in optical communications to optimize the OSNR performance of the system. When mapping our bits into symbols, we make sure that neighboring symbols on the constellation diagram differ for as few bits as possible. Intuitively, if noise causes a wrong detection, this will most likely make us detect one of the symbols closest to the transmitted one. So, the fewer the wrong bits, the better the BER. Figure 2.8 shows a possible Grey coding for QPSK and 8PSK. In the case of 16QAM things are a little bit more complicated and the problem of encoding will be discussed in Section 3.2.6.4.

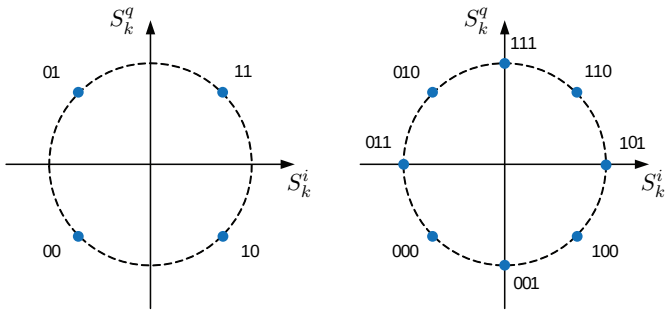

Figure 2.8: Example of Grey coding for (a) QPSK and (b) 8PSK.

Differential encoding is a completely different concept. The bits to be mapped into symbols are encoded to be representative of phase differences. So, the kth symbol depends on the difference between the phases of the signal sampled in two adjacent symbol slots, $\phi_k - \phi_{k-1}$. This idea holds great potential for three reasons. First, it

allows for direct detection since knowing the phase of the signal (with respect to a local oscillator) is not necessary anymore, we just need to make the signal interfere with a delayed version of itself at the receiver to retrieve the phase difference. Second, also in the case of a coherent receiver with DSP (see Section 2.4.8 and [12]), thanks to differential encoding we do not need synchronization sequences in the data[1]. Third, talking about noise, what matters is how much the phase changes between two neighboring symbols. This means that the higher the symbol rate, the lower the impact of phase noise! This is an astonishingly good reason to use differential encoding. On the other hand, every time we wrongly detect a bit we will have two errors, because also the following one will be wrong. In this way the number of errors will double itself, resulting in a penalty of 3 dB [6].

2.1.11 OSNR Definition

The *optical signal-to-noise ratio* (OSNR) is defined as optical signal power over noise power. It is an extension of the concept of SNR (signal-to-noise ratio) to the optical domain, and gives a measure of how much the signal is corrupted by the noise. In optical communications, it is common use to draw BER-OSNR plots to display the system performance. It is indeed crucial to be able to assess the impact of increasing levels of noise on the BER.

For these reasons we need to establish a precise definition of OSNR, which is not a totally trivial task, as it will be shown below. Having a clear and thoroughly understood definition of OSNR is necessary in order for a comparison with the literature on the topic to be possible. We set

$$\mathrm{OSNR} = \frac{\langle P(t) \rangle}{p \cdot N_0 \cdot B_{ref}} \tag{2.35}$$

where at the numerator we have the mean signal power, while at the denominator we have the number of polarizations in which noise is present p, the single-sided noise spectral density per polarization N_0, and a reference bandwidth B_{ref}, which is 0.1 nm

[1] Many constellations are symmetric with respect to rotation. In this case, when a symbol is received, a phase ambiguity arises. For example, a BPSK signal has a π phase ambiguity, QPSK and square-16QAM ones have $\pi/2$ phase ambiguities. Differential encoding makes this ambiguity irrelevant, since what matters is not the absolute phase but the phase difference with respect to the previous symbol.

(or 12.5 GHz) in our model, as generally found in literature [15]. p can be either 1 or 2, depending on whether we have noise in only one or both polarizations (x and y).

Notice that in (2.35) N_0 is a constant spectral density. This is of course not true for all kinds of noise. In this definition of OSNR this is perfectly verified, since the noise we are considering here is ASE noise, which has typically a Gaussian distribution with constant spectral density.

2.1.12 Relationship Between OSNR and SNR

The signal-to-noise ratio can be defined in various ways. The way we conceive it in our model is one of the most widespread in literature,

$$\mathrm{SNR} = \frac{E_b}{p \cdot N_0}, \tag{2.36}$$

where E_b is the energy per bit, p the number of polarizations in which we have noise, and N_0 is again the single-sided noise spectral density per polarization.

Note that both OSNR and SNR will be measured at the receiver input, more precisely just before the optical filter preceding the actual receiver. It is important to define these quantities clearly and carefully, since a large chunk of our results will deal with BER curves, and these are shifted if we change our definitions. As should be readily understood, a factor of 2 in the equations (for example due to the number of polarizations involved) would in fact shift such curves of 3 dB. Ultimately, what one wants most often to assess is the robustness of a system with respect to noise, and OSNR and SNR are our ways to measure the amount of noise with respect to the signal power in a hopefully generally understood way.

It is now also important to relate the two ratios, since in section REF4.1 we will compare to numerous papers in the attempt of showing the validity of our model. Some of these publications make use of the SNR as defined in 2.36, for which reason we need to be able to switch safely between the two definitions. Calling m the number of bits in one symbol (so that the number of points in the constellation will be M), we set the general conversion equation as

$$\mathrm{OSNR} = \frac{\mathrm{SNR} \cdot R_S \cdot m}{B_{ref}}, \tag{2.37}$$

which in dB becomes

$$\mathrm{OSNR}_{\mathrm{dB}} = \mathrm{SNR}_{\mathrm{dB}} + 10 \log_{10} \left(\frac{R_S \cdot m}{B_{ref}} \right). \tag{2.38}$$

From now on OSNR and SNR will always be given in dB, and the subscript will be dropped for simplicity.

2.1.13 System Overview

To conclude this part dedicated to a general review of the main concepts needed for understanding this work, we will present an overview of a typical optical communication system, at least in the form we will use later for our investigations. Here we give just some guidelines about the different components, that will be discussed in detail in the following part. The goal is to take a comprehensive look at the system so to see how the several main blocks connect and position themselves. Figure 2.9 should be observed while reading. Note that the portrayed system is valid only for direct detection, since a coherent receiver has a slightly different structure (see 2.4.8 and [12]).

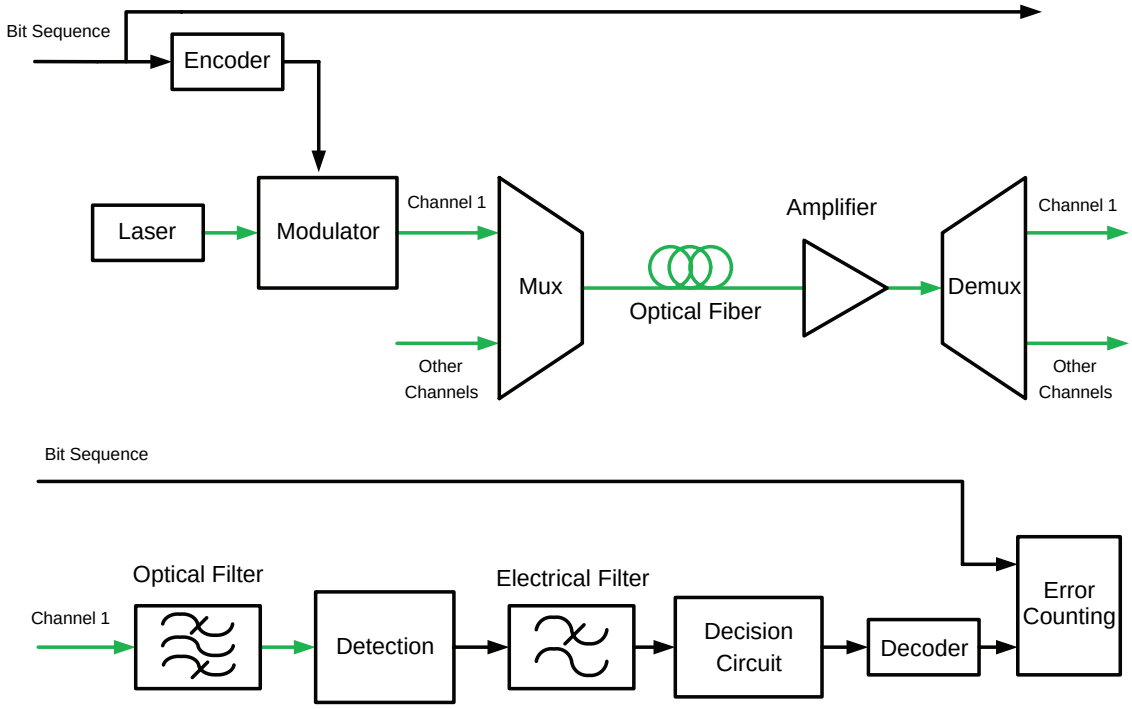

Figure 2.9: Block diagram of a generic multiple channel optical communication system with direct detection. The upper scheme continues in the lower part, as indicated by the labels on top of the arrows.

One or more bit sequences constitute the input of this system (in the block diagram only one bit sequence was shown to avoid excessive complexity). They come as digital

electrical signals (currents or voltages) and are encoded to apply, if needed, Grey coding and/or differential encoding. There might be several outputs from the encoder (only one shown in the figure), depending on the order of the modulation we are going to perform. Here the digital domain ends and the signals are amplified and a DC component is added so that they are suitable driving signals for the optical modulator.

In our system we always have a laser as light source, and its emission is coupled into the optical modulator, whose output will be a modulated optical signal carrying the information encoded in the input bit sequences. This will be one channel, then we may have extra channels, and they will be multiplexed either according to the OTDM or the PolMux techniques. So far, noise has been introduced by the laser in the form of phase noise and intensity noise (the noise added on the electrical signals will not be considered and is negligible in most practical situations). The components mentioned so far are described in Section 2.2.

The optical signal is transmitted over an optical fiber, which is responsible for major variations in the signal itself, depending on characteristics of the fiber such as length, nonlinear coefficient, dispersion curve, and loss per unit length. Losses are then compensated by amplifying the signal. Optical amplifiers introduce ASE noise, which is what mostly limits the length of the fiber link, since longer links mean more losses and therefore more amplification and noise. All these topics are thoroughly discussed in Section 2.3.5.

After demultiplexing, each channel goes through an optical filter, which has the goal of suppressing as much out-of-band noise as possible. White noise will have a spectral density constant at all frequencies. The signal will have a spectrum somewhat limited in frequency. As long as we do not modify the signal spectrum, the signal will look untouched in the time domain. The more noise we manage to suppress, the fewer errors we will get. This explains the presence of the optical filter, which should have a frequency response centered on the optical carrier frequency and a bandwidth larger than the signal bandwidth.

Our direct detector will convert the optical signal into one or more analog electrical ones (as many as the modulator driving signals). How this is carried out will be left to later explanations (see Section 2.4). In this block shot and thermal noise are added to the signals. An electrical filter aiming at suppressing as much noise as possible follows.

The analog signals are then processed by a so-called decision circuit, which will sample them at a constant rate producing an output bit sequence for each of the input signals. 1s and 0s are discerned by means of a threshold. When the analog signal is above this threshold, the corresponding bit is a 1, otherwise a 0. This process is detailed in Section 2.4.4.

To conclude, a decoder should retrieve the original bit sequences which will then be compared to the transmitted ones to check if any errors have occurred.

All of the described parts will be discussed in much ampler detail in the remainder of this chapter.

2.2 Optical Transmitters

Here we present the theory regarding optical transmitters. This is a vast topic, and it was one of the main areas of interest for this work. For this reason, this section will be particularly detailed. The notions here introduced will prove necessary to understand the modeling of such components as presented in Chapter 3.

Optical transmitters necessitate an emitter, i.e. a light source of any kind. We will concentrate on lasers, namely continuous wave (CW) lasers and mode-locked (ML) lasers. Typical noise sources are contextually discussed. We follow with a section about external modulation, where phase modulators, Mach-Zehnder modulators, and IQ modulators are explained in detail. To conclude, we show how signals can be OTD-multiplexed.

2.2.1 Light Sources

Light sources can emit constant or pulsed power. The latter can be employed for RZ formats and OTDM systems, while the former is the only possible solution for the NRZ ones and does not allow for time division multiplexing.

There are a number of light sources, from incandescence bulbs to enormous industrial lasers, most of whom are of no interest whatsoever for optical transmission, and discussing them all is by far out of the scope of this work. The most performing light source for multilevel modulation is definitely a laser. A laser is an emitter made up of two main parts: an active medium (which is somehow provided with energy so to emit photons) and a cavity (simply an optically confined area where energy is stored, most

often a pair of mirrors that reflect the light back and forth). Many books about lasers have been written, and we do not want to summarize such a fascinating and enormous topic in a few simplistic lines. If unsatisfied after the reading of the following sections, the eager reader can refer to [16] or [17], just to cite the two we most abundantly looked into when studying the subject.

The reason why we did not consider other light sources (like light emitting diodes) when working on high-order modulation formats is that this sort of transmission is highly complex and costly to implement. For the foreseeable future it will be of interest for high data rate connections, where the focus is more on performance than on costs (or at least where the cost of an expensive laser can be shared by a very high number of users). Lasers are the natural choice in this case, providing the lowest noise levels (sources of noise in lasers are going to be clearly understood in the upcoming sections).

Ideally, a perfect CW optical carrier (i.e. the optical signal before modulation) should present a single, sharp frequency component. By definition, a laser is indeed an emitter whose output is collimated (i.e. a well confined ray) and characterized by a single frequency. In practice it is not possible to obtain a signal whose spectrum presents an infinitely narrow peak at the desired optical frequency. This is due to phase noise. The reasons for this are not trivial and we will explain them in Section 2.2.1.2. A perfect CW laser would also have a truly constant output power. This is not verified in practice either, where intensity noise disturbs the signal amplitude, as we will see in Section 2.2.1.3.

This section on light sources continues with the analysis of mode-locked lasers, before introducing an unusual pulse source we will study later on in this work. A brief description of an ulterior non-ideality coming into play when the output power is not constant but periodic, the timing jitter, concludes this section.

2.2.1.1 CW Lasers

As we previously said, a laser always presents a cavity. Only light at some well determined frequencies can build up increasing energy and actually lase. This happens if the phase shift experienced by light in a round trip in the cavity equals an integer number of times 2π, so that constructive interference can take place. This is verified for wavelengths λ such that

$$l = \frac{q\lambda}{2}, \tag{2.39}$$

where l is the length of the cavity (assuming a simple cavity with two mirrors at the extremities) and q an integer number. Remembering that $f\lambda = c/n$, with n refractive index of the medium filling up the cavity, the frequencies that can resonate in the cavity are called *longitudinal modes* and calculated as

$$f_q = q\frac{c}{2nl}. \tag{2.40}$$

The distance between two adjacent resonance frequencies is called *free spectral range* (FSR) and is given by

$$\text{FSR} = \frac{c}{2nl}. \tag{2.41}$$

If this is not clear, further analysis is carried out in [17]. One should at this point understand that, if the active medium in the cavity amplified all frequencies in the same way, one would have a laser output spectrum made up of all these many peaks equally strong. However, the gain medium has a limited bandwidth, so that just a finite number of modes can survive in the cavity. This would be a multi-mode laser, and the output power would be more or less constant because of the absence of any coherence between the various modes (this concept will be clear after discussing mode-locking, see Section 2.2.1.4). A single mode laser can be obtained by artificially increase the losses in correspondence of all the modes but one.

We can adapt (2.16) to the description of a CW laser output by making power and polarization independent of the time, moreover the phase modulation term is deleted,

$$E(t) = \sqrt{P_0}e^{j\omega_0 t}. \tag{2.42}$$

So, the main parameters defining a CW laser are output power P_0 and central frequency $f_0 = \omega_0/2/\pi$. The spectrum will show a peak at f_0 (and symmetrically at $-f_0$), if we assume that the laser is single-mode. From the spectrum in Figure 2.10, we notice that the peak has a certain width, which is called *linewidth* and label with $\Delta\nu$, and is determined by the amount of phase noise, as explained in the following section. The linewidth is usually measured as the FWHM of the power spectrum peak. A finite linewidth is due to phase noise, indeed we recall that frequency shifts are caused by phase jumps, as expressed by (2.34). The physical reason for the phase noise will be clear in the next section.

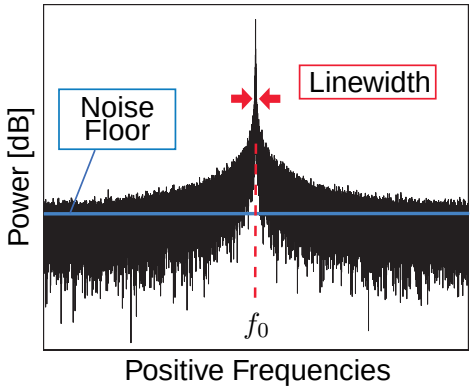

Figure 2.10: Spectrum of a single mode CW laser.

Looking again at the spectrum of a CW laser, we notice a noise floor, which comes from the joint contribution of phase noise and intensity noise. Introducing terms accounting for these two noise sources, (2.42) becomes

$$E(t) = \sqrt{P_0 + \delta P(t)} e^{j(\omega_0 t + \delta\phi(t))}. \tag{2.43}$$

Today there is a variety of solutions for CW lasers, but in this analysis we have limited ourselves to single mode lasers, which offer better performances in terms of phase noise, having a single line in the spectrum, instead of a number of incoherent lines (the concept of coherency will become much clearer after reading Section 2.2.1.4). Distributed feedback (DFB) lasers and external cavity lasers (ECL) are typical choices, and they offer linewidths narrower that 1 MHz [16]. The description of the mentioned noise sources follows.

2.2.1.2 Phase Noise

To understand the origin of laser phase noise, one needs to grasp some of the basic concepts of photonics. We will hereby provide as short and naive an explanation as possible. Since the topic is mastodontic and complex, a trade-off between rigor and simplicity is needed. Hopefully, the well informed reader will forgive us. An excellent reference is [16].

Light emission and absorption takes place in three ways:

- Absorption,

- Stimulated emission,
- Spontaneous emission.

A photon can be absorbed by a medium with the consequence of an electron jumping to a higher energy level. Momentum and energy have to be conserved for basic principles of physics. The more the "low-energy" states are populated with electrons and the "high-energy" ones are depleted, the more absorption we will experience. For simplicity, let us assume that only two energy levels exist in the medium, and let us call them 2 (higher energy), and 1 (lower energy). The absorbed photon must have energy $E = E_2 - E_1$. This means that its frequency f will verify the well known equation

$$E = hf, \tag{2.44}$$

where h is Planck's constant.

Emission takes place in two forms. When an incoming photon traverses a medium, an electron can give up part of its energy and jump from 2 to 1, liberating a photon with energy and momentum such that the aforementioned conservations still hold true. This is the so-called stimulated emission, and the emitted photon will be characterized by being identical to the stimulating one in frequency, phase, direction and polarization. The probability of a photon to induce stimulated emission will be enhanced for an higher population of electrons in 2 and a lower population in 1.

In nature, electrons populate the different levels following a probability distribution. Normally, the low-energy levels are by far more populated than the high-energy ones, and absorption is the prevailing phenomenon. In a laser the active medium is "pumped" by means of a current or another light source. Without going into the details, this simply means providing it with energy so that many more electrons will be in an excited states, ready to participate in the stimulated emission, while the low-energy states will be almost depleted and absorption will therefore be a minor contribution. Therefore, photons travel back and forth in the cavity and stimulate the emission of other photons. The mirrors let a small part of the photons go through, so that an output is constituted.

According to this scenario, the spectrum of a laser should present a sharp peak at the photon frequency f_0, since stimulated emission generates photons with identical phase and frequency. Spontaneous emission is the reason for a finite linewidth. Excited

electrons have a probability to fall to 1 and emit a photon (this is explained in quantum mechanics with the concept of vacuum field [18]). Unfortunately, these spontaneously emitted photons will not have the same phase, it will indeed be completely random. Since the direction is also random, just a minority of these photons contribute to the laser output. Nonetheless, they will cause small phase jumps in the electric field. Recalling the relation between the time derivative of the phase and the frequency shift (2.34), it should be readily understood that these phase jumps turn into a frequency broadening of the output field. Spontaneously emitted photons also have random polarization, whereas the frequency matches the one of the carrier frequency of the laser light, in this idealized scenario where we just have two sharp energy levels[1].

Phase noise is one of the most impairing non-idealities in an optical communication system employing high-order modulation formats. If the absolute value of phase of the field[2] carries information, noise disturbing the phase is clearly detrimental. When employing differential encoding, what matters is the phase difference between consecutive symbols. By increasing the symbol rate we obviously shorten the symbol slot, meaning that the phase noise will have less time to corrupt the phase of the field from a symbol to the following one. Therefore, almost uniquely in telecommunications, the phase noise is an impairment whose weight becomes less for higher symbol rates, provided that we employ differential encoding.

More details will be provided when discussing the implementation of phase noise in Section 3.2.2.3.

2.2.1.3 Intensity Noise

Light is quantized. It is not a continuum but made up of a finite number of photons. The same holds true for matter. The electrons participating to the phenomena described in the previous section are countable. Absorption and emission are regulated by statistical laws that apply to every single particle. Macroscopically, the output power might be steady and flat, but microscopically myriads of recombination events take place. This

[1] For reasons of brevity and simplicity we have not discussed the fact that energy levels are in practice broadened (due to Heisenberg's uncertainty principle) and that atomic systems have of course more than two levels, even energy bands in the case of semiconductors. All the desired information is found in [19]

[2] The phase is relative, and cannot be measured on absolute terms. What we mean is the absolute value with respect to the phase of a local oscillator. This concept will be clarified in Section 2.4.8.

means that the power level will slightly oscillate over time. According to the discussions above, one should understand that the populations of electrons and photons depend on each other. Therefore oscillations of the pumping agent (for example the current that pumps the active medium) will be converted into noise in the population of excited electrons and in turn into intensity noise. There are also other causes behind intensity noise, but these will do for our purposes.

For lasers it is customary to define the *relative intensity noise* (RIN),

$$\int_0^{\Delta f} \mathrm{RIN}\left(f\right) df = \frac{\left\langle \Delta P\left(t\right)^2 \right\rangle}{\left\langle P\left(t\right)^2 \right\rangle}, \tag{2.45}$$

in which Δf is an integration reference bandwidth, the brackets $\langle\rangle$ stand for time average, $P\left(t\right)$ is the signal power, constant in the case of a CW laser, and $\Delta P\left(t\right)$ the deviations from the expected power (i.e. intensity noise).

Typical values of RIN for semiconductor lasers range from -160 dB/Hz to -130 dB/Hz [6]. Intensity noise is generally not one of the most impairing noise sources in an optical communication system. Further information about intensity noise will be provided contextually with its modeling in Section 3.2.2.2.

2.2.1.4 Mode-Locked Lasers

When we need to generate pulses, a possible solution is the direct modulation of a laser. This implies changing the pumping current to modulate the output power. This is not an interesting technique for high performance systems like the ones we will investigate. Direct modulation is indeed slow (the population of electrons takes a finite time to adjust to variations in the pumping current and the photons also require some time to adjust to the new levels) and just a few devices can today work at symbol rates in the order of tens of Gb/s. Moreover, direct modulation introduces chirp in the laser output, since a variable population of electrons in the active medium causes the refractive index to vary. This introduces phase changes and in turn frequency shift.

Mode-locked lasers are in most cases the best solution when we need a pulse source. The theory of mode-locking is very complicated and an entire thesis could be devoted to it. Here we just aim at giving some basic understanding of the principles standing behind this technique.

Let us consider N harmonic oscillators with angular frequencies equally spaced by δ (which could be the longitudinal modes of a laser cavity, separated by FSR) and centered on ω_0, and the same initial phase ϕ_0,

$$x_n(t) = x_0 \sin(\omega_n t + \phi_0), \tag{2.46}$$

where $\omega_n = \omega_0 + n\delta$ and n is an integer in the range between $-\frac{(N-1)}{2}$ and $\frac{(N-1)}{2}$.

By summing up all of the oscillators, and performing a number of trigonometric acrobatics (see [20]), one would end up with

$$X(t) = x_0 \frac{\sin(\omega_0 t + \phi_0)\sin\left(\frac{N\delta t}{2}\right)}{\sin\left(\frac{\delta t}{2}\right)} = A_N(t)\, x_0 \sin(\omega_0 t + \phi_0). \tag{2.47}$$

Note that the sinusoidal term indicates the fast oscillations of the field at the carrier frequency, while the factor $A_N(t)$ is a variable amplitude and it is shown in Figure 2.11(a) for different values of N. The higher the number of modes, the higher and narrower the peaks. Moreover, the spacing in time between peaks is exactly $1/\frac{2\pi}{\delta}$, which is 1/FSR for a laser.

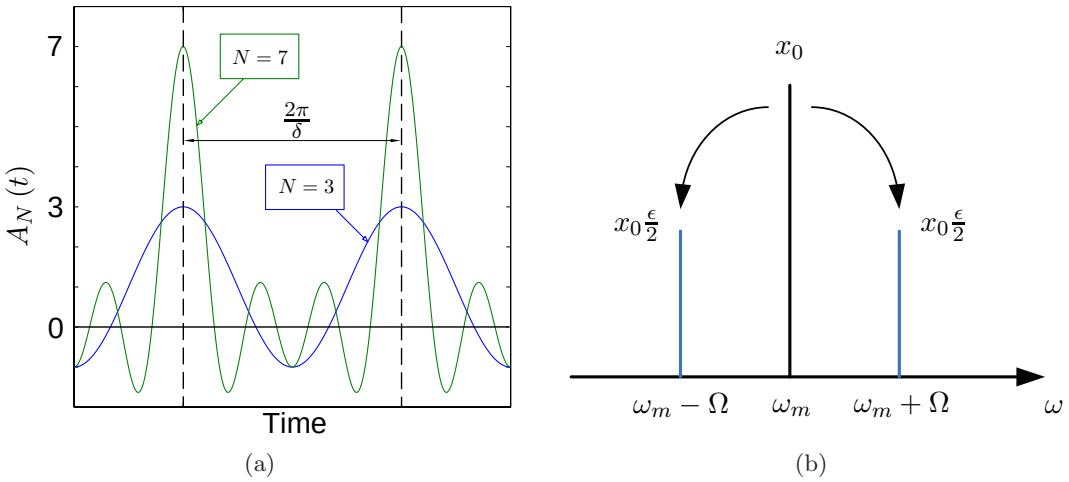

Figure 2.11: (a) $A_N(t)$ as defined in (2.47). (b) Sidebands generated by amplitude modulation of a carrier.

We have seen that the power of several modes can be rearranged in time so that a train of pulses is generated. A multi-mode laser will normally give a constant output power, but, if the modes have the same initial phase ϕ_0, and there is no phase noise,

then the output becomes pulsed. Mode-locking a laser simply means making sure that this condition on the phases is verified.

How is this done in practice? Lots of information about this topic are found in [21]. For simplicity, of the many techniques that have been devised over the years, we will just briefly discuss the *amplitude modulation locking*. Let us sinusoidally modulate the amplitude of the m-th mode at a angular frequency Ω and with a modulation factor ϵ. We get

$$x_m(t) = x_0 (1 + \epsilon \cos(\Omega t)) \sin(\omega_m t + \phi_m). \tag{2.48}$$

After some manipulations one can express $x_m(t)$ as

$$x_m(t) = x_0 \left\{ \sin(\omega_m t + \phi_m) + \frac{\epsilon}{2} \sin[(\omega_m + \Omega) t + \phi_m] + \frac{\epsilon}{2} \sin[(\omega_m - \Omega) t + \phi_m] \right\}. \tag{2.49}$$

In the frequency domain this is a carrier with two coherent sidebands (see Figure 2.11(b)). This means that, if we choose Ω = FSR, then the sidebands of any mode will fall exactly on the two adjacent modes. This is true for any of the several modes of a multi-mode laser. In this way, all of them will be coupled to each other. Since stimulated emission is the driver to energy build up in the cavity, all the photons in one mode will tend towards the same phase, which should in turn be the same for all the modes thanks to the locking provided by the amplitude modulation. Ideally, all the modes should therefore have the same phase and the output should be a train of pulses.

Amplitude modulation in practice achieved by means of an amplifier positioned in the cavity and sinusoidally pumped at a frequency equal to FSR. Other methods employ saturable absorbers or other devices, but we will not discuss them here since they do not add much to the understanding of the topic in relation to what is needed within this thesis.

Note that in practice things do not work so well. The locking is not perfect and the modes undergo a continuous adjustment. Every mode has in fact a contribution from the sidebands of the neighboring modes plus a contribution initiated by spontaneous emission at that frequency. Even though ideally the locking should prevail, it is never complete and perfect as in the theory developed above. This results in deviations from the ideal train of pulses. We will not discuss mode-locked lasers to this level of detail,

and the only non-idealities we will consider are phase noise, intensity noise, and timing jitter.

Phase noise has been explained already, we just need to define the concept of linewidth also for a mode locked laser. We decided to define it as the FWHM of the central mode, i.e. the one with the highest power. Intensity noise was defined in all generality with (2.45). Timing jitter is briefly touched in the Section 2.2.1.6.

2.2.1.5 Generation of Pulses by Phase Modulation of a CW Source and Group Velocity Dispersion

Mode-locked lasers are not the only way to produce a pulse train. In this project, we have extensively studied a less popular technique, which allows to generate a series of pulses by phase modulating a CW source and then making the signal propagate through a span of optical fiber. The idea was first (to our knowledge) presented in [22]. Here we just aim at giving some basic theoretical understanding of the way this works, while in Section 3.2.2.5 we will discuss in finer detail the way we model such a system.

The explanation should be quite easy on an intuitive level. It is important to have the concepts of chirp (briefly introduced in Section 2.1.7) and dispersion (still to be touched, will be in Section 2.3.3[1]) clear in mind, in order to grasp the functioning of this pulse source. By phase modulating the signal we can introduce some chirp, i.e. a frequency modulation (as appears from (2.34)). After this step, the CW signal will alternate lower frequencies to higher frequencies, following the phase modulation. If we now propagate the light through a dispersive medium (like an optical fiber), so that group velocity dispersion take place, different frequencies will travel at different speeds. As a result, pulses will start forming.

Proving this analytically would be more complicated and would not add anything to the understanding of the concept. For more detail one should refer to [22]. Let us just give a couple of definitions that will come at hand later on.

[1] The reader will forgive us for necessitating a concept that has not yet been explained. Unless we wrote a massive introduction to optical communications, which someone surely more knowledgeable already did in [4], there would be no way to avoid this, since concepts are correlated to form an entangled and sometimes annoying net. We therefore preferred to keep this pulse source after the only other, i.e. the mode-locked laser, instead of putting it at the end of this chapter, where it would have been easier to understand but completely out of place.

Assuming a sinusoidal phase modulation, the electric field after the modulator could be expressed as

$$E(t) = \sqrt{P_0} e^{j(\omega_0 t - \Delta\Theta \sin 2\pi f_m t)}, \tag{2.50}$$

where f_m is the frequency of the phase modulation and $\Delta\Theta$ the amplitude of such modulation. We then borrow from [22] a parameter collecting all the system characteristics, and defined as

$$B = \left| \frac{\delta f}{\delta t} \right|_{max} \cdot \frac{\delta \tau_g}{\delta f}, \tag{2.51}$$

in which the first term represents the contribution of the phase modulation, and the second one (where τ_g is the group delay, expressed in s and described in Section 2.3.3) the contribution of the group velocity dispersion. It will be useful to refer to B from time to time, as we will show in Section 4.2.

Now we face the most difficult problem of this section: find a name for such a pulse source. We will need to name it quite often later on, and we should hence find a nice acronym. After thinking long and hard, we could not come up with anything better than PMCW pulse source, which recalls the fact that the pulses are originated from the phase modulation of a continuous wave laser. We are sorry for not accounting for the dispersive element in such an acronym, but we wanted to keep it short enough.

2.2.1.6 Timing Jitter

Timing jitter is a well known uncertainty in the pulse repetition rate. It is noticed both in ML lasers and pulses generated by external modulation. Simply, the instant in time at which we have the peak of the pulse can shift slightly. This is caused by different factors depending on the system implementation and components. Just to mention one, it can generate from phase noise in the oscillators used by the electronics driving the optical modulators. Also a non-ideal locking of the modes in a ML laser results in jitter. We will limit ourselves to these few lines for what concerns timing jitter.

2.2.2 Optical Couplers

It is often necessary to split the optical signal, or combine two optical signals together. This is achieved through optical couplers. We discuss them here, before discussing most of the other components, because they are utilized at the transmitter as well as at the receiver. We will not look into the way a real device works, we are just interested in

giving a few details that will be necessary to understand later on how some components work.

A coupler will be represented as the one shown in Figure 2.12. It has two inputs and two outputs, the optical signal coming from the upper input will be split so that half the power goes into the lower output and half the power into the upper output. The same holds true for the second input. Since the power is equally split (at least ideally), this component is generally referred to as 3-dB coupler.

On top of this there is a peculiar property we should mention. When the signal goes from the upper input to the lower output or from the lower input to the upper output (red and blue arrows in Figure 2.12, respectively), it acquires a phase shift of $-\pi/2$. It is important to consider this every time we want to work with the phase of the signal within an interferometric structure. If we do not, we will have an unexpected overall phase shift for our signal at the output.

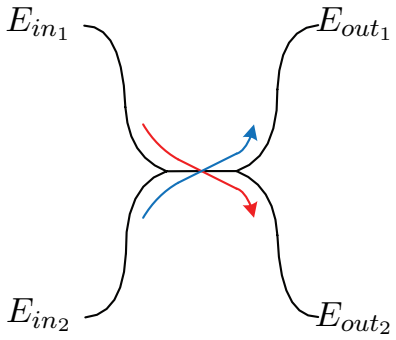

Figure 2.12: 3-dB coupler. The red and blue arrows indicate the paths introducing $-\pi/2$ phase shift.

Notice that in many figures the couplers will be represented with only an input, or only an output. This is because in most practical situations we use them as power splitters or combiners, and we do not need all of the four ports. In these cases, unless otherwise specified, we will always use the upper input or output. Sometimes, for simplicity, we will also neglect the phase shift introduced by the 3-dB coupler, and we will make sure this is clear from the description in the text.

2.2.3 External Modulators

In optical communications there is a variety of external modulators that, together with light sources and interferometric structures can be combined to obtain the desired mod-

ulation formats. In this section we concentrate on three different external modulators, namely phase modulators (PM), Mach-Zehnder modulators (MZM), and IQ modulators (IQM).

2.2.3.1 Phase Modulator

A phase modulator is a device that applies a phase shift to the input optical signal, depending on the driving voltage accordingly to

$$\Delta\phi\left(t\right) = \pi\frac{V\left(t\right)}{V_{\pi}}, \tag{2.52}$$

where $V\left(t\right)$ is the voltage and V_{π} a characteristic parameter of the modulator, clearly measured in Volts and indicating the applied voltage necessary to have a phase shift of π. Its value is in most cases between 3 and 6 V. Practically a phase modulator consists of a waveguide realized in a substrate of $LiNbO_3$ (most often), stacked between two electrodes (see Figure 2.13(a)). When we apply a voltage to the electrodes, the refractive index of the the material through which the light propagates will change, thus modulating the wavelength and in turn the phase [6].

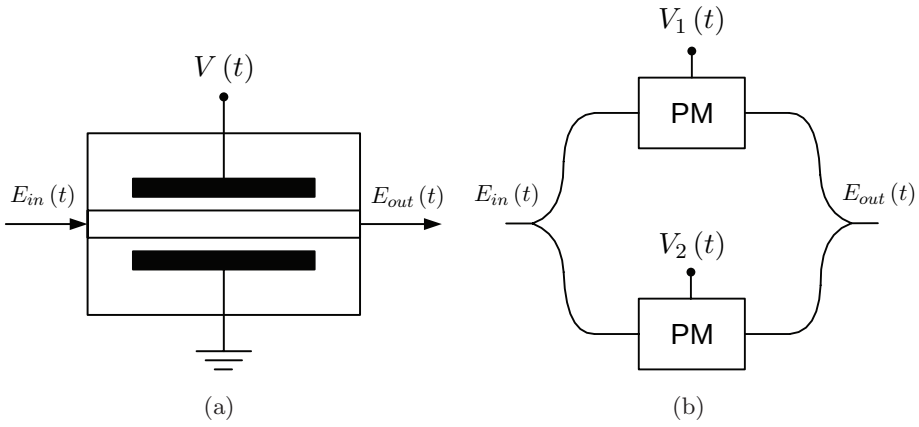

Figure 2.13: (a) Optical phase modulator and (b) Mach-Zehnder modulator.

V_{π} depends on a variety of parameters, both related to the geometry of the device and the materials employed [23]. Without going into the details, we should accept that V_{π} is inversely proportional to the length of the PM. Intuitively, the longer the device, the less voltage we need to apply to obtain the same phase shift (assuming that the electro-optic effect responsible for the modulation takes place over the entire length

and in the same fashion). One could therefore produce longer devices to reduce the voltages required to perform useful modulations. Unfortunately, longer devices have smaller bandwidth.

So far, we have indeed assumed an instantaneous response by the modulator, which is not the case in practice. A precise and extensive analysis of the problem can be found in [23], here we will just report the major findings. There are basically two reasons for the mentioned bandwidth limitation:

1. The metallic electrodes together with the crystal form a capacitor,
2. Light takes a finite time to travel throughout the modulator.

The electrodes will constitute a capacitor whose capacitance C will be directly proportional to the area of the electrodes themselves. On top of this, we will also have a load resistance R_L with the purpose of matching the load impedance with that of the transmission line. This means that, from the source, we will see an equivalent RC circuit, whose 3-dB bandwidth will be $1/(2\pi R_L C) \propto 1/l$, where l is the length of the device. Clearly, the longer the device the lower the bandwidth.

The limitation due to transit time is even more intuitive. The light wave will take a certain time to travel in the crystal. Ideally, the driving voltage should be constant over this time, but, if we increase the frequency indefinitely, at some point the symbol slot T_S will be shorter than or at least comparable to the above mentioned transit time. In this case the light will not be phase modulated properly. At some point a photon will experience the modulations corresponding to more than one symbol during its transit throughout the crystal, so that there is no meaningful modulation anymore.

This bandwidth limitation should not be perceived up to frequencies of many tens of GHz [23], but since we will be working at 40 GBd/s or higher, we had better take it into account.

2.2.3.2 Mach-Zehnder Modulator

A Mach-Zehnder modulator is made up of two phase modulators, as shown in Figure 2.13(b). The transfer function, without considering the phase shifts introduced by the couplers, will be

$$\frac{E_{out}(t)}{E_{in}(t)} = \frac{1}{2}\left(e^{-j\Delta\phi_1(t)} + e^{-j\Delta\phi_2(t)}\right), \tag{2.53}$$

where $\Delta\phi_1(t)$ and $\Delta\phi_2(t)$ are the phase shifts introduced by the two phase modulators, according to (2.52). Assuming that both the phase modulators have the same V_π and after substituting and performing simple maths,

$$\frac{E_{out}(t)}{E_{in}(t)} = \cos\left(\frac{\pi}{2V_\pi}\left(V_2(t) - V_1(t)\right)\right) e^{-j\frac{\pi}{2V_\pi}(V_1(t)+V_2(t))}, \tag{2.54}$$

where $V_1(t)$ and $V_2(t)$ are the voltages applied to the two PMs.

While a phase modulator will always chirp the signal (recall (2.34)), it is possible to operate a MZ modulator in chirp-free mode (called also push-pull operation), by setting $V_1(t) = -V_2(t)$. This is generally achieved by making sure that the two voltages have opposite DC components and complementary data. The transfer function under such conditions becomes

$$\frac{E_{out}(t)}{E_{in}(t)} = \cos\left(\frac{\pi\Delta V(t)}{2V_\pi}\right), \tag{2.55}$$

in which we have defined $\Delta V(t) = V_1(t) - V_2(t)$. By squaring (2.55) we find the power transfer function,

$$\frac{P_{out}(t)}{P_{in}(t)} = \frac{1}{2} + \frac{1}{2}\cos\left(\frac{\pi\Delta V(t)}{V_\pi}\right). \tag{2.56}$$

In Figure 2.14(a) one can visualize the transfer functions of such a modulator. The arrows suggest two possible ways to achieve amplitude and phase modulation starting from a two-level electrical signal. In this work, intensity modulation will be performed with a DC bias of $-2V_\pi/2$ and a peak-to-peak of V_π, while phase modulation will be obtained by biasing at $-V_\pi$ and having a peak-to-peak voltage of $2V_\pi$.

One simple remark about phase modulation: when performing it in the described chirp-free configuration, the signal phase will jump directly from 0 to π and viceversa, and the power will ideally be constant for an electrical signal with no rise/fall times. Of course such signals do not exist in practice, and smoother edges result in deeps at the border between neighboring bits where we have a transition (see Figure 2.14(b)). Every time we move from a one to a zero or viceversa, the phase is flipped and we see a deep in the output optical power.

Let us close this section by setting a useful convention. From now on, when referring to the voltage driving a MZM, we will always mean $\Delta V(t)$ and not, for example, $V_1(t)$. So, if we need to use a MZM to apply a standard amplitude modulation, we will state that a peak-to-peak of V_π and a DC component of $-V_\pi/2$ are needed. This is, in our opinion, the simplest approach, since one can refer to Figure 2.14(a) straight forwardly.

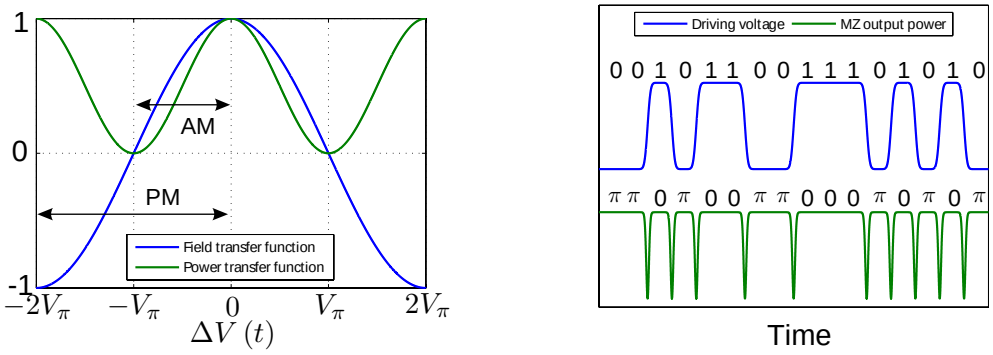

(a) (b)

Figure 2.14: (a) Mach-Zehnder modulator transfer functions and possible voltage spans for amplitude modulation (AM) and phase modulation (PM). (b) Effect of rise and fall times on the output signal.

2.2.3.3 IQ Modulator

After discussing the MZ modulator, we can concentrate on an element central to many of the discussions that will follow in Chapter 4, the IQ modulator. This device employs two MZMs and a PM to reach every possible point on the complex plane. Let us show how this is achieved.

The signal is split into two arms, the upper one consists of a MZM driven in push-pull mode by the signal $V_I\,(t)$, the lower one incorporates a MZM, driven in push-pull mode by $V_Q\,(t)$, and a PM whose driving voltage is constant. The output signal is given by the coupling of the two arms (see Figure 2.15(a)). The upper arm will modulate the field of the signal without introducing a fixed phase shift, reason why it is called I for *in-phase*. If the PM introduces a fixed phase shift of $\pi/2$, the second MZM will operate on the *quadrature* (out-of-phase) component of the output field, from which the label Q. This should be easily understood once one has clear in mind that we are talking about field vectors in the complex plane (or complex numbers) and that every time we couple them we are therefore summing their real and imaginary parts. When performing this sum the phase difference between the two fields plays a key role, allowing for complete freedom as depicted in Figure 2.15(b). Note that the reachable area on the complex plane is square if the power is equally split in all the couplers and decouplers and this area grows for larger signal powers.

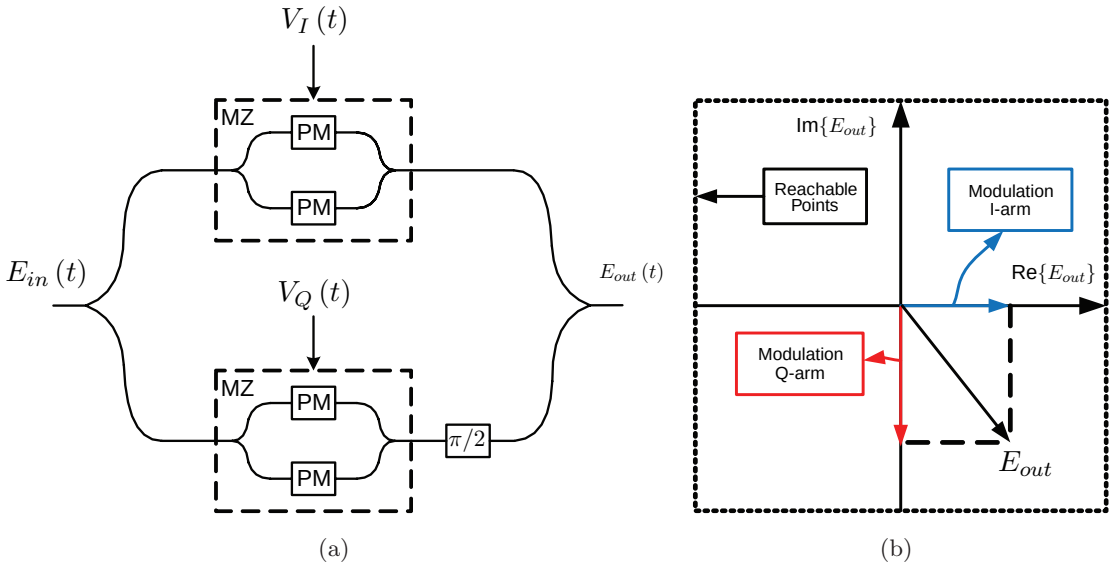

Figure 2.15: (a) Structure of an IQ modulator and (b) its principle of operation on the complex plane.

Now some equations. Recalling 2.55, the phase differences introduced by the two MZMs are, for the I-arm and Q-arm respectively,

$$\Delta\phi_I(t) = \frac{\pi V_I(t)}{V_\pi}, \quad \Delta\phi_Q(t) = \frac{\pi V_Q(t)}{V_\pi}, \tag{2.57}$$

where we have once more assumed that V_π is the same for the four PMs within the MZMs (not necessarily for the phase shifter in the Q-arm). Neglecting the phase shifts introduced by the couplers, the field transfer function can be calculated as

$$\frac{E_{out}(t)}{E_{in}(t)} = \frac{1}{2}\cos\left(\frac{\Delta\phi_I(t)}{2}\right) + j\frac{1}{2}\cos\left(\frac{\Delta\phi_Q(t)}{2}\right). \tag{2.58}$$

This shows once more how the I-arm allows to modulate the real part of the output field and the Q-arm the imaginary one, as visualized in Figure 2.15(b).

2.2.4 Pulse Carvers

There are different ways of carving pulses out of a CW source. Generally this is performed by means of one or more MZMs. Depending on the driving voltage the duty cycle of the output pulses varies. Our choice was to create 50% pulses, which means that the FWHM of the pulse is 1/2 of the symbol slot. This is achieved by driving the MZM with a $\Delta V(t)$ characterized by a DC component of $V_\pi/2$ and a sinusoidal one

of peak-to-peak value of $-V_\pi/2$, exactly as the amplitude modulation we discussed in Section 2.2.3.2. This results in a pulse repetition rate equal to the frequency of the sinusoid.

2.2.5 Optical Multiplexers

Multiplexing channels in the time domain is theoretically quite simple. Figure 2.16 should be self-explanatory. It shows an example of OTD multiplexing of four channels. A laser output is split into four branches (note that this can be done by using three couplers) and each of them is modulated to form a channel. Delays are applied so that we have as little cross-talk as possible. Note that the original pulse width should be narrow enough for this to be possible.

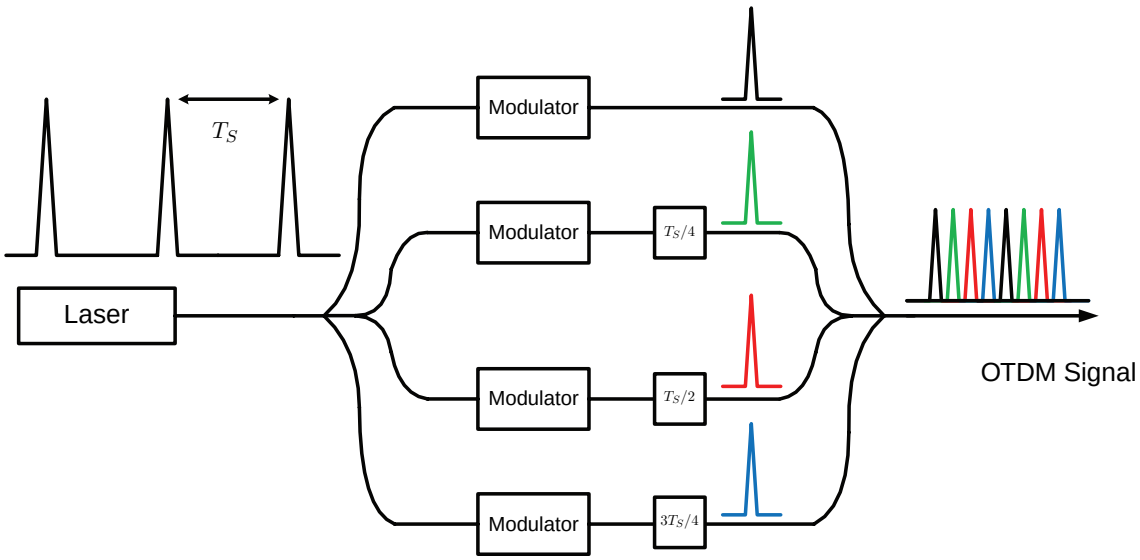

Figure 2.16: 4-channel OTD multiplexer.

Multiplexing two orthogonally polarized signals into a PolMux signal requires a device called *polarization beam combiner*, which works as a coupler but allows just orthogonally polarized waves at the two inputs. As already stated, PolMux is not treated in this thesis and more details can be found in [12].

2.3 Optical Channel

The optical channel we are interested in is the optical fiber. This is the means through which optical signals are transmitted over long distances. Optical fibers are an impressively performing medium when it comes to loss and bandwidth. Compared to copper cable, the former is tiny and the latter enormous.

Light propagates along a fiber thanks to a phenomenon called *total internal reflection*. A fiber is basically made up of two parts, an inner cylinder, called *core* (refractive index n_1), and an outer adherent layer, called *cladding* (refractive index $n_2 < n_1$), as shown in Figure 2.17(a). Other layers provide protection and insulation, but we will neglect to discuss them since they do not interest our research within this work. Any interface between two different refractive indices is a mirror. It can be shown that whenever a ray of light hits the interface from n_1 to n_2, it experiences complete reflection (i.e. no energy is lost) if the incidence angle is larger than a critical angle $\phi_c = \arcsin n_2/n_1$ (see Figure 2.17(b)). This is the way light is propagated over optical fiber.

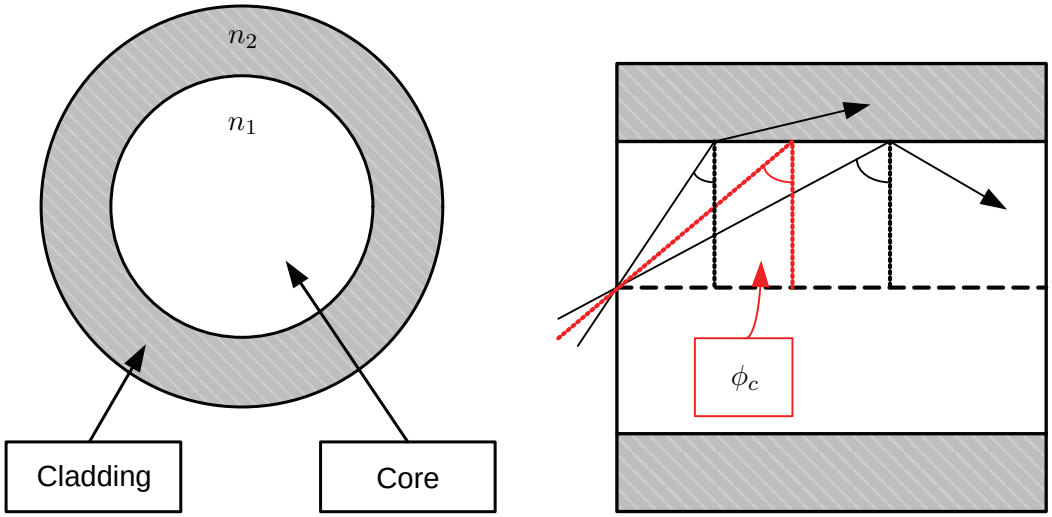

Figure 2.17: (a) Frontal view of an optical fiber. (b) Lateral view of an optical fiber with the visualization of the concept of total internal reflection.

Another aspect of light propagation in optical fiber has to be briefly discussed before we move on. When solving Maxwell's equations, one finds that a finite number

of solutions exist, once we have set n_1, n_2, core radius, and light carrier frequency. Larger differences between the refractive indices, larger core radii, and lower frequencies increase the number of allowed modes in the fiber (see [17]). Today's single mode fibers allow for just one mode at the wavelengths of interest, which are around 1310 nm (zero dispersion wavelength) and 1550 nm (lowest losses). The advantages of a *single-mode fiber* (SMF) over a *multi-mode fiber* (MMF) will be explained in the following sections, which will cover the main aspects related to fiber transmission, namely losses, dispersion, and nonlinearities.

2.3.1 Non-Linear Shrödinger Equation

The complex envelope $A(z,t)$ (we consider the space dependence in this case) that we have introduced in Section 2.1.1 is often referred as *slowly varying envelope* (unless the modulation is almost as fast as the carrier frequency, far from being realized in our case). Its evolution during propagation in optical fiber is described by the so-called *generalized nonlinear Schrödinger equation* (NLSE),

$$\frac{\delta A(z,t')}{\delta z} = -\frac{\alpha}{2}A\left(z,t'\right)+j\frac{\beta_2}{2}\frac{\delta^2 A(z,t')}{\delta t'^2}+\frac{\beta_3}{6}\frac{\delta^3 A(z,t')}{\delta t'^3}-j\gamma\left|A\left(z,t'\right)\right|^2 A\left(z,t'\right), \quad (2.59)$$

where we have used a new time coordinate that relates to the usual time t according to $t' = t - \beta_1 z$. This will correspond to using a time axis that moves as fast as the carrier frequency of the light. In this way, fixed a certain t', we will monitor the change of a specific point of the envelope (for example the peak of a pulse) at different positions in the fiber. Remember that $|A(z,t)|^2 = P(z,t)$. Notice also that we have neglected the polarization. We will assume no interaction between the two polarizations (in the case of a PolMux, for example). This is not a very realistic assumption, but it is needed to make an analytical discussion of nonlinearities possible (or at least to avoid indecently complicated maths).

On the right side of the equation, the first term relates to the losses, the second and third ones to chromatic dispersion (up to the third-order dispersion), and the last one to the nonlinear Kerr effect. These aspects will be discussed in the following three sections.

The derivation of (2.59) is long and cumbersome, moreover it depends on several assumptions and hypotheses. One can find a well detailed explanation in [24][1].

[1]The reader might notice some differences between 2.59 and the cited source. This is due to our

2.3.2 Losses

Light propagating in an optical fiber will irremediably incur in losses. There are at least three factors of loss in a fiber:

- Material absorption,
- Rayleigh scattering,
- Waveguide Imperfections.

Light traveling through a medium is absorbed. In an optical fiber, both silica and impurities contribute to this. Material absorption depends strongly on the frequency of the light (a very complete an fascinating analysis of material losses is carried out in [19]).

Moreover, photons are scattered when they encounter discontinuities in the refractive index, and some of them are deviated so strongly that they exit the fiber or start propagating backwards. These phenomena are explained by the quantum nature of matter. Silica molecules move randomly on a microscopical level during the fabrication of the fiber, when silica is still fluid. When the material solidifies, the density is not homogeneous, and this turns into small variations of the refractive index. This phenomenon is called Rayleigh scattering and it also depends on the frequency.

With waveguide imperfections we mean excessive bends, slight fractures of the core-cladding interface, and other defects causing losses. These are generally independent of the frequency.

It is in general a good approximation to assume that changes in the optical power in a fiber follow Beer's law [17], which states

$$\frac{dP}{dz} = -\alpha P, \tag{2.60}$$

where α is called *attenuation coefficient*, is measured in m^{-1}, and accounts for all the sources of losses. If L is the fiber length, the relation between the power at the input and at the output of the fiber becomes

$$\frac{P_{out}}{P_{in}} = e^{-\alpha L}. \tag{2.61}$$

different phase convention, as stated in Section 2.1.1.

It is customary to express α in dB/km, and standard values for single mode fibers are between 0.2 and 0.25 dB/km at wavelengths of 1550 nm (see [4]). The reason why in optical communications one most often works at 1550 nm is indeed that here losses are the lowest for standard SMFs.

2.3.3 Dispersion

Pulses broaden when traveling over an optical fiber. This phenomenon is in general called *dispersion*, and has two contributions, *intermodal dispersion* and *intramodal dispersion*. The former takes place only in multi-mode fibers, where each mode travels at a different velocity, therefore undermining the compactness of the pulse and resulting in broadening. Single-mode fibers have the great advantage of not presenting this impairment. However, intramodal dispersion still takes place. Pulses have spectra obviously comprising different frequencies. Each frequency travels at a slightly different speed through the fiber, so that the pulse will broaden. Intramodal dispersion is most often referred to as *group velocity dispersion* (GVD) or *chromatic dispersion* (CD). Let us dig a little bit into this.

A specific frequency component will travel a length L of fiber in a time L/v_g, in which v_g is called *group velocity* and is defined as

$$v_g = \left(\frac{d\beta(\omega)}{d\omega} \right)^{-1}. \tag{2.62}$$

Here β is the propagation constant, i.e. the component of the wave vector along the direction of propagation, in this case k_z. βL is the phase shift undergone by light over a distance L. $\beta = \overline{n}(\omega)\,\omega/c$, where $\overline{n}(\omega)$ is the so-called *mode index*, a refractive index depending on the refractive indexes of core and cladding and on the mode confinement (see [4]). β depends therefore on the frequency, and so does the group velocity.

The *group delay* per length unit is the delay undergone by a specific frequency per length unit. It is defined as

$$\tau_g'(\omega) = \frac{d\beta(\omega)}{d\omega}. \tag{2.63}$$

This is measured in s/m, and can be related to the τ_g of Section 2.2.1.5 by multiplying it by the fiber length.

Mathematically, one can describe GVD by Taylor expanding the propagation constant at a frequency ω_0, most likely the carrier frequency,

$$\beta(\omega) = \beta_0 + \beta_1(\omega - \omega_0) + \frac{1}{2}\beta_2(\omega - \omega_0)^2 + \frac{1}{6}\beta_3(\omega - \omega_0)^3 + ..., \tag{2.64}$$

where $\beta_0 = \beta(\omega_0)$ and $\beta_i = \left(d^i\beta(\omega)/d\omega^i\right)|_{\omega=\omega_0}$. Clearly, v_g is constant and we do not have dispersion if the frequency derivative of β is constant, which is true only if $\beta_i = 0$ for $i \geq 2$.

Generally, fiber dispersion is defined through two parameters, denoted as dispersion and dispersion slope respectively,

$$D = \left.\frac{d\tau_g'(\lambda)}{d\lambda}\right|_{\lambda=\lambda_0} = -\frac{2\pi c}{\lambda_0^2}\beta_2. \tag{2.65}$$

$$S = \frac{dD}{d\lambda} = \left.\frac{d^2\tau_g'(\lambda)}{d\lambda^2}\right|_{\lambda=\lambda_0} = \left(\frac{2\pi c}{\lambda_0^2}\right)^2\beta_3 + \frac{4\pi c}{\lambda_0^3}\beta_2. \tag{2.66}$$

In standard single-mode fibers D is typically zero at a wavelength of 1310 nm and grows for longer wavelengths to 17 ps/(nm·km) at 1550 nm. This means that two frequency components separated by 1 nm around a wavelength of 1550 nm will experience a delay of 17 ps/km. S in standard single-mode fibers is about 0.058 ps/(nm^2·km) [4].

A frequency ω will experience a delay per unit length with respect to the frequency ω_0 of $\beta_2(\omega - \omega_0) + \frac{1}{2}\beta_3(\omega - \omega_0)^2 + ...$ The broader the spectrum of our signal, the more important the contribution from higher-order dispersion terms. In this work we study high-speed optical transmission, therefore our signal will be modulated fast and have a wide spectrum. At baud rates as high as 40 GBd/s, the contribution of β_3 can be noticeable in standard single-mode fibers.

Note that $\beta_2 < 0$ for standard single-mode fibers. This means that high frequencies travel faster than low frequencies. Consequently, an initially positively chirped pulse (i.e. a pulse with a red shift in the leading edge and a blue shift in the trailing one) will experience compression before broadening again.

A *dispersion length* is commonly used to assess over which length of fiber a pulse undergoes a noticeable broadening. It is the length that it takes to a Gaussian pulse to get broadened of a factor of $\sqrt{2}$, and is calculated as

$$L_D = \frac{T_0^2}{|\beta_2|}, \tag{2.67}$$

where T_0 is the full width of the pulse at 1/e of the peak value.

Dispersion causes penalty. Broadened pulses interfere with each other, moreover the extinction ratio (i.e. the ratio between peak value and minimum value) decreases, making it more difficult to detect the bits correctly (the same noise power generates more errors). Thus, narrow spectra are preferable for transmission, since they suffer less from chromatic dispersion.

Dispersion Compensating Fibers (DCFs) can be developed to provide negative D and compensate for the dispersion accumulated over a fiber link. This is possible being dispersion a linear operator (i.e. it does not depend on the signal power). Second-order dispersion can be fully compensated by making sure that $D_{SMF}L_{SMF} = -D_{DCF}L_{DCF}$. Of course the effects of higher-order dispersion would still be uncompensated. Dispersion compensation is a vast topic, but these basic ideas will be enough for this thesis. Standard values for SMFs and MMFs as found in [4] and [5] are reported in Table 2.1.

Table 2.1: Standard values for single-mode and multi-mode fibers [4], [5].

Parameter	SMF	DCF
α [dB/km]	0.2	0.5
D [ps/(nm·km)]	17	-95
S [ps/(nm^2·km)]	0.058	-0.323
A_{eff} [μm^2]	80	19

Note that it is also possible to make fibers with $D = 0$ at 1550 nm. These fibers are not a good choice for transmission. Dispersion is indeed a useful phenomenon to contain the effect of nonlinearities, as we will discuss in the next section. It is usually preferable to transmit on SMF and then compensate for the accumulated dispersion over a much shorter DCF.

2.3.4 Nonlinear Kerr Effect

The refractive index depends on light intensity. Proving this requires several nontrivial steps, which can be found in [24]. Here we will just report the main results. We can express the dependence of the refractive index on the signal power as

$$n = n_0 + n_2 \frac{|A(z,t)|^2}{A_{eff}}, \tag{2.68}$$

where n_0 is the *linear refractive index* and n_2 is called *nonlinear index coefficient*, expressed in m^2/W. The reader should remember that A_{eff} is the fiber effective area, generally 80 μm^2 in single-mode fibers, and that $|A(z,t)|^2$ is the optical signal power.

The propagation constant becomes dependent on the intensity as well, and a *nonlinear propagation coefficient* is defined as

$$\gamma = \frac{n_2 \omega_0}{c A_{eff}}. \tag{2.69}$$

In single-mode fibers γ is typically 1.3 $W^{-1}km^{-1}$ [24]. A *nonlinear length* can be defined as

$$L_{nl} = \frac{1}{\gamma P_p}, \tag{2.70}$$

in which P_p is the peak power. L_{nl} is the length over which a Gaussian pulse undergoes a phase shift of 1 rad (-1 rad with our phase convention) in correspondence of its peak when there are neither dispersion nor losses.

Let us show the implications of the Kerr effect on a signal propagating along a fiber. Assuming that we have neither losses nor dispersion, a simple solution of 2.59 is

$$A(z,t') = A(0,t')\, e^{-j\gamma |A(0,t')|^2 z}. \tag{2.71}$$

Clearly, the intensity dependence of the refractive index induces a phase modulation of the signal. This effect is called *self-phase modulation* (SPM). No broadening in the time domain is noticed, just the spectrum gets widened due to the frequency shift caused by phase modulation. If dispersion is present, the spectral broadening is converted in pulse broadening.

An interesting phenomenon is *soliton* transmission. Solitons are particular hyperbolic secant pulses whose parameters verify

$$N^2 = \frac{\gamma P_p T_0^2}{|\beta_2|} = \frac{L_D}{L_{nl}}, \tag{2.72}$$

where N is a positive integer defining the soliton order. In this case, a balance between SPM and dispersion is achieved. Dispersion broadens the pulse. SPM induces a positive chirp in the pulse, and, for $\beta_2 < 0$, this is such that the pulses tend to be squeezed by dispersion while propagating throughout the fiber. If (2.72) is verified, the contribution of SPM is exactly counterbalanced by the one of dispersion so that the pulses remain

untouched. If we consider also higher-order dispersion, losses, noise and maybe other channels, (2.72) is not exact any longer. A thorough study of solitons is found in [4].

When considering WDM systems, in which we have signals at different frequencies, also *cross-phase modulation* (XPM) occurs. As long as two channels are overlapped in time, they mutually modulate their phases. The impact of this phase shift can be shown to be twice as strong as the one of SPM [4]. Dispersion is useful to mitigate the impact of XPM. Different channels travel at different speeds, so that a each symbol experiences XPM from many other symbols and only for the time intervals during which there is overlap. In this way, all the symbols experience a similar impact from XPM. If dispersion is negligible, symbols overlapped to high power symbols will experience a lot more XPM than the symbols paired to low power ones.

A third effect is *four-wave mixing* (FWM), which consists in the generation of new frequency components and the power transfer between them. This is also limited if dispersion is not negligible. More information about XPM and FWM is not needed for our purposes, since we do not treat WDM systems. For further information refer to [24].

To conclude, we should have understood that high signal powers are detrimental for transmission, since nonlinearities would be substantially higher and they can not be compensated. For this reasons, the power over the fiber is generally kept between 1 and 100 mW, with this value strongly dependent on the fiber nonlinear propagation coefficient and the transmission length.

2.3.5 Amplification and ASE Noise

At this point it should be clear that whenever we transmit an optical signal losses will take place. In general, it will be necessary to amplify the signal before receiving it. The higher the power the less thermal noise will impair the system (this will be explained better in Section 2.4.3). For this reason, almost all optical links are terminated with an optical amplifier. In long-haul systems, other optical amplifiers will be installed at different distances in the fiber to sustain the signal.

We do not need to discuss optical amplifiers in fine detail, which would take several pages. Simply, one should understand that amplification in optical fibers is achieved by pumping the fiber medium so that electrons jump onto excited states and can liberate energy, namely photons, when stimulated by the signal light. This is the same principle

standing behind lasers, as explained in Section 2.2.1, just without any cavity. Clearly, spontaneous emission takes place in the amplifier. Spontaneously emitted photons have random phase, as we know from previous discussion, and therefore constitute a noise contribution for both quadrature and in-phase components of the field carrying information. Also, they are generated in both polarizations.

Clearly, a spontaneously emitted photon will experience gain while propagating in the amplifier, and more optical energy for the noisy field is built up. This phenomenon is referred to as *amplified spontaneous emission* (ASE) While in lasers spontaneous emission contributes almost exclusively as phase noise, since the cavity feedback makes stimulated emission dominant, in optical amplifiers there is no cavity and, if the signal power is too low, the effect of ASE noise manifests itself also as signal power fluctuations. Now the convenience of the concept of OSNR should be even more striking.

In optics, there are several types of amplifiers, namely *Raman amplifiers*, *semiconductor optical amplifiers* (SOA), and *erbium-doped fiber amplifiers* (EDFA). EDFAs are the most used as in-line amplifiers for optical communication systems, especially at high symbol rates. No need for further detail in this context, one should refer to [4].

2.4 Optical Receivers

In this section we look at the receiver for an optical communication system. Here we concentrate on the part of the receiver that welcomes the optical signal, and somehow transforms it into a bit stream in the electrical domain. It is therefore a conversion from optical to digital-electrical. We will not discuss the logical operations that follow, namely decoding and error counting, since we have already explained their general meaning and the actual implementation will be shown in the next chapter. We will hereby concentrate on OTD-demultiplexer, front end and decision circuit. Let us first provide a general scheme with Figure 2.18.

First, an optical filter eliminates the out-of-band noise, i.e. the ASE noise at frequencies which are not comprised in the spectrum of the signal. This reduces the noise power and therefore improves the receiver sensitivity. A photodetector follows. This is in our case a photodiode, which is a device converting optical power into current (see Section 2.4.1). Note that the photodiode is to be substituted by more complex structures if we want to detect modulation formats other than OOK (see Section 3.2.6).

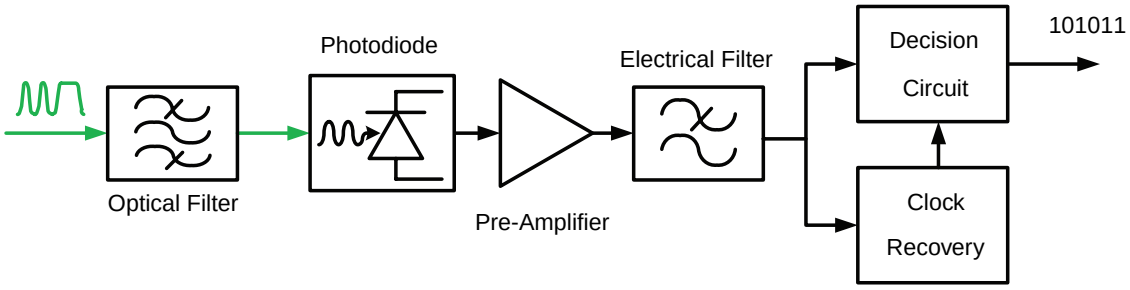

Figure 2.18: Simplified block diagram of a generic direct detection receiver front end and decision circuit, just after the demultiplexing.

Shot noise comes into play here (see Section 2.4.2). Before processing the electrical signal, this is generally amplified by a pre-amplifier that introduces thermal noise (see Section 2.4.3). Photodetector and pre-amplifier constitute the front end. An electrical filter suppresses as much thermal and shot noise as possible, before the signal is split and the clock is recovered on one arm. The other arm exploits the recovered clock to sample the signal and produce a bit stream (see Section 2.4.4. Clock recovery will not be addressed here.

We will conclude this section with the description of balanced detection (a technique that allows for an improvement of the receiver sensitivity at the expense of hardware complexity) and a comparison between direct and coherent detections.

2.4.1 Photodetectors

A photodetector is a device that measures the power of the incident light. The devices we will consider are semiconductor diodes called *photodiodes*. Practically, these work thanks to optical absorption, as explained in Section 2.2.1.2. If the photons have the proper energy, they will be absorbed by the medium and their energy will excite electrons to high energy states. If the medium is properly doped and polarized, current will flow in the form of excited electrons moving due to the polarizing voltage. Understanding why unexcited electrons do not flow as a consequence of the electric field and the exact reasons why this works require at least some basics of solid state physics. We do not think that providing here a better explanation would significantly improve the quality of this work. A simple analysis can be found in [4], for a more thorough discussion one could also refer to [19].

In a photodiode, the current is related to the optical power through

$$I = R \cdot P, \tag{2.73}$$

where R is called *responsivity* and measured in A/W. The efficiency of the conversion from photons to electrons is called *quantum efficiency* and is given by

$$\eta = \frac{\text{electron generation rate}}{\text{photon incidence rate}} = \frac{h\nu R}{q}, \tag{2.74}$$

with q charge of the electron.

Note that the absorption takes place only at the frequencies at which the material can absorb light. For a photodiode, which is a semiconductor device, we have energy bands instead of energy levels. This means that the device works over a certain range of frequencies. On top of this, we also observe a bandwidth limitation, i.e. a limited speed in the way the current can adjust to variations of the optical power. This is due to the fact that newly excited electrons take some time to reach the electrical contacts. Moreover the circuitry surrounding the photodiode is also bandwidth limited. The devices we will be using and modeling are the so-called *pin*-photodiodes[1]. These have the advantage of being small, and faster than the more primitive *pn*-photodiodes [4].

When no signal light is present at a photodiode input, one can still measure some output current. This is called *dark current* and is due to background radiation and some other reasons related to the pn-junction which we do not need to investigate here. It is generally negligible compared to the signal current levels, but still it is to be accounted as a source of noise in the receiver.

Specifically, we report in Table 2.2 some typical values for InGaAs (indium gallium arsenide) pin-photodiodes, as found in [4]. InGaAs photodiodes are among the fastest commercial devices and operate over the range of wavelengths of interest.

Note that the bandwidths reported in Table 2.2 are clearly not very suitable for baud rates in the order of tens of GHz, as it will be the case for our simulations. However, the source is not extremely recent and today's InGaAs photodiodes can work up to 70 GHz or more, as many datasheets available online prove. The rest of the data is still pretty up-to-date.

[1] The reason for the name is that pin-photodiodes feature a p-i-n junction. Explaining what this is would be too cumbersome and we leave this task to the aforementioned sources.

Table 2.2: Typical values for an InGaAs photodiode.

Parameter	Typical value
Operating wavelengths [μm]	1-1.7
Responsivity [A/W]	0.6-0.9
Quantum efficiency [%]	60-70
Dark current [nA]	1-20
Bandwidth [GHz]	1-10

2.4.2 Shot Noise

Even for constant optical input power, the photocurrent shows some oscillations. These are due to shot noise. It is a manifestation of the fact the an electrical current is made up of a finite discrete number of electrons. Their contribution to the overall current is random and can be analyzed statistically. Since their number is enormous, the macroscopic behavior is predictable. All in all, shot noise is due to current quantization. The magnitude of shot noise increases for larger currents, as it will be clear when looking at its implementation (see Section 3.4.2).

2.4.3 Thermal Noise

Electrons move randomly in a conductor at a finite temperature. This phenomenon is particularly noticeable in resistors, and this random motion of electrons results in a fluctuating current. Thermal noise is therefore present also in the absence of applied voltage. In our receiver, the main source of thermal noise is the load resistor present in the preamplifier. Thermal noise is completely independent of the photocurrent, and becomes negligible for increasing photocurrents.

2.4.4 Decision Circuit

The decision circuit is in charge of translating the analog photocurrent into a digital signal, i.e. a stream of bits. The decision is performed in a specific instant in time, whose repetition rate is determined by the clock recovery circuit[1], and according to one

[1]In practice the clock recovery gives the frequency at which the decision circuit samples, which corresponds to extracting the symbol slot duration from a partially unknown signal. The sampling point within the symbol slot is generally optimized somehow else, for example simply changing it until an optimum BER is obtained.

or more thresholds. In the case of single threshold, the concept of threshold is easy: if the photocurrent at the sampling time is higher than the threshold, then we have a 1, otherwise a 0 (or viceversa, depending on the convention). For multiple thresholds we detect groups of bits instead of single ones. This will not be the case in this thesis.

Clearly, the signal at this point will be noisy, because of all the noise sources we have discussed so far. Noise will introduce errors in the detection, so that a certain BER can be measured. This should appear quite clearly from Figure 2.19. Sampling point and thresholds can be optimized to minimize the BER.

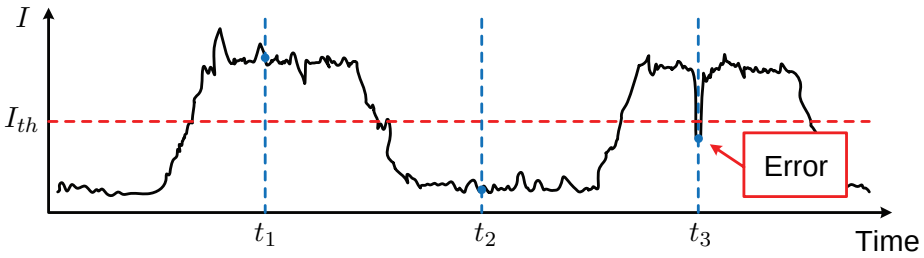

Figure 2.19: Example of decision within a basic decision circuit with single threshold current I_{th}. The photocurrent is sampled at three times, t_1, t_2, and t_3, and an error occurs in the last one.

2.4.5 Receiver Sensitivity and Power Penalty

The performance of the system can be improved by increasing the received power. Larger powers mean larger photocurrents (as long as we do not burn the photodetector), which in turn diminish the relative magnitude of thermal noises. It is customary to define as *receiver sensitivity* the received power necessary to operate at a certain BER. Of course, in a real situation the sensitivity of a receiver will depend also on the amount of noise that is applied to the optical signal both in the generation (phase noise, RIN, etc.) and in the transmission (ASE noise).

In general, if we increase the transmitted power, we will have a larger OSNR. In fact, an optical amplifier adds approximately the same amount of ASE noise regardless of how much optical power flows through it, which means that the ASE noise becomes less and less noticeable for larger powers[1]. Typically, we will draw plots where the y-axis

[1]Here we have assumed that the optical signal is amplified just once and in front of the receiver. If we had other amplifiers along the optical link, then their ASE noise would also be amplified by the following amplifiers. Still, having a larger transmitted power would limit the effect of the ASE noise

is the BER, whereas the x-axis is the OSNR (most conveniently in dB) measured just before the receiver. On these plots one can determine a slightly different sensitivity, which is expressed as the OSNR needed to obtain a given BER (see Figure 2.20). Sampling point and thresholds can be optimized to minimize the BER. In the good old times, optical communication systems where defined as "error-free" for a BER of about 10^{-9}. With the advent of digital signal processing and consequently FEC (see Section 2.1.10), a BER between 10^{-3} and 10^{-4} became sufficient to declare a system error-free.

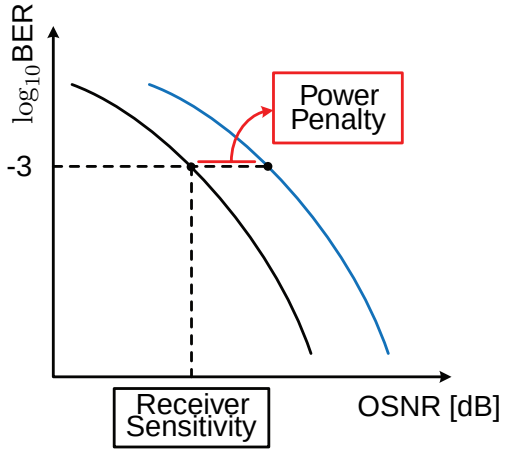

Figure 2.20: Example of BER-OSNR plot with highlighting of a power penalty.

We hereby also introduce the concept of *power penalty* (PP), which will be used several times in this thesis. When a change occurs in a system, for example the fiber is prolonged or the number of channels increased, the BER-OSNR curve will be shifted. At a certain BER, the difference between the corresponding OSNR values is called power penalty. Basically, it measures how much the OSNR should be increased to obtain the same BER performance as before the modification in the system. A negative penalty means that an improvement in the BER performance has taken place.

In this thesis, unless otherwise specified, the OSNR sensitivities (that in turn allow to talk about power penalties) will be determined after a linear fitting of curves log_{10}BER as a function of OSNR (expressed in dB), where the y-axis is logarithmic. At least five well separated points will be determined before performing the fitting. Note that the theoretical trend of such a plot is actually linear under some circumstances [4].

introduced by the last amplifier.

2.4.6 Delay Line Interferometer

A *delay line interferometer* (DLI) is an optical component used to make the optical signal interfere with a delayed version of itself. It will be needed for correctly receiving differentially encoded signals. It is a quite simple structure, as one can see in Figure 2.21. The signal is split in two branches, to one of them is applied a delay of a symbol period, and to the other a phase shift, if needed. Note that the two couplers introduce phase shifts, as explained in Section 2.2.2.

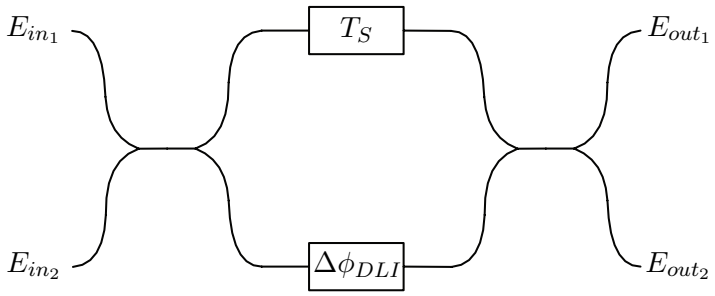

Figure 2.21: Delay line interferometer.

2.4.7 Balanced Detection

As we will see when presenting the actual receiver structures in Section 3.4, very often the signal will pass through a DLI. Consequently, if we just took one of the two outputs, we would lose half of the optical power. This can be avoided in a very simple way, although it requires an extra photodiode for each interferometer at the receiver. We detect both outputs of the DLI and we subtract the two currents (in practice this is done by connecting the wires in the proper way). As a result, a 3-dB improvement in the receiver sensitivity is achieved. A few equations might help understanding this concept better. One can find them in [12]. Some more information is found in [25].

2.4.8 Direct Detection and Coherent Detection

So far we have discussed a direct detection receiver. The photodetectors convert optical power into electrical current. Clearly, all the information related to phase and frequency of the light gets lost. This is not a problem if we have adopted an intensity modulation, where the signal carries information exclusively in its power. Also

some phase modulations can be properly received with direct detection if differential encoding is employed, as we will show in Section 3.2.6.

To be able to retrieve information about the signal phase and frequency we need a local light source at the receiver. This is called *local oscillator* (LO) and we will show its functioning in a short while. It is important that the phase of the LO be constantly equal to the one of the incoming light, therefore receivers employing an LO are called *coherent receivers*. This is a marvelously extended and fascinating topic, and we do not mean to thoroughly discuss it since a more detailed explanation can be found in [12]. We will just give a tiny introduction.

The reasons for the interest in coherent detection are at least two. First, the receiver sensitivity can be significantly improved (up to 20 dB [4]), second it allows us to successfully detect phase and frequency modulations, which in turn are desirable for all the reasons listed in Section 2.1.6.

So, neglecting to consider polarization, if we suppose to combine the signal light with the LO whose field is described as

$$E_{LO} = \sqrt{P_{LO}} e^{j(\omega_{LO} t + \phi_{LO})}, \tag{2.75}$$

we get a signal with power

$$P(t) = P_s(t) + P_{LO} + 2\sqrt{P_s(t) P_{LO}} \cos(\omega_{IF} t + \phi_s(t) - \phi_{LO}), \tag{2.76}$$

where we have supposed that no frequency modulation be applied to the signal. $\omega_{IF} = \omega_0 - \omega_{LO}$ is called *intermediate frequency*. When $\omega_{IF} = 0$ we have the so-called *homodyne detection*, otherwise we are in the case of *heterodyne detection*. We will only apply the former, for more information about the latter one might refer to [4].

Clearly, from (2.73) and (2.76), the photocurrent becomes

$$I(t) = R(P_s(t) + P_{LO}) + 2R\sqrt{P_s(t) P_{LO}} \cos(\omega_{IF} t + \phi_s(t) - \phi_{LO}). \tag{2.77}$$

It contains information on both phase and intensity of the signal, as we had anticipated at the beginning of this section. Note that the received power is largely enhanced by the LO which generally delivers an intensity much higher than the signal one. This reduces the impact of thermal noise improving the receiver sensitivity.

Of course, noise in the LO will impair the detection and cause errors. Especially demanding is the phase relation between LO and signal. Basically the difference of

their phases should be stable and just the phase modulation of the signal should induce variations in the sinusoidal term of (2.77). Phase noise is therefore a problem, since the detected phase might be different from the correct one. A feedback is needed to maintain this phase locking. This is achieved by means of an optical phase-locked loop (OPLL) in analog systems.

2.4.8.1 Coherent Receiver Front-End

In the previous section we have discussed the basic principle of coherent detection. Here we want to show how the front end of a coherent receiver differs from the one of a direct detection receiver (as described in 2.4). We will assume that both signal and LO have the same polarization, so that the beating between the two is fully achieved. A scheme of the front end is found in Figure 2.22.

LO and signal enter an interferometric structure called 90° *optical hybrid*. This is simply a net of couplers and phase shifters, whose structure can be found in [12]. The four outputs result to be the ones written in Figure 2.22. For different implementations the outputs could slightly vary, but the important point is that, after balanced detection, we end up with two photocurrents corresponding to in-phase and quadrature components of the input electric field. One could convince himself of this by referring to [12] or by doing the calculations himself. Electrical filters close the front-end.

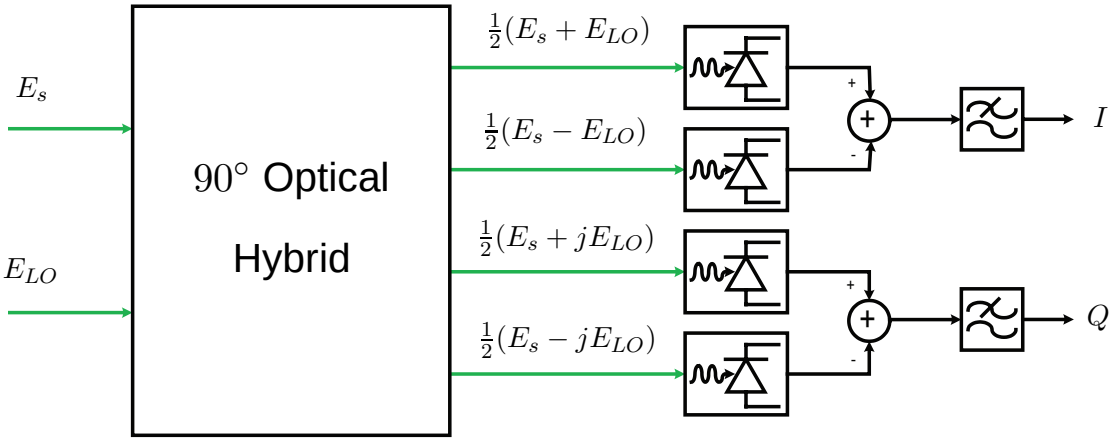

Figure 2.22: Front-end of a coherent receiver.

2.4.9 Coherent Detection with DSP

Coherent receivers are not very practical in many cases, since they require OPLLs, which are extremely complicated to implement. Moreover ω_{IF} should be as close to zero as possible, which might not be trivial to achieve. *Digital signal processing* (DSP) allows to elaborate digital samples of the photocurrent to estimate the phase error between LO and signal, and then correct it. This allows us to perform coherent detection without the uttermost complex OPLL.

On top of this, a DSP allows for processing of the signal so to estimate and correct the frequency offset between LO and signal, and many others. The only difference with respect to the coherent detection described in the previous section is that we will need *analog-to-digital converters* (ADC). These devices simply sample the analog photocurrent at a certain sampling rate, that should be a multiple of the symbol rate, so that each symbol is represented by a fixed number of samples. The samples are then processed by a CPU. This should be done on-line, so in real time with respect to the information flow. Of course this requires fast electronics, which are very expensive. On top of this electronics are slower than optics (in most cases and for sure in future potential), therefore one could parallelize the processing, which is very feasible if OTDM is employed.

We hope that this short introduction to coherent detection with DSP helped clarify the reasons for so much interest in this topic, which is the one we devoted our attention in this thesis together with [12]. As a simplistic summary, we want coherent detection because it allows for high-order modulation formats, and we want DSP because it makes it possible to perform coherent detection without OPLL. A lot more information about this topic is also found in [6].

2.4.10 Optical Demultiplexers

There is a variety of ways to demultiplex our OTDM channels. Within this work we have just studied a method suitable for a coherent receiver. This is part of [12], so here we will just show the block diagram of our OTD demultiplexer (see Figure 2.23).

The signal is split in as many branches as the number of OTDM channels plus one. One branch is reserved to a clock recovery circuit which produces a clock at the symbol rate. A pulse source works as LO producing pulses at the symbol rate. The pulses beat

with the signal, each channel has a differently delayed version of the LO so that, once we have centered the pulses on one channel properly (this is done by means of tunable delay line), also all the others will overlap with the respective channel. In this way on each branch a channel is magnified by the beating with the LO, according to what we explained in Section 2.4.8, and becomes by far dominant with respect to the others. Each channel is then detected in a dedicated front-end. The delays to be applied to the LO pulses at each step in the chain depend on the number of channels. If the scheme is like the one in Figure 2.23, then each version of the LO pulses is delayed of T_S/N_{ch}, where N_{ch} is the number of channels. Note that in the figure we have simplified all the splitters. Normally these would be combinations of couplers as the ones described in Section 2.2.2.

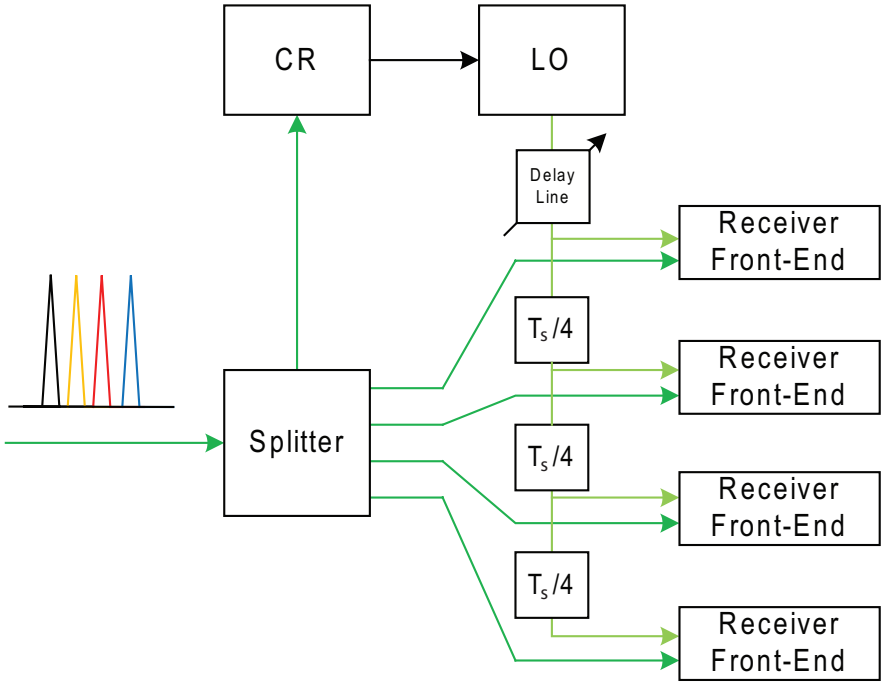

Figure 2.23: Block diagram of our 4-channel OTD demultiplexer for coherent detection.

The demultiplexing of a PolMux signal is done in two steps. First a polarization beam splitter decouples the two orthogonal polarizations of signal and LO into two different branches. We will not hereby delve into the details of this particular device. Then a normal coherent detection is performed separately for x and y polarizations. The actual demultiplexing takes place digitally during the signal processing. The algorithm

devoted to this function is discussed in [12].

3

Numerical Model

This chapter will be devoted to the description of the Matlab® model created and utilized to obtain all the numerical results discussed within this thesis. The model has been written from scratches and in collaboration with my colleague and friend Francesco Patarnello [12].

Describing every single function and detail would be too burdensome and, we believe, quite uninteresting for the reader. Thus, we will concentrate on the most significant and crucial parts, so that the rest of the modules should be easily reproducible starting from the directions we will give. Light blue areas will highlight actual code. We will try to report quite some code, so that the reader be able to grasp what we exactly did. Of course we would not be able to show all the code, but just a tiny amount, which we will try to select among the most significant lines.

This chapter will have five main sections. The first will introduce the reader to the way we setup our simulations, which consists in creating the necessary numerical environment and data sequences. The second section is devoted to the transmitter model, from the laser to the various modulators. We thereby also show the block diagrams of the transmitters for all the modulation schemes we study within this thesis. The third section is about the modeling of an optical fiber. In the fourth section we discuss the implementation of an optical receiver, we show the block diagrams of all the receivers we have employed, and we describe the technique we use to determine the BER in our system. Finally, the last section delves into the details of the operations we perform in the frequency domain, like filtering and spectrum analysis.

Let us stress once more the fact that this thesis concentrates itself mainly on transmitter and fiber, so that the fine details about the receiver are left to [12].

3.1 Simulation Setup

In a numerical simulation we need to describe real analog signals with sequences of numbers. We must therefore sample in time, moreover we have to limit ourselves to a finite time interval, so to have a finite number of samples. This is the purpose of a time array we create at the beginning of all simulations.

The numerical precision we decide to use is the default one in Matlab®, i.e. `double`, which allows us to reproduce the amplitude of the signal in an almost continuous way, since every value is represented by as many as 64 binary digits, according to IEEE® standard 754. We will therefore forget from now on that our numerical signal is digital, and we will treat and discuss it as only discrete on the time axis. The quantization error introduced by the numerical format used is in fact by far negligible if compared to the other limitations of the model. Just to mention a couple of them, the finiteness of the sampling frequency, and the fact our model does not reproduce all the non-idealities of a real optical communication system.

This section is devoted to the first steps one should follow to generate a proper simulation environment. Time and frequency arrays are to be created, to be able to work in both time and frequency domain. On top of this, one has to generate one or more suitable data sequences to transmit, and electrical driving signals are to be produced from these sequences.

3.1.1 Time and Frequency Arrays

The three parameters that determine the backbone for the simulator are number of symbols (N_S), samples per symbol (SPS) and symbol rate (R_S). Once we have set these three, all the others will come consequently. The length of the time window is of course obtained by multiplying N_S and SPS, while the time resolution is

$$dT = \frac{1}{\mathrm{SPS} \cdot R_S}. \tag{3.1}$$

A time array is generated, which is simply a vector of time values, where the difference between consecutive times is dT and the length is $N_S \cdot \text{SPS}$. In Matlab® syntax the time array is defined as

```
TimeArray = (1:Nsymbols*SamplesPerSymbol)*dT;
```

We also need a frequency array, since the filtering will be performed in the frequency domain, moreover we will want to show the spectra of our signals. The understanding of this might result slightly more difficult, but not much. The resolution in frequency will be determined by the longest measurable time in our simulation, which happens to be $\text{SPS} \cdot N_S \cdot dT$. Thus,

$$dF = \frac{1}{\text{SPS} \cdot N_S \cdot dT}. \tag{3.2}$$

The maximum measurable frequency can be intuitively linked to the time resolution, and the Nyquist criterion suggests that $f_{max} < f_S/2$, where f_S is the sampling frequency. From this, we trivially set

$$f_{max} = \frac{1}{2dT}. \tag{3.3}$$

Hence, the frequency array is a vector with as many elements as the number of samples, centered on frequency zero, and with a granularity of dF. It is generated as

```
FrequencyArray = (-Nsamples/2:Nsamples/2-1)*dF;
```

3.1.2 PRBS Generation

A communication system needs some data to be fed with. A numerical one needs data as well. Generating a sequence of bits is not a difficult task, but a reliable test requires as random a data pattern as possible. The definition of *random* is out of the scope of this work, but what good scientists know is that the same system delivers different performances (that we measure as BERs) for different inputs. This is due to *inter-symbol interference* (ISI), i.e. the interaction between neighboring symbols. Basically, the way a system processes one symbol depends on which symbols have been processed before. This is due to the response time of all the components, whose behavior and adjustment will be slightly influenced by their previous operation. For an ideal system where the response is instantaneous (or, equivalently, the bandwidth infinite) the data sequence will not influence the performance.

The dependence of the system on the already transmitted symbols is called *memory*, and its magnitude can be measured as the number of symbols preceding a given symbol that still influence the probability of wrong detection of the bits within that symbol.

The best way to put our model in all possible trouble is to feed it with a *pseudo-random bit sequence* (PRBS), derived from a seed of n_b bits. Such patterns are characterized by being $2^{n_b} - 1$ bits long (and then repeating themselves periodically) and containing all possible combinations of 1s and 0s shorter than n_b bits, except for a sequence of n_b 0s. A detailed theory of PRBS is presented in [26].

Therefore, we generated the bit sequences we needed starting from a seed of variable length, and applying a technique known as *shift register*. According to this method, the seed may be any but the all-zeros one, and the pattern is obtained by xoring the output of the line of registers with the output of the last but one register, and then using the result as an input for the first register. This is immediately understood by looking at Figure 3.1.

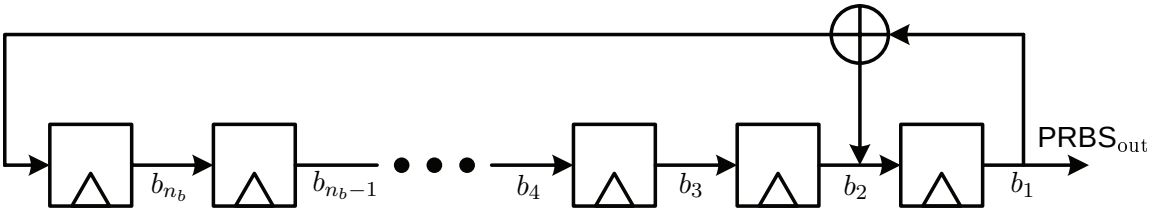

Figure 3.1: PRBS generation scheme.

The PRBS so obtained lacks the n_b consecutive zeros, so we solved the problem by searching for the longest sequence of zeros and adding an artificial one. The result is a beautiful PRBS as long as 2^{n_b} bits that presents all possible subsequences to give as hard a time as possible to our system. This sort of bit sequences are called *De Bruijn bit sequences* [6].

When choosing the length of the seed, we should estimate the memory of our system. In our case, inter-symbol interference is caused by optical and electrical filtering, as well as by linear and nonlinear fiber degradation effects. Estimating the system memory is difficult to do, and we will always stick to a default value of $n_b = 7$, which is fairly commonly accepted for numerical simulations. It is indeed very computationally demanding to use longer sequences, as it will become clear after reading Section 3.4.6.

Note, the fact that the sequence length is a power of 2 is pretty convenient from the programming point of view. The main reason of this is that the fast Fourier transform (FFT) algorithm we use to Fourier transform in our model has the lowest computational complexity when fed with vectors whose lengths are powers of 2. Note that the FFTs are one of the key bottlenecks for the speed of the simulation, and they are widely employed in the fiber model as well as for the filtering. To make sure that we work with a power of 2 number of samples, it is required that also SPS be a power of 2.

For the sake of honesty it is to be pointed out that in our model most often these PRBSs are processed by encoders, as we will show later on, with the result of losing the pseudo-randomness. Overcoming this issue would take some time, since we should generate ad-hoc patterns for each encoder, so that the optical signal maintain its character of PRBS. This was not done for reasons of time, but we believe that the impact on the results is negligible. In any case, a detailed analysis of the problem would be too committing if compared to the advantages provided by a possible solution.

An even more important issue is that, when performing multi-level modulation, we have symbols which contain several bits. Hence, the problem is shifted to the generation of M-ary pseudo random sequences. We have not had the time to address this problem, which could be subject to further research. Some information is found in [6].

3.1.3 Electrical Signal Generation

After generating a proper bit sequence, we have to make it suitable for the time array we previously created. This is achieved by a function that produces a vector compatible with the time array. For each bit we have SPS values, following an ideal square wave. This is basically an interpolation, so this step might be seen as a sort of digital-to-analog converter (DAC). Please, note that our convention is to have high voltage for 1-bits and zero voltage for 0-bits. Moreover, one should observe that the output is not analog, since our time axis is discrete, but what we are trying to simulate is indeed an analog signal. The higher SPS, the closer we get to a continuous time axis.

To resemble a more realistic electrical signal (which we will exploit as driver for our modulators) we proceed to a filtering of the ideal square wave with a Gaussian filter giving certain rise and fall times (this step is described in section 3.5.2.1). We define the rise time in the classically accepted way, i.e. the time it takes to the signal to grow

from 10% of the peak value to 90% of the peak value. The schematic of the signal generation process can be visualized in figure 3.2.

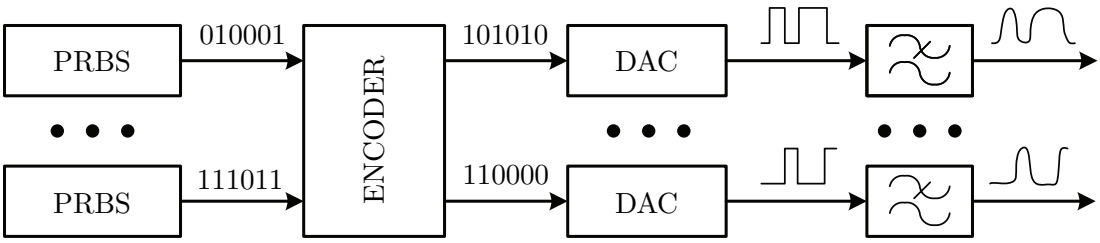

Figure 3.2: Driving voltages generation process.

3.2 Transmitter Model

Here we describe our model of optical transmitter. The definition of the optical signals is a crucial step in our model. Such signal is much more complex than a simple voltage, since we have two polarization axes. The first part of this section will deal with this issue. We then move to analyzing our models of lasers in the second part. The third part is devoted to the description of the external modulators models, before looking at our model of OTD multiplexer. This section is concluded with a list of all the transmitters we use for the various modulation formats we study, and for all of them a block diagram is provided.

3.2.1 Optical Signal Representation

When setting up and running numerical simulations, we have to consider the requirements in terms of time and frequency windows. Intuitively, if the signal varies at a faster pace, i.e. the signal spectrum has higher frequency components, numerically we will need a higher sample rate to be able to track these variations. Practically, this means that the array representing our optical signal will be longer, making the simulation much more burdensome, which is to be avoided at all costs. This is an especially severe problem for optical signals whose frequency will be in the order of hundreds of THz, much higher than the modulation frequency, typically 40 GHz in this work.

The simplest solution to the problem is to represent a base-band version of the signal, obtained by subtracting a reference frequency f_{ref} from the actual frequency of

the oscillating electric field. Our signal will look like

$$E(t) = \sqrt{P(t)} e^{-j\phi(t)} e^{j\left(\omega_0 - 2\pi f_{ref}\right)t}. \tag{3.4}$$

Each sample will therefore be a complex number.

To describe the polarization state we exploit the data type called *structure* in Matlab®, so that each signal is a pair of arrays, one for x-polarization and one for y-polarization, and each element of both arrays a complex number. The power of the signal will be the sum of the power in both polarizations, namely

```
power = abs(signal.x).^2+abs(signal.y).^2;
```

Figure 3.3(a) should help visualize and understand how the data relative to the optical signal is stored and structured. From now on, when showing the code of our model, we will show just the code for one polarization, implicitly implying that the one for the other polarization is the same.

3.2.2 Laser Models

The approach we follow for the presentation of our laser model consists in starting from the simplest entity, which is a laser emitting constant power, following up with the description of the two impairments we modeled, i.e. intensity noise and phase noise, and concluding with the extension to a pulsed source and its timing jitter.

3.2.2.1 CW Laser model

In our model, the most primitive light source is a CW laser. The objective of the function modeling the laser is to fill the data structure describing the emitted optical signal in as realistically a way as possible. Consistently with what has been written so far, this structure is made up of two vectors, one for each polarization. Recalling (2.42) and (3.4), we generate a complex field

$$E(t) = \sqrt{P_0 + \delta P(t)} e^{-j(\delta\phi(t) + \phi_0)} e^{j\left(\omega_0 - 2\pi f_{ref}\right)t}, \tag{3.5}$$

where $\delta P(t)$ stands for the intensity noise, $\delta\phi(t)$ is the phase noise, and ϕ_0 is the initial phase of the laser. ϕ_0 is randomly set with a value between 0 and 2π. This is done by means of the command `rand`, which returns a number drawn from a uniform distribution in the interval $[0, 1]$, and then multiplying by 2π, namely

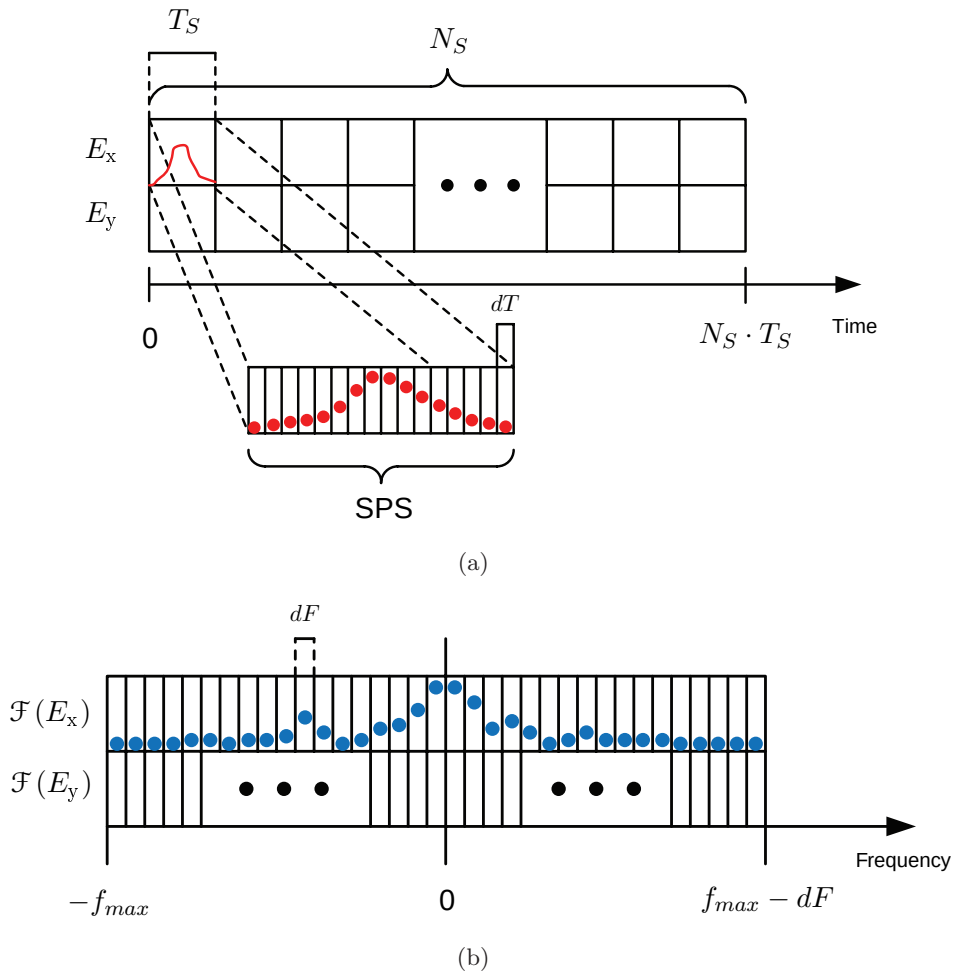

Figure 3.3: Signal representation (a) in the time domain and (b) in the frequency domain. Note that each point represents a complex number.

```
phi(1) = rand*2*pi;
```

where `phi(1)` is the first element of a vector of signal phases. The code for (3.5) looks like

```
CW = sqrt(P+intensity_noise).*exp(1i*(2*pi*(f0-
    ReferenceFrequency)*TimeArray)+1i*phase_noise);
```

in which `intensity_noise` and `phase_noise` are vectors describing the aforementioned noise sources, one value for each time sample of the signal. How these are generated will be shown in the next two sections.

Our laser model allows for a linearly polarized output wave. If the laser is set to x-polarization, then the previously generated vector is assigned to the corresponding part of the output optical signal structure, while the part corresponding to y-polarization is filled up with zeros. If the laser is set to y-polarization, vice versa.

3.2.2.2 Intensity Noise Implementation

Physics and definition of intensity noise were given in Section 2.2.1.3. Here we discuss how such a noise source can be modeled. It is largely accepted to assume a Gaussian distribution for the intensity noise in a laser.

We decided to generate a zero-mean AWGN to be superimposed on the clean signal. In Matlab® a Gaussian random process with constant spectral density can be reproduced by means of the commands `random` or `randn`. The required inputs are mean (which we set to zero), standard deviation (which we calculate below), and noise vector length (there should be one noise instance per sample, so the vector should be as long as the time array). We obtain a vector of AWGN with a spectral density extended over the whole frequency array we have created to set up our simulation.

However, the spectral density of the intensity noise is not constant in practice, as shown in [27]. It is flat up to a certain resonance frequency, that can vary from laser to laser but is in the order of hundreds of kHz, so well within our frequency array, that will always be larger than at least a few tens of GHz. Therefore we cannot assume the RIN to be white. Since it is so easy to create AWGN numerically, while it is much more complicated to produce noises with tailored spectral densities (if at all possible), we will have to generate white noise anyway.

We need to determine the standard deviation of the RIN, starting from some input. From (2.45), and for a CW laser, one can write the RIN variance as

$$\sigma_{RIN}^2 = P_0^2 \int_0^{\Delta f} \mathrm{RIN}\,(f)\,df = P_0^2 \cdot \mathrm{RIN}_{\mathrm{tot}}. \tag{3.6}$$

We face a choice here:

1. Either our input is the RIN in dB/Hz and we suppose that it is a white noise over our whole frequency array, so that the integral in (3.6) becomes simply $\Delta f \cdot$RIN, where Δf is the width of the frequency array,

2. Or we have $\mathrm{RIN}_{\mathrm{tot}}$ in dB as input, and we do not need to calculate the integral.

In the first case, we definitely overpower the intensity noise, since our frequency array will almost always be much larger than the RIN bandwidth, as explained above. In the second one we have the same overall RIN, but its power at a given frequency will be different. We chose to implement intensity noise in the second way. Consequently, the relative code will be

```
sigma_intensity_noise = sqrt(Total_RIN)*P;
intensity_noise = random('norm',0,sigma_intensity_noise,[1,
    length(TimeArray)]);
```

We are conscious that neither of the two presented solutions is fully satisfactory. At the present time, it has not been possible to devise a better one without devoting a large amount of time. Since time is limited, we have preferred devoting it to more crucial and novel topics within this thesis. Moreover, intensity noise is generally fairly negligible at today's levels of -150 dB/Hz with a bandwidth of about 100 kHz, compared to other impairments, for example phase noise, ASE noise, and dispersion.

3.2.2.3 Phase Noise Implementation

Our model of a CW laser allows also for the simulation of the effects of a finite linewidth, responsible for phase noise, as described in Section 2.2.1.2.

It is important to have it clear in mind that there is a relation between the instantaneous value of the frequency shift and the time derivative of the phase in any sinusoidal signal, as shown by (2.34). Hence, we can reproduce a spectral broadening by somehow modulating the phase. These phase jumps are naturally called phase noise. Every time

spontaneous emission takes place inside the laser cavity, the phase undergoes a jump, that in turns means a frequency shift. The phase noise is of primary interest in this work, since it is one of the most impairing factors in optical systems in the case we employ phase modulation and a coherent receiver.

[28] suggests that the frequency noise can be modeled as a white Gaussian stochastic process, i.e. it follows a normal distribution and the spectral density N_0 is constant. From equation (2.34), a phase noise process starting at $t = 0$ is linked to the frequency noise one by

$$\phi_n(t) = 2\pi \int_0^t \Delta f\left(t'\right) dt'. \tag{3.7}$$

This may suggest that the phase difference between two time instants must have Gaussian statistics in order for the frequency noise to be Gaussian itself. This is much easier to see in a discrete time frame, which happens to be the situation in any numerical simulation. The integral becomes a sum,

$$\phi_n(m \cdot dT) = 2\pi \sum_0^{m \cdot dT} \Delta f(m \cdot dT), \tag{3.8}$$

so that the phase difference between two neighboring times can be written as

$$\phi_n((m+1)\,dT) - \phi_n(m \cdot dT) = 2\pi \Delta f((m+1)\,dT). \tag{3.9}$$

Equation (3.9) clearly shows that we just need to make sure that the phase difference between two consecutive samples follows a Gaussian distribution.

This results in a random walk of the phase over time (see figure 3.4(a)), that is known as Wiener process. We now need to somehow relate the linewidth of a laser spectrum to the variance of the Gaussian phase noise process. Note that in this work we define the linewidth of a CW laser as the FWHM of the single-sided spectral density of the output field. We will label it with $\Delta\nu$ and it will be measured in Hz, being a frequency difference. The following derivation can be found in wider detail in [29], we will report here just the main steps in order to justify our final conclusions.

We will start by writing once more the equation for the complex electric field, assuming phase noise ϕ_n but no intensity noise,

$$E(t) = \sqrt{P_0} e^{j(\omega_0 t + \phi_n(t))}, \tag{3.10}$$

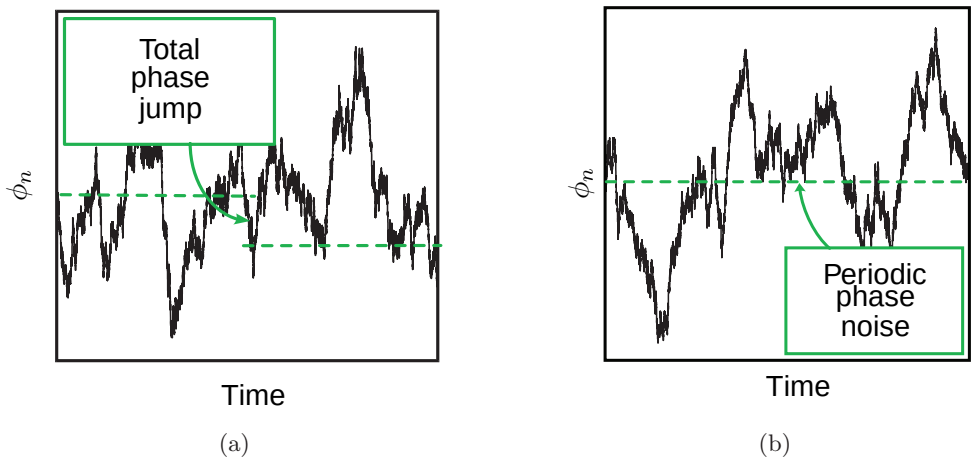

Figure 3.4: (a) Phase noise for a laser (notice the absence of periodicity). (b) Periodic phase noise after the modification described in the text.

where we have assumed no RIN, called the phase noise $\phi_n(t)$, and forgotten the base-band representation for ease of calculation. Note that ϕ_0 can be neglected. In fact, ϕ_0 is randomly and uniformly distributed in the interval $[0, 2\pi]$, making the phase noise stationary. From these observations one can redefine the phase noise as

$$\phi_n'(t) = 2\pi \int_{-\infty}^{t} \Delta f\left(t'\right) dt', \tag{3.11}$$

and the autocorrelation function is conveniently determined as (see [29])

$$R(\tau) = \frac{P_0}{2} e^{j2\pi f_0 \tau} e^{-2\pi^2 N_0 |\tau|}. \tag{3.12}$$

By Fourier transforming the above equation one gets the power spectral density of $E_0(t)$,

$$S(f) = \frac{A^2 N_0/2}{(\pi N_0)^2 + (f - f_0)^2}. \tag{3.13}$$

It happens to be a Lorentzian spectrum whose 3-dB bandwidth (what we define as linewidth) is

$$\Delta\nu = 2\pi N_0. \tag{3.14}$$

Now we just need to link the variance of the process describing the difference between the phase noise in neighboring time instants in our model to the linewidth we just calculated. It is a pure mathematical exercise (see again [29]), which results in

$$\mathrm{Var}\left\{\phi_n(t) - \phi_n(t - dT)\right\} = \sigma_{\phi_n}^2 = (2\pi)^2 N_0 dT. \tag{3.15}$$

After substituting (3.14) in (3.15), we reach the desired result,

$$\sigma_{\phi_n} = \sqrt{2\pi\Delta\nu dT}. \tag{3.16}$$

To conclude, we generate phase noise in the laser by having a Gaussian random process of standard deviation given by (3.16) which defines the phase difference between neighboring times on our time array. The resulting optical signal will have a spectrum showing the wanted linewidth. Namely,

```
sigma_phase_noise = sqrt(2*pi*linewidth*dT);
phase_noise_jump = random('norm',0,sigma_phase_noise,[1,length
    (TimeArray)-1]);
for i = 2:(length(TimeArray))
    phase_noise(i) = phase_noise(i-1)+phase_noise_jump(i-1);
end
```

In [30] issues related to discontinuities in the phase in numerical simulations are studied. Without going into the detail of such a topic, it is showed that a model is more robust when the phase is periodic with a period as long as the time window we consider, i.e. our time array. To ensure this, we simply determine the difference in phase between the first and the last samples after the generation of phase noise, and we divide it by the number of samples. Finally, this is subtracted from each phase sample, assuring that the phase noise noise be periodic (see Figure 3.4(b)). The previous code has to be modified according to

```
total_jump = mod(abs(sum(phase_noise_jump)),2*pi);
delta = total_jump/(length(TimeArray)-1);
for i = 2:(length(TimeArray))
    phase_noise(i) = phase_noise(i-1)+phase_noise_jump(i-1)-
       sign(total_jump)*delta;
end
```

3.2.2.4 Mode-Locked Laser Models

In Section 2.2.1.4 we have shown how a pulse train in the time domain is characterized by a series of modes in the frequency domain, and these modes are equally separated and phase-locked. We have thought of two ways to model such a device. One consists in shaping the pulse train in the time domain (let us call it model A), the other in generating as many coherent oscillators as the desired modes, so that a pulse train results in the time domain (labeled as model B).

Model B would be interesting because it would allow us to break the coherence of some modes as we like. Unfortunately, a practically realistic extent of these deviations is totally unknown to us, also after discussing the problem with renowned experts and consulting several references. Model A is fairly simple to implement, and would allow us to easily introduce timing jitter in the pulse train. Also implementing phase noise would be much easier. For this reasons, model A was preferred and developed.

Let us now discuss the actual implementation. We first repeat the same operations as we did for a CW laser, with the only exception that we will use the average signal power when determining the standard deviation for the intensity noise (see Section 3.2.2.2). Then, once we have a CW signal in the time domain, we simply shape it as a Gaussian train of pulses or a hyperbolic secant one, depending on our preference. To do this we first need to create a vector `pulse` containing the values of, for example, a Gaussian function,

```
for i = 1:length(TimeArray)/SamplesPerSymbol
    for j = 1:SamplesPerSymbol
        pulse((i-1)*SamplesPerSymbol+j) = exp(-((j-
            SamplesPerSymbol/2)*dT+timing_jitter(i))^2/(2*T0^2)
            );
    end
end
```

where `T0` is the full width at 1/e of the pulse, and `timing_jitter` an array of values of the pulse timing jitter. The way this is generated will be explained in the next section.

Once this is done we just have to multiply by the CW wave,

```
ML = CW.*pulse;
```

and then assign to the right polarization within the structure constituting the output of our model.

On top of the parameters characterizing the CW laser function, here we also have pulse shape, duty cycle, and timing jitter. The pulse repetition rate is automatically calculated to suit the value assigned to R_S, while the duty cycle D determines how narrow the pulses are. It is defined as

$$D = \frac{T_{FWHM}}{T_S} = T_{FWHM} * R_S. \tag{3.17}$$

Note that T_{FWHM} is the FWHM of the pulse. D is a very convenient parameter when working with OTDM systems. The smaller D is, the less cross-talk will take place between neighboring channels because of multiplexing.

3.2.2.5 PMCW Pulse Source Model

Let us describe the way we implement the pulse generation technique discussed in Section 2.2.1.5. We suggest the reader to keep an eye on Figure 3.5 while following this brief discussion.

First we generate a sinusoidal voltage signal with en electrical oscillator at a frequency f_m and with a peak-to-peak voltage V_{pp},

$$V(t) = \frac{V_{pp}}{2} \sin 2\pi f_m t. \tag{3.18}$$

We will set f_m to be equal to the symbol rate. This is a natural choice, since we will want to use these pulses in our OTDM system, either as a data carrier or as a LO.

Our model supports phase noise for this oscillator. In practice, an electrical oscillator shows indeed small fluctuations in the instantaneous frequency, which are related to the phase of the sinusoid by (2.34). This immediately turns into timing jitter, since the peaks are obviously shifted from the expected positions. A nice overview of this non-ideal behavior of electrical oscillators can be found in [31]. In this thesis we will not discuss this further, since our studies are not fully satisfactory yet. We will thus assume a noise-free electrical oscillator.

The optical source is a CW laser, followed by a Mach-Zehnder modulator working as a pulse carver. To achieve this, we need an amplifier of gain G_1 such that the peak-to-peak of the differential voltage driving the MZM be $V_\pi/2$. We also add a DC component of $-V_\pi/2$. Between the oscillator and the amplifier we also have a delay element, to make sure that the pulses generated by the MZM are centered on the pulses produced by the rest of the setup, so that they do not counteract each other. All this red part in Figure 3.5 is optional, but improves the quality of the pulses by enhancing the extinction ratio significantly, as we will show in Section 4.2. Of course pulses would be generated after the MZM without the rest of the system, which adds complexity and cost. However, a pulse carver like this produces 50% pulses, hardly suitable for multiplexing two channels. Thanks to this overall setup, we will generate much narrower pulses, as we will show in Section 4.2.

To phase modulate the signal we obviously use a PM. Let us here define a *modulation index* (MI), as the ratio between the peak-to-peak voltage driving the PM and its V_π,

$$\mathrm{MI} = \frac{V_{pp_{PM}}}{V_\pi} = \frac{2}{\pi}\Delta\Theta, \tag{3.19}$$

where in the last equality we have inserted the $\Delta\Theta$ introduced in Section 2.2.1.5.

As dispersive element, an optical fiber follows. This is defined by a fiber length L and values of D and S.

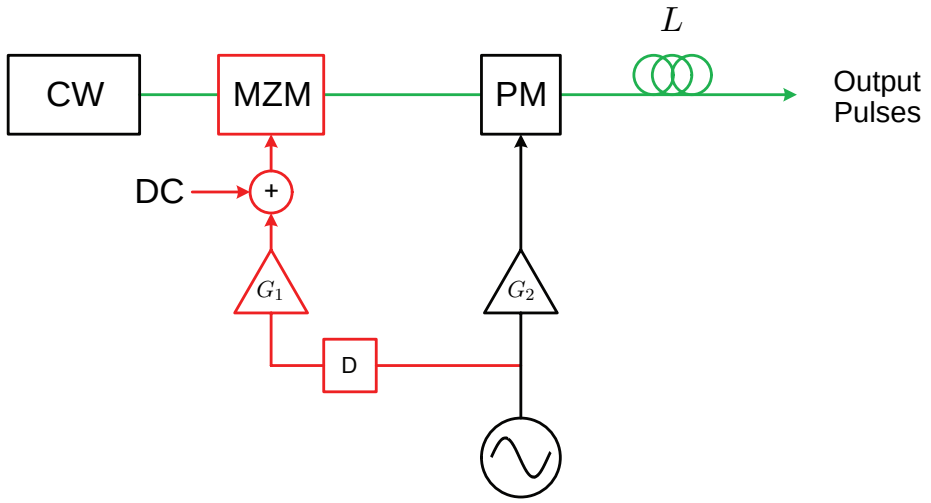

Figure 3.5: Overview of the schematics for our model of PMCW pulse source.

Let us conclude by calculating B, as defined in Section 2.2.1.5, as a function of parameters typical of this implementation. The first term of (2.51) can be calculated by taking the time derivative of (2.34) and then substituting according to (2.50). One ends up with

$$\left|\frac{\delta f}{\delta t}\right|_{max} = 2\pi f_m^2 \Delta\Theta. \tag{3.20}$$

The second term can be derived from (2.63) remembering the relation between τ_g and τ_g' and the definition of β_2. This yields

$$\frac{\delta\tau_g}{\delta f} = 2\pi L\beta_2. \tag{3.21}$$

As a consequence, B will result

$$B = 4\pi^2 f_m^2 \Delta\Theta L\beta_2 = 2\pi^3 f_m^2 \mathrm{MI}\cdot L\beta_2. \tag{3.22}$$

3.2.2.6 Timing Jitter Implementation

Understanding the physical reasons of timing jitter in a mode-locked laser well enough to model them in a refined way is by far out of the scope of this thesis. We assume a Gaussian distribution for the timing jitter. This is not sustained by a specific research finding, but it is a reasonable choice in absence of better knowledge and time for acquiring it.

A zero-mean random process with Gaussian statistics is created and each pulse is shifted (anticipated or delayed) of the respective time, as seen in Section 3.2.2.4. The input used to generate this source of noise is simply its standard deviation given in s. Note that we just need as many instances of timing jitter as the number of pulses we want to generate, which happens to be equal to the number of symbols. Consequently, the right code will be

```
timing_jitter = random('norm',0,sigma_timing_jitter,[1,length(
    TimeArray)/SamplesPerSymbol]);
```

3.2.3 Optical Coupler Model

After understanding Section 2.2.2, modeling a 3-dB coupler should be fairly easy. We implemented a non-ideal behavior of the coupler in the repartition of the power, as follows:

- The ratio of the optical powers measured at the two outputs when a signal is present at the first input but not at the second one can be different from 1/2,
- The ratio of the optical powers measured at the two outputs when a signal is present at the second input but not at the first one can be different from 1/2.

This leads us to the definition of *power split ratio* as

$$r_1 = \left.\frac{P_{out_1}}{P_{out_2}}\right|_{P_{in_2}=0}, \tag{3.23}$$

$$r_2 = \left.\frac{P_{out_2}}{P_{out_1}}\right|_{P_{in_1}=0}. \tag{3.24}$$

On top of this, we allowed the user to disable the phase shift introduced by the coupler, since sometimes it is a bit simpler and more convenient not to have it. In

practice one could compensate for it if needed by means of a phase shifter (a phase modulator driven by a constant voltage). The code of our coupler, for just the x-polarization and when we decide to apply the phase shift, looks like

```
E_out1.x = E_in1.x*sqrt(r1)+E_in2.x*sqrt(1-r2)*exp(-1i*pi/2);
E_out2.x = E_in1.x*sqrt(1-r1)*exp(-1i*pi/2)+E_in2.x*sqrt(r2);
```

where `r1` and `r2` are clearly the power split ratios.

3.2.4 External Modulators Models

Our models of external modulators are described here. The implementation should be pretty obvious once the theory lying behind has been understood (see Section 2.2.3). However, our models incorporate a few non-idealities that deserve attention, especially considering that an extensive study will be carried out in the next chapter.

3.2.4.1 Phase Modulator Model

The way we model a PM is very simple. We only shift the phase of the input field in both polarizations by an amount depending on the corresponding sample in time of the driving voltage, according to (2.52). Note that this means we neglect any dependence of the device response on the polarization of the signal.

The bandwidth limitation can be modeled by low-pass filtering the driving voltage. This is done by means of a 1^{st} order Gaussian electrical filter, whose model will be described later (see 3.5.2.2). The choice of such a filter is purely arbitrary, and we will show in the next chapter that the system behaves very similarly with other filter types. Let us observe that we filter the driving voltage and not the optical output. A similar outcome would have been achieved by band-pass filtering the optical signal around its carrier frequency.

The code is very simple, as it follows just for the x-polarization,

```
V_filtered = Electrical_Filter(V,'GAUSSIAN',1,bandwidth);
optical_out.x = optical_in.x.*exp(-1i*V_filtered/Vpi*pi);
```

where the meaning of the different parameters should be pretty straightforward.

3.2.4.2 Mach-Zehnder Modulator Model

Our implementation of a MZ modulator starts from the theory presented in 2.2.3.2 and adds a number of non-idealities that affect the functioning of real devices. In this thesis, all the MZ modulators will be driven in push-pull mode, so to achieve chirp-free operation. As inputs they require an optical signal and a driving voltage, divided into AC component and DC offset. A list of the modeled non-idealities follows:

- The non-idealities of the two couplers,
- The non-idealities of the two PMs,
- The delay between the electrical signals driving the two PMs can different from 0.

Not all of these appreciably affect the output signal in practice. MZ modulators are produced as integrated structures, and power split ratios and delays are certainly very well optimized. What one may notice is instead the bandwidth limitation, especially when operating the device at high frequencies (in the order of the tens of GHz). All these limitations will be thoroughly analyzed in the next chapter.

Real MZMs have a limited extinction ratio when performing amplitude modulation. This limitation is due to contributions from a number of non-idealities, both the ones we have listed and possibly others we have not thought about. Our model allows for the imposition of a fixed ER of 15 dB, a typical value for commercial devices.This is achieved by setting the input power split ratio of the interferometric structure to 0.67, that happens to result in the desired ER.

3.2.4.3 IQ Modulator Model

Our model of IQ modulator has two electrical inputs, which are what we called $V_I(t)$ and $V_Q(t)$, plus the obvious optical input for the signal to be modulated. Our implementation takes into account a number of non-idealities:

- The non-idealities of the two couplers,
- The non-idealities of the two MZMs,
- There might be some delay between $V_I(t)$ and $V_Q(t)$,

- The phase shift applied to the Q-arm might be not totally accurate.

These are more likely to be noticed in practice than the ones described for a MZM. In fact, an IQ modulator is a complex device of which the MZMs are components. Optimizing all the delays and power splitters will thus be more difficult. Even assuming that the manufacturers did a great job, there would be at least two aspects they could not control fully. First, the two driving signals I and Q are the outputs of an encoder and will be provided through two cables which will therefore introduce delays. We can try to find very similar cables, but some difference in the propagation time could still exist. Second, the phase shift is most often applied by regulating the voltage driving the PM on the Q-arm until the output constellation looks fine. This is clearly an intrinsically imprecise way of performing this operation. It is indeed based on mere observation and if any other parameters of the system are not totally ideal, then the optimization of the phase shift will become even more difficult to carry out because performed on an already suboptimal signal.

3.2.5 OTD Multiplexer Model

In our model we do not multiplex different streams of data, we just multiplex together several delayed versions of the same pulse train. This is very similar to what we did during our laboratory experience (see Section 5.1.1).

Doing this numerically is very easy. We employ the Matlab® embedded function `circshift`, which allows to shift the elements of a vector back or forth in a circular way, meaning that an element exiting the array at one end enters the same array on the other side.

The first issue to consider is that the precision of the shift is limited by the time resolution of our time array. There is not much one can do about this. The simplest approach is to simply delay of the number of samples closest to the analog ideal delay. The complicated one consists in interpolating the signal so to have a larger number of samples per symbol, and then applying a very accurate shift before decimating to the original value of SPS. We apply the former method, since it is much lighter from a computational point of view and since we anyway have enough samples per symbol (namely 32 per OTDM channel) to make sure that the error introduced by the finiteness of dT be negligible.

The second issue relates to the amount of which we want to delay our signal. What we do is to apply a OTDM technique that preserves the PRBS nature of the bit stream [32]. Before we explain how this work, we should emphasize once more that, in most cases, our optical signal is not pseudo random. This is due to the process of encoding and to the fact that multi-level signals require M-ary PRBSs and not simple PRBSs, as we already observed in Section 3.1.2. However, the mentioned PRBS preserving OTDM technique is not particularly complicated to implement.

Let us explain how it works (please, follow on Figure 3.6. Assuming to have a signal carrying the bits of a PRBS of N bits, the first stage of multiplexing consists in summing to the signal a delayed version of itself, where the delay amounts to half the length of the PRBS. The result will be a 2-channel OTDM signal for which the overall bit sequence of $2N$ bits is still pseudo random (meaning that it presents all the possible combinations of 1s and 0s as long as $\log_2 2N$). In the figure the colored arrows indicate the position of a specific bit before and after multiplexing. The following stage will repeat the same operation but with a halved delay. The result will be a 4-channel OTDM signal for which the bit sequence is a PRBS of $4N$ bits.

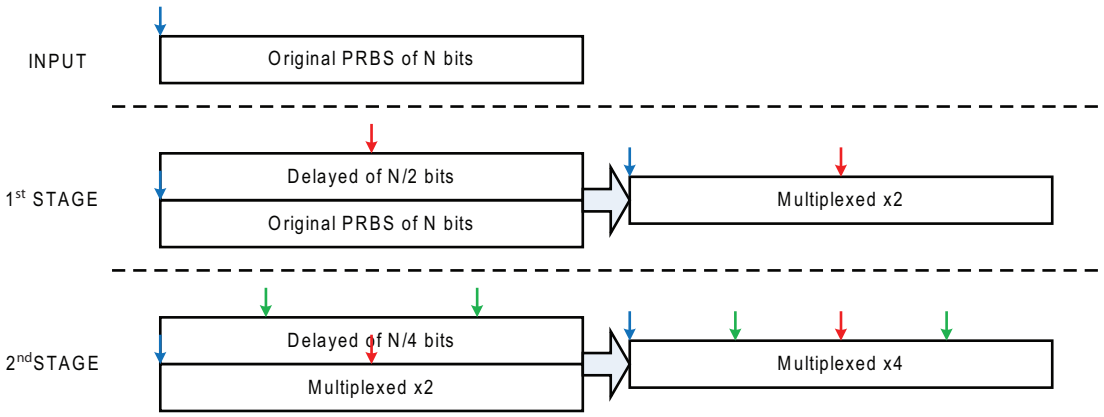

Figure 3.6: Exemplification of the concept of PRBS preserving OTD multiplexing.

Doing this is very easy once one has understood that our signal is defined over a time array comprising as many symbols as 2^{n_b}, where n_b is the length of the seeds utilized to generate our PRBSs. The shift applied at the first stage will therefore be equal to half the length of the time array, plus a small adjustment of half a symbol slot to make sure that the pulses our equally distanced. The same happens for the second

stage. The following code for a 4-channel multiplexing and for only one polarization should solve any doubts about our implementation,

```
delay1 = Nsymbols/2*SamplesPerSymbol+SamplesPerSymbol/2;
delay2 = round(Nsymbols/4)*SamplesPerSymbol+round(
    SamplesPerSymbol/4);
E_mid.x = r*E_in.x+r*circshift(E_in.x,[1,delay1]);
E_out.x = r*E_mid.x+r*circshift(E_mid.x,[1,delay2]);
```

Note that `r` can be either 1 or $1/\sqrt{2}$, depending on whether we want to simulate the losses related to each stage of couplers (necessary in practice to split the signal) or not. The divisions by 4 necessitate a `round` to make sure we obtain a finite number, the ones by 2 do not, since both `Nsymbols` and `SamplesPerSymbol` are powers of 2 in our model.

3.2.6 Transmitter Types

In this section we present the transmitter schemes for all the modulations utilized in this work. Some readers might argue that such a topic should have been discussed in the previous chapter. They would have their share of reason, no doubt about it. Nevertheless, we have preferred to postpone this topic up to this point because we will give specific details concerning the implementation in our model. There are indeed a number of ways of realizing an optical transmitter, especially for higher-order modulations. Here we will define and motivate our choices. We will also give the exact rules for the employed encoding.

Let us underline the fact that all these transmitters can be realized both as NRZ and RZ. We will show just the NRZ versions, but the RZ ones can be obtained by simply using a pulse source or a pulse carver after a CW laser.

3.2.6.1 OOK Transmitter

The OOK or binary ASK is the simplest form of optical modulation. High optical power stands for a 1, while low optical power stands for a 0. This is achieved by modulating the amplitude of a CW light in a MZM. The voltage should present an offset of $-V_\pi/2$ and a peak-to-peak of V_π.

The output power can be calculated from (2.55):

$$P_{out} = P_s \cos^2\left(\frac{\pi V(t)}{2V_\pi}\right). \tag{3.25}$$

The block diagram of such a transmitter can be visualized in Figure 3.7(a). The way the bits are encoded in the two symbols in the constellation is shown in Figure 3.7(b).

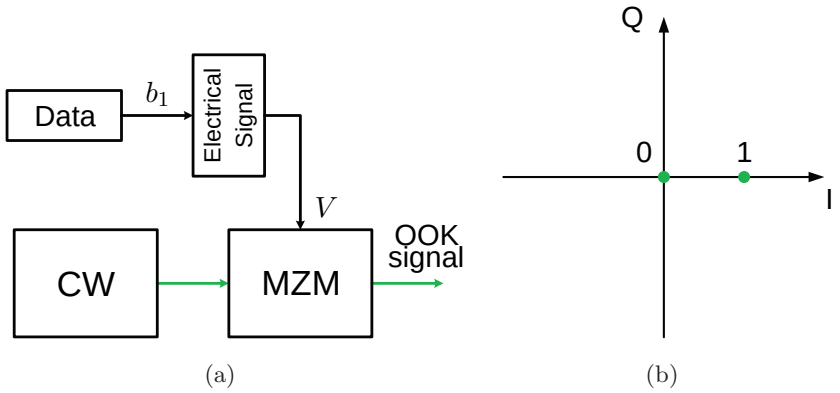

Figure 3.7: (a) Block diagram of our OOK transmitter and (b) constellation and bit mapping of our OOK signal.

3.2.6.2 DBPSK Transmitter

The generation of a binary phase modulated signal is pretty simple. It can be achieved by means of a phase modulator. There are two good reasons for not doing this but employing a MZ modulator instead. First, a phase modulator introduces chirp, second, it transfers all the amplitude noise of the electrical signal to the optical one. A MZ modulator operated in push-pull configuration does not chirp the signal and, exploiting the flatness of the transfer function at 0 and $-2V_\pi$ (see Figure 2.14(a)), the amplitude noise of the electrical signal is largely suppressed [33]. Of course a MZ modulator is more complex and costly than a simple phase modulator. We will always employ a MZ modulator to phase modulate in this work (see Figure 3.8 for the schematic of our DBPSK transmitter). The phase modulation is carried out in the way described in Section 2.2.3.2.

Our BPSK is differentially encoded. We listed the pros of differential encoding in Section 2.1.10, and all the points apply here. Specifically, it allows us to employ direct detection and resolves the π phase ambiguity arising from the rotational symmetry of the constellation. The encoding follows the logical operation

$$y_k = y_{k-1} \oplus x_k. \tag{3.26}$$

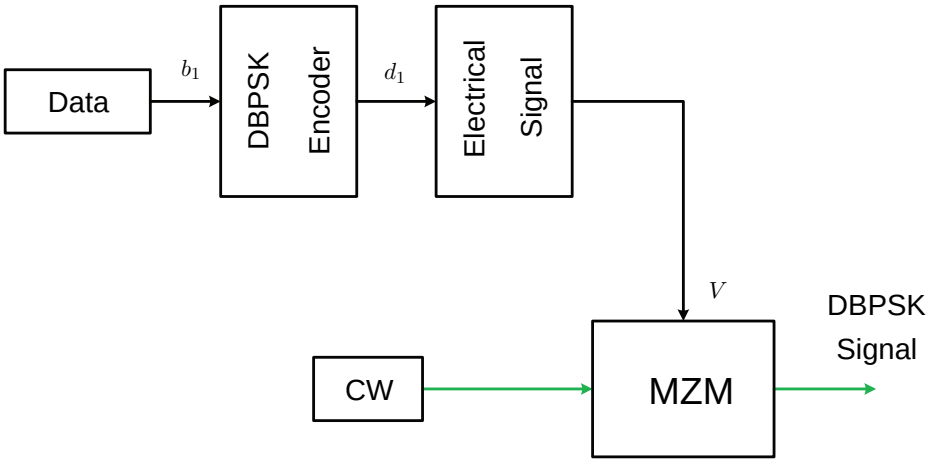

Figure 3.8: Block diagram of our DBPSK transmitter.

When we have a phase change of π, a 1-bit is produced, while 0-bits correspond to no phase change.

Similarly to the case of OOK, we can calculate the output field as

$$E_{out} = \sqrt{P_s} \cos\left(\frac{\pi V(t)}{2V_\pi}\right). \tag{3.27}$$

In this way, for $V(t) = 0$ the resulting phase shift is 0, and for $V(t) = -2V_\pi$ we have a phase shift of π. The constellation is consequently the one showed in Figure 3.9. Note that the bits we report on the constellation are the ones after performing the differential encoding.

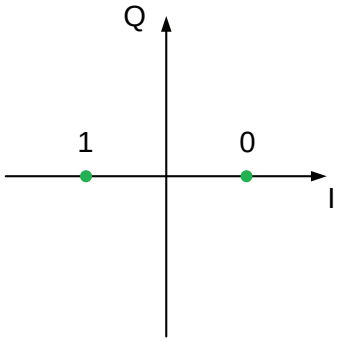

Figure 3.9: Constellation and bit mapping of our DBPSK signal.

3.2.6.3 DQPSK Transmitter

The more we enhance the modulation order, the more different ways of performing the desired modulation exist. Choosing among them is a matter of tradeoff between complexity/cost and performance, and also depends on how many levels our electrical signal can have. Since we are hereby interested in the optical domain more than the electrical one, we assume our driving voltages to be binary, and we shift as much complexity as possible to the optical modulator.

We decided to employ an IQ modulator for our simulations because it is highly resilient with respect to the amplitude noise of the electrical signal (for the same reasons explained in the previous section about DBPSK). It is also a good choice for a practical implementation. IQ modulators are indeed commercially available and all the inner connections and components are supposedly optimized by the manufacturers, so that we are left with a little bit less freedom in the settings than in the case of serial configurations employing phase and MZ modulators, probably resulting in a lower proneness to error. On the other hand, an IQ modulator might be one of the costliest solutions. The schematic of such a transmitter can be visualized in Figure 3.10.

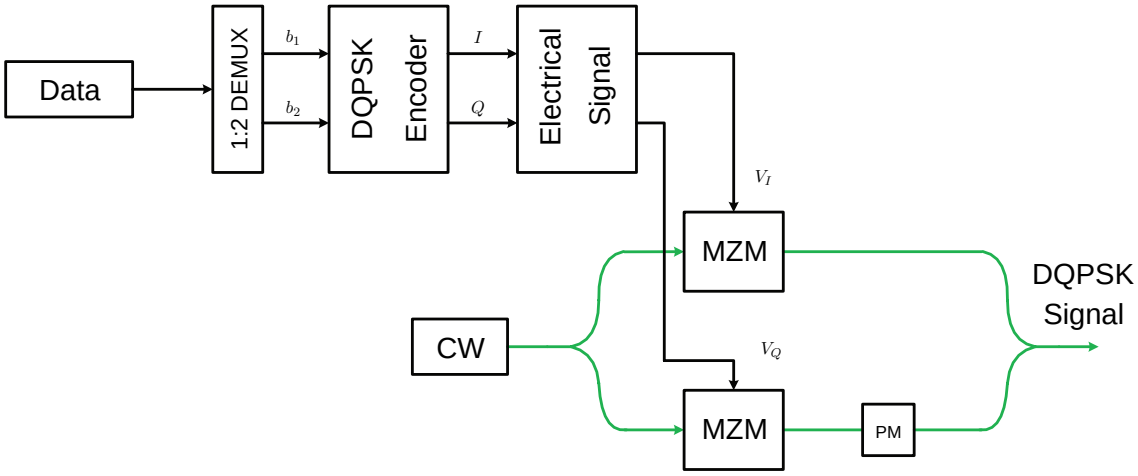

Figure 3.10: Schematic of our DQPSK transmitter.

The way an IQ modulator achieves modulation in the whole complex plane should be clear from the reading of Section 2.2.3.3. We phase modulate the signal on both branches, according to the standard phase modulation defined in 2.2.3.2. The equation

of the output field can be simply written as

$$E_{out} = \frac{1}{2}\sqrt{P_s}e^{-j\phi_s}, \tag{3.28}$$

where the phase can assume one of the four values of the constellation according to

$$\phi_s = \begin{cases} \pi/4 & \text{if } V_I = 0 \text{ and } V_Q = 0 \\ 3\pi/4 & \text{if } V_I = -2V_\pi \text{ and } V_Q = 0 \\ -3\pi/4 & \text{if } V_I = -2V_\pi \text{ and } V_Q = -2V_\pi \\ -\pi/4 & \text{if } V_I = 0 \text{ and } V_Q = -2V_\pi \end{cases} \tag{3.29}$$

Differential encoding is utilized here as well, together with Grey coding, to optimize the BER performance. Of course differential encoding is in this case more complicated, since we have two inputs and two outputs for our encoder. We have implemented the differential encoding suggested in [34], whose logical equations are

$$I_k = \overline{(u_k \oplus v_k)}(u_k \oplus I_{k-1}) + (u_k \oplus v_k)(v_k \oplus Q_{k-1}), \tag{3.30}$$

$$Q_k = \overline{(u_k \oplus v_k)}(v_k \oplus Q_{k-1}) + (u_k \oplus v_k)(u_k \oplus I_{k-1}). \tag{3.31}$$

The constellation with the employed bit mapping can be seen in Figure 3.11. Once more the shown bits are the ones produced by the encoding and not the original ones, the most significant bit of each pair (the one to the left) is taken from the Q bit sequence, the least significant one from the I sequence.

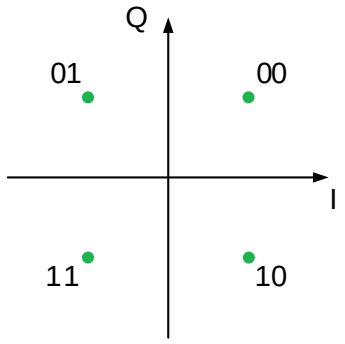

Figure 3.11: Constellation and bit mapping of our DQPSK signal.

3.2.6.4 16QAM Transmitter

As already introduced in Section 2.1.6, we will only work with square-16QAM signals, which have better BER performance (due to more homogeneous distances between the symbols on the constellation) and are easier to modulate and detect.

There are a multitude of ways of implementing such a transmitter, and we chose to use two IQ modulators in parallel, both applying a QPSK modulation to the signal. One of the two IQ modulators is responsible for defining the quadrant to which the symbol is mapped, while the other one, whose output is attenuated of 6 dB, determines the position of the symbol within the quadrant. The way this functions should be quite intuitive, and a block diagram of the transmitter is provided in Figure 3.12.

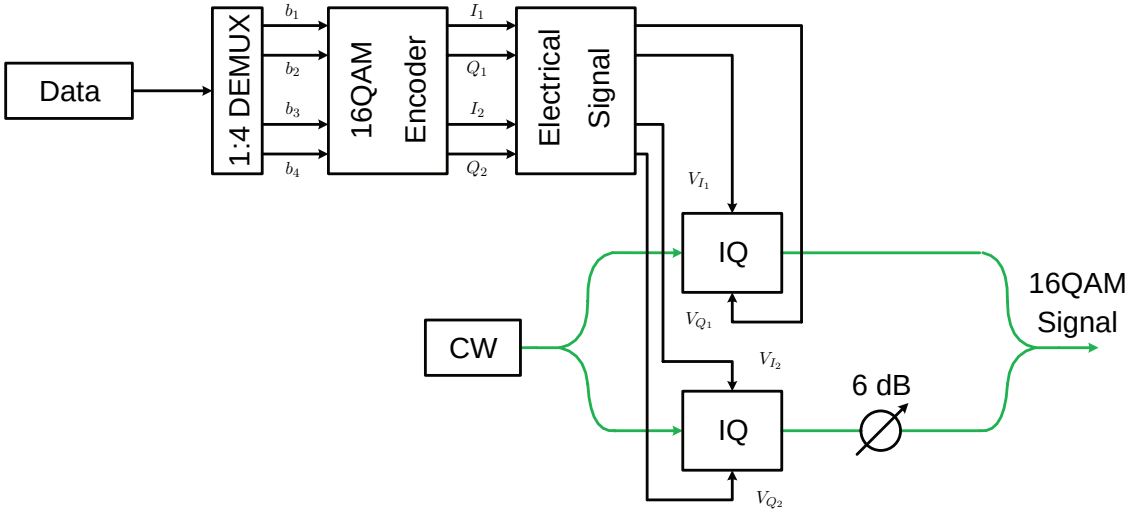

Figure 3.12: Schematic of our 16QAM transmitter.

It is not possible to employ direct detection with 16QAM. Coherent detection is therefore needed. Moreover, In the case of 16QAM the differential encoding becomes even more complicated than in the case of DQPSK. Every time we receive a symbol, a $\pi/2$ phase ambiguity arises. This is basically an uncertainty about which quadrant the symbol belongs to. This can be solved by performing a *differential quadrant encoding*, which simply consists in encoding two bits (we do it for the most significant ones) in the DQPSK way, so that they can be unambiguously recovered. The other two bits should be such that the four symbols mapped into each quadrant be rotationally symmetric with respect to these two bits. Unfortunately, Grey coding cannot be implemented anymore, with the consequent decrease in BER performance. On the other hand, this encoding makes it possible to operate without synchronization sequences. The constellation with the bit mapping can be seen in Figure 3.13.

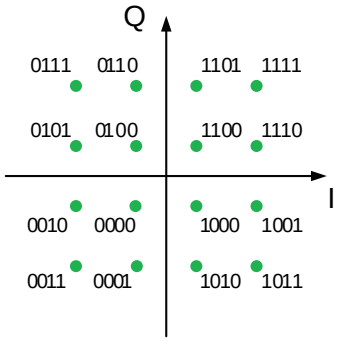

Figure 3.13: Constellation and bit mapping of our 16QAM signal.

3.3 Optical Channel Model

As thoroughly discussed in Section 2.3, our optical channel will be made up of two main parts: the fiber and a number of amplifiers.

The complexity of the modeling of an optical fiber depends tremendously on the factors we want to take into account. We believe we chose a good compromise between realizing a sufficiently realistic model[1] and avoiding excessive complexity. The motivations for our choices will be given in the following sections, where our implementations of losses, dispersion, and nonlinearities will be presented.

Amplification in optical amplifiers is also a complex phenomenon. In our simulations we will never actually employ optical amplifiers. It is customary to apply all the ASE noise at the end of the link, before receiving the signal. In Section 3.3.4 we will discuss how we impose the ASE noise and to what extent this way of doing it is acceptable.

3.3.1 Losses Implementation

Implementing losses is extremely easy, once one has accepted Beer's law as described in Section 2.3.2. If we consider only losses, the solution of the generalized NLSE (2.59) will be

$$A\left(z,t'\right)=A\left(0,t'\right)\exp\left(-\frac{\alpha}{2}z\right). \tag{3.32}$$

[1] A model of a system can be defined realistic or reliable only in relation to certain system conditions. There is no such thing as a perfect or totally reliable model. In optical communications, especially symbol rate (or better the pulse width) and signal power determine the behavior of the fiber. Very short pulses will experience a lot of dispersion due to their larger spectra, high power signals will cause a lot of nonlinearities to take place.

Clearly, we just need to multiply the optical signal by the right exponential, depending on loss coefficient and fiber length. However, α is generally expressed in dB/km, according to the equation

$$\alpha_{dB} \cdot z = 10 \log_{10} \frac{P(z,t')}{P(0,t')}, \tag{3.33}$$

where z was expressed in km. This yields

$$A(z,t') = \frac{A(0,t')}{\sqrt{10^{\frac{\alpha_{dB} z}{10}}}}. \tag{3.34}$$

Consequently, the code for one polarization will be

```
E_out.x = E_in.x/sqrt(10^(alpha*L/10/1e3));
```

Note that `alpha` is the attenuation coefficient expressed in dB/km and `L` the fiber length in m, as they are in our model.

3.3.2 Dispersion Implementation

Implementing chromatic dispersion can be a little bit more challenging. We should start from the generalized NLSE (2.59). Let us keep just the terms related to dispersion,

$$\frac{\delta A(z,t')}{\delta z} = j\frac{\beta_2}{2}\frac{\delta^2 A(z,t')}{\delta t'^2} + \frac{\beta_3}{6}\frac{\delta^3 A(z,t')}{\delta t'^3}. \tag{3.35}$$

This equation could be written as

$$\frac{\delta A(z,t')}{\delta z} = \mathbb{D} A\left(z,t'\right), \tag{3.36}$$

where we have conveniently identified a linear operator $\mathbb{D}$,

$$\mathbb{D} = j\frac{\beta_2}{2}\frac{\delta^2}{\delta t'^2} + \frac{\beta_3}{6}\frac{\delta^3}{\delta t'^3}, \tag{3.37}$$

which, after Fourier transforming[1], becomes

$$\tilde{\mathbb{D}}(\omega) = -j\frac{\beta_2}{2}(\omega-\omega_0)^2 - j\frac{\beta_3}{6}(\omega-\omega_0)^3, \tag{3.38}$$

where $\tilde{\mathbb{D}}$ denotes the Fourier transformed version of our operator. So, if we Fourier transform (3.36), we get

$$\frac{\delta \tilde{A}(z,\omega)}{\delta z} = \tilde{\mathbb{D}}(\omega)\,\tilde{A}(z,\omega). \tag{3.39}$$

[1]To perform this step one should remember that the operation of time derivation corresponds, after Fourier transform, to a multiplication by a factor of $j(\omega-\omega_0)$. Note that this is true for our definition of Fourier transform.

Now, this differential equation is extremely easy to solve. The solution is an exponential,

$$\tilde{A}(z,\omega) = \tilde{A}(0,\omega) \exp\left[-j\frac{\beta_2}{2}(\omega-\omega_0)^2 z - j\frac{\beta_3}{6}(\omega-\omega_0)^3 z\right]. \tag{3.40}$$

After this discussion one should have a pretty clear idea of how we can model dispersion. β_2 and β_3 can be determined from D and S according to (2.65) and (2.67), and $\tilde{\mathbb{D}}(\omega)$ will be given by

$$\tilde{\mathbb{D}}(\omega) = -j\frac{\beta_2}{2}(2\pi(f+f_{ref}-f_0))^2 - j\frac{\beta_3}{6}(2\pi(f+f_{ref}-f_0))^3, \tag{3.41}$$

where we have kept into account that in our model frequencies are expressed with respect to a reference frequency f_{ref}. Consequently, the code for the x-polarization will look like

```
E_out_f.x = E_in_f.x.*exp(-1/2*1i*beta2*(2*pi*(FrequencyArray+
    ReferenceFrequency-f0)).^2*L).*exp(-1/6*1i*beta3*(2*pi*(
    FrequencyArray+ReferenceFrequency-f0)).^3*L);
```

In the code above, we perform a multiplication between the Fourier transform of our input `E_in_f` and the exponential term $\exp\tilde{\mathbb{D}}(\omega)L$. Afterwards, we would inverse-transform to bring the signal back to the time domain. The way Fourier transforms are performed in our model will be discussed later on in Section 3.5.1.

Dispersion is a linear operation since it does not depend on the signal power. Consequently, we can apply dispersion and losses in any order we like. Problems arise when also nonlinearities are present.

3.3.3 Nonlinearities Implementation

When considering nonlinearities and chromatic dispersion together, the generalized NLSE does not have analytical solutions anymore (apart from the special case of solitons). If we have only nonlinearities but not dispersion or losses, then a solution is given by (2.71). In this case the implementation will be easy, and the code might look like

```
E_out.x = E_in.x*exp(-1i*gamma*(abs(E_in.x).^2)*L);
```

Note that such a model would support only one polarization at a time. In practice, when we multiplex the two polarizations of a PolMux system, nonlinearities behave differently and the two channels influence each other in this respect. The theory becomes significantly more complicated, and we have not looked into it. For this reason,

our model of nonlinearities will loose accuracy when applied to PolMux signals, and this should be avoided. The way we handle the two polarizations is by treating them as two completely separated signals, which is not physical.

When losses, dispersion, and nonlinearities are to be simulated all together, then numerical solutions of the generalized NLSE are needed. Commonly, one employs the so-called *split-step Fourier method* [24]. Let us explain how this method works.

Basically, the problem about predicting the evolution of the optical signal in the fiber is that the Kerr effect depends on the signal power in that specific instant in time[1], and the power will change due to pulse broadening caused by dispersion and/or losses. The idea is to cut the fiber into as many slices as possible, and, for each slice, treat the three phenomena separately. The length of a slice will be called step length or step size. Clearly, if the step length approaches zero, then the estimate provided by such a method will get close to the actual behavior of a real fiber.

We have already described how we model losses, dispersion, and Kerr effect. Now we need to understand in which order we simulate the three of them and in which way we determine the step size. There are a few different possible choices for deciding what to perform first and what last. The idea is to minimize the number of Fourier transforms, which are computationally very demanding, while getting as close as possible to the ideal solution obtained with infinitely short step lengths.

Before moving on, we should find a way to determine the error of a solution with respect to the ideal one. Let us define a norm as

$$\|A(t)\| = \sqrt{\int |A(t)|^2 \, dt}, \tag{3.42}$$

where $A(t)$ is a complex function, in our case the complex slowly varying envelope. The integral is performed applying the so-called *Simpson's rule*, which states that

$$\int_a^b f(x)\, dx \approx \frac{b-a}{6}\left[f(a) + 4f\left(\frac{a+b}{2}\right) + f(b)\right]. \tag{3.43}$$

Remembering that in our model the signal is defined only at intervals of dT, the code for the integration is

[1]This is true if we assume that the Kerr effect is instantaneous, or at least much faster than our sampling rate $1/dT$. This assumption is backed up by the literature on the topic, and the derivation of the NLSE presupposes an instantaneous Kerr effect in the first place.

```
N = length(f);
if mod(N,2)==0
    integral = 0;
    for i = 1:2:N-2
        integral = integral+(2*dT/6*(f(i)+4*f(i+1)+f(i+2)));
    end
else
    integral = f(1)*dT;
    for i = 2:2:N-2
        integral = integral+(2*dT/6*(f(i)+4*f(i+1)+f(i+2)));
    end
end
```

If we have a perfectly accurate solution $A_a(t)$, then we define the *relative global error* of any other generic solution $A(t)$ as

$$\frac{\|A(t) - A_a(t)\|}{\|A_a(t)\|} = \sqrt{\frac{\int |A(t) - A_a(t)|^2 \, dt}{\int |A_a(t)|^2 \, dt}}. \tag{3.44}$$

Note that we will never have a perfectly accurate solution, but we can generate one with such a short step size that its error will be negligible compared to the one introduced by the solutions we would normally obtain in shorter and more reasonable times.

We need at least two Fourier transforms for each step, since dispersion is to be calculated in the frequency domain, while losses and nonlinearities in the time domain. We follow these steps:

1. We apply losses for a length equal to half the step,
2. We calculate the Kerr effect for half the step size as well,
3. We Fourier transform the resulting optical signal,
4. Dispersion is applied for the whole step length,
5. The optical signal is inverse Fourier transformed to go back to the time domain,
6. Point 2 is repeated,
7. Point 1 is repeated.

Figure 3.14 should help visualize the process. Note that this is a symmetric implementation, meaning that anything that takes place in the first half of the step is repeated

in inverted order in the second half. It can be proved that symmetric steps yield a lower error [24].

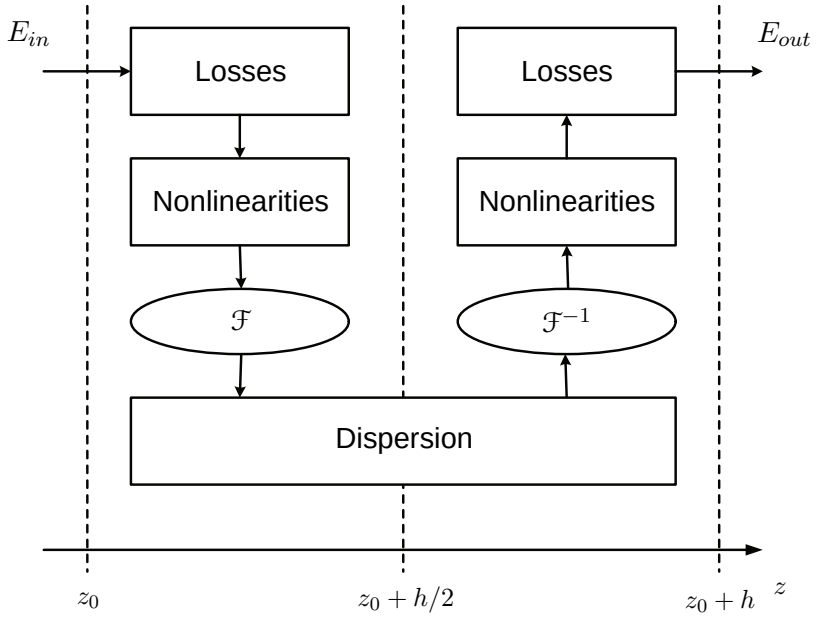

Figure 3.14: Sequence of operations within a step of the split-step Fourier method as it was implemented in this work.

Now we need to determine the step size. There is a variety of techniques when doing this, we have limited ourselves to implementing just three of them:

1. Constant step size,
2. Step size depending on nonlinear phase rotation,
3. Step size depending on relative local error.

Constant Step Size Using a constant step size is the simplest method, on the other hand it is also the least computationally efficient of the three [35]. The other two deserve a bit more attention.

Step Size Depending on Nonlinear Phase Rotation For a step length of h and at the instant t, self-phase modulation will induce a phase shift of

$$\phi_{nl} = -\gamma \left| A\left(0,t\right)\right|^2 h, \tag{3.45}$$

as one can easily see from (2.71). The idea is to set the step length so that the phase shift due to SPM be no larger than a certain set value, which we can call ϕ_{nl}^{max}. This leads to a step length

$$h = \frac{|\phi_{nl}^{max}|}{\gamma |A(0,t)|^2}. \tag{3.46}$$

The lower ϕ_{nl}^{max}, the more precise our solution will be.

Before we are ready to implement this, we still have to solve a problem. (3.46) requires the signal power at a specific time. This does not make sense, since the signal will most likely have very different powers at different instants. We have two choices: either we take the average power, or the peak power. The first one is not suitable if we want to simulate a signal which has very low power for most of the time window, and then a peak, for example an isolated pulse. In this case, we would use a step size much longer than the required one, and the result would be affected by very large error. The second solution could be a little bit too conservative, since we determine the step length depending on the peak power, resulting in steps sometimes shorter than the actual need. In our model we implemented the latter solution. The code is utterly simple,

```
Pp = max(Power(E_in));
h = phi_nl_max/Pp/gamma;
```

Notice that this method is practically equivalent to having a fixed step size in absence of losses and for limited deformations of the signal. In fact, if the peak power does not change (as in the case of first order solitons), the step length will not change either. In practice SPM and dispersion can cause significant change in the peak power and thus a change in the step length.

Step Size Depending on Local Relative Error First a goal local relative error δ_G is set. We start from a given step length h (we determine it by using the previously described method of nonlinear phase shift). Then, we act as follows until we cover the entire fiber length:

1. We generate two solutions, one for a step length of $2h$, and one obtained by taking two steps of length h each. We will call them rough solution A_r and fine solution A_f.

2. The relative local error $\delta = \|A_r - A_f\| / \|A_f\|$ is calculated.

3. If $\delta \geq 2\delta_G$ the solution is discarded and we repeat from 1 with half the step size.

4. The following step length h is determined according to:

   - If $\delta_G \leq \delta < 2\delta_G$ the step size is obtained by dividing h by $2^{1/3}$.
   - If $1/2\delta_G \leq \delta < \delta_G$ we use once more the same h.
   - If $\delta < 1/2\delta_G$ the step size is obtained by multiplying h by $2^{1/3}$.

The final solution will then be given by

$$A = \frac{4}{3}A_f - \frac{1}{3}A_r = A_a + O\left(h\right), \tag{3.47}$$

where we have shown that the so obtained solution presents an error of fourth order in the step length with respect to the exact solution [35]. This is the most complicated way of choosing the step size, but it is also the most robust for arbitrary systems [35] and very often the most computationally efficient (see Section 4.4 and [35]), even though a single step requires 50% extra FFTs due to the calculation of the rough solution.

3.3.4 ASE Noise Implementation

As explained in Section 2.3.5, normally long-haul links will present a number of amplifiers equally spaced, plus probably a preamplifier just before the receiver. As long as nonlinearities are not considered, the optical power over the fiber does not matter, and adding all the amplifiers at the end of the link is absolutely fine. In our model, we will never have amplification along the fiber link.

Generally, we will artificially impose a certain amount of noise just before the receiver. This is a widespread method for analyzing optical systems. In this case, the OSNR becomes an input value, and noise must then be generated accordingly, so that

$$\text{OSNR} = \frac{\langle P\left(t\right)\rangle}{p \cdot N_0 \cdot B_{ref}} \tag{3.48}$$

be verified. We have already discussed (3.48) in Section 2.1.11, we hereby just remind the reader that we set $B_{ref} = 0.1$ nm and that N_0 is a single-sided noise spectral density that we assume constant. The noise we add to the signal should simulate the optical channel noise, which is mainly ASE noise due to the amplifiers. This noise can be modeled as Gaussian noise on the electric field, so that both the in-phase and quadrature components of the field be noisy.

Once we have determined N_0 from the desired value of OSNR and p, we can calculate the standard deviation of the Gaussian process as

$$\sigma_{ASE} = \sqrt{\frac{N_0}{2dT}}. \tag{3.49}$$

N_0 is a single-sided power spectral density, so we multiply it by $1/dT$, which is the width of our baseband frequency span. Note that this is per quadrature, so it will be necessary to generate different instances of the noise for the real and imaginary parts of the electric field, and for x and y polarizations. This explains the factor 2 at the denominator.

Now we just need to actually generate the in-phase and quadrature instances of the noise and add them to the field. Note that we add the noise in just one polarization if $p = 1$, in both polarizations if $p = 2$. The code follows:

```
switch p
    case 2
        ASE.x = random('norm',0,sigma_ASE,[1,Nsamples])+1i*
            random('norm',0,sigma_ASE,[1,Nsamples]);
        ASE.y = random('norm',0,sigma_ASE,[1,Nsamples])+1i*
            random('norm',0,sigma_ASE,[1,Nsamples]);
        E_out.x = E_in.x+ASE.x;
        E_out.y = E_in.y+ASE.y;
    case 1
        ASE.x = random('norm',0,sigma_ASE,[1,Nsamples])+1i*
            random('norm',0,sigma_ASE,[1,Nsamples]);
        E_out.x = E_in.x+ASE.x;
        E_out.y = E_in.y;
end
```

3.4 Receiver Model

Our model features a wide variety of receivers, from the simplest direct detection to a much more complex coherent receiver with digital signal processing (DSP). The latter is thoroughly described and analyzed in [12], so here we will limit ourselves to the description of one of the basic blocks, the photodiode, and of a few direct detection receivers of particular interest for this work.

We will discuss the model of photodiode, which, through the realization of shot and thermal noises, accounts also for a number of effects introduced by the electronics of

the receiver, and the decision circuit. The electrical filter will be explained in Section 3.5.2.2 and we will not write about the clock recovery circuit. In our model this is not required, since the clock frequency is known as a general parameter, and the sampling point can be optimized as we will explain in Section 3.4.5.

3.4.1 Photodiode Model

After the theoretical introduction provided in Section 2.4.1, the modeling of a photodiode is quite easy. In the ideal case we simply convert the optical power into current according to 2.73, knowing the responsivity.

Our implementation supports a bandwidth limitation, and it is simulated by low-pass filtering the photocurrent with a Gaussian filter of 1st order. The code will be

```
I = R*Power(E_in);
I_filtered = Electrical_Filter(I,'GAUSSIAN',1,bandwidth);
```

Shot noise and thermal noise are also added within this block, for simplicity. Their implementation is discussed in the following two sections.

3.4.2 Shot Noise Implementation

If $P(t)$ is the optical power, R the responsivity of the photodiode, and $i_S(t)$ the shot noise contribution, the instantaneous detected current can be written as

$$I(t) = R \cdot P(t) + i_S(t). \tag{3.50}$$

$i_S(t)$ can be described by a random process with Poisson statistics, approximated to a Gaussian process [4].

In [4] one may follow the derivation that leads to the variance of the just mentioned random process,

$$\sigma_S^2 = 2q(RP + I_d)\Delta f, \tag{3.51}$$

where q is the electron charge, I_d the dark current (i.e. the current measured at the photodiode output for no incident light) and Δf the effective noise bandwidth of the receiver ($\Delta f = \int_0^\infty |H_T(f)|^2 df$, in which $H_T(f)$ is the total frequency response of the receiver circuit).

3.4.3 Thermal Noise Implementation

Thermal noise is modeled as a Gaussian random process [4]. Also in this case we skip the derivation, which can be found in [4] and give the final result,

$$\sigma_T^2 = \frac{4k_B T F_n \Delta f}{R_L}, \tag{3.52}$$

where k_B is Boltzmann's constant, T is the temperature in K, F_n is the noise figure of the amplifying circuitry following the photodiode, and R_L is the load resistance, which is the prime cause of thermal noise. Note that the noise figure is just a simple way to account for all the electronics of a typical front end circuitry, which can enhance the thermal noise, especially in the case of amplifiers. F_n is defined as the ratio between the SNR just after the photodiode and the one at the output of the receiver circuit.

Being both thermal and shot noises approximated to Gaussian processes, and assuming they are uncorrelated, they can be expressed as a single Gaussian process of variance

$$\sigma_{tot}^2 = \sigma_S^2 + \sigma_T^2. \tag{3.53}$$

So, after calculating σ_S^2 and σ_T^2 from (3.51) and (3.52) respectively, and summing them up, we can generate a random process as done for the ASE noise and add it to the current,

```
noise = random('norm',0,sigma_tot,[1,length(TimeArray)]);
I_out = I_filtered+noise;
```

Note that the noise is to be added after the filtering, since the bandwidth limitation of the photodiode does not apply to the following electronic circuitry, whose bandwidth limitation is already accounted for by the paramenter Δf.

3.4.4 Receiver Types

We hereby describe the way we receive our signal in all its different formats. We just describe direct detection receivers, leaving the description of our coherent receiver with DSP to [12]. Note that the 16QAM cannot be received with direct detection, and necessarily requires a coherent receiver. In general, since this work is more centered on transmission, we will devote a little less attention to this part.

3.4.4.1 OOK Receiver

Receiving an OOK signal is utterly simple. We just utilize a photodiode to convert optical power into current. A decision circuit follows.

3.4.4.2 DBPSK Receiver

Thanks to differential encoding, it is possible to employ direct detection also with some phase modulations. DPSK can be received quite simply when utilizing a DLI with no phase shift on the lower branch. In this way, the photocurrent will depend on the phase difference between two consecutive symbols, as we planned when adopting differential encoding. The absolute phase of the signal is unimportant. Two photodiodes follow to perform balanced detection. The scheme of our DBPSK receiver is shown in Figure 3.15.

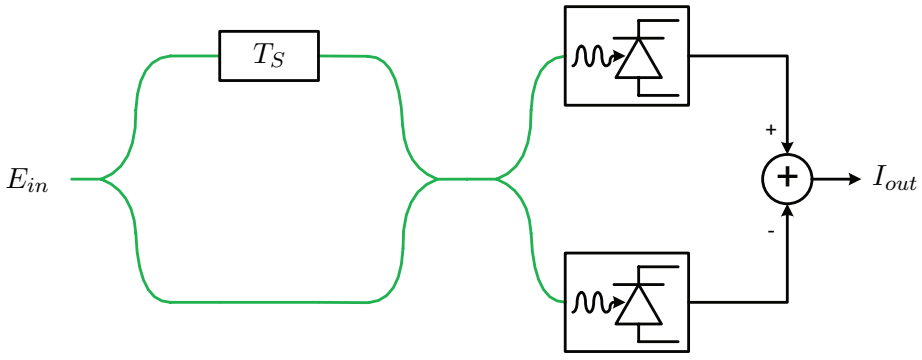

Figure 3.15: Schematic of our DBPSK receiver.

3.4.4.3 DQPSK Receiver

The direct detection receiver for a DQPSK signal is a bit more complicated. We will just show how we implement it, but we redirect the reader to [12] for an explanation of the reasons why it works.

We split the signal into two arms by means of a coupler. The upper one will go through a DLI applying a phase shift of $\pi/4$, the lower one will do the same but with a phase shift of $-\pi/4$. After writing a few equations, one could convince oneself that the upper arm differentially detects the in-phase component of the signal, whereas the

lower arm takes care of the quadrature component. The scheme is shown in Figure 3.16.

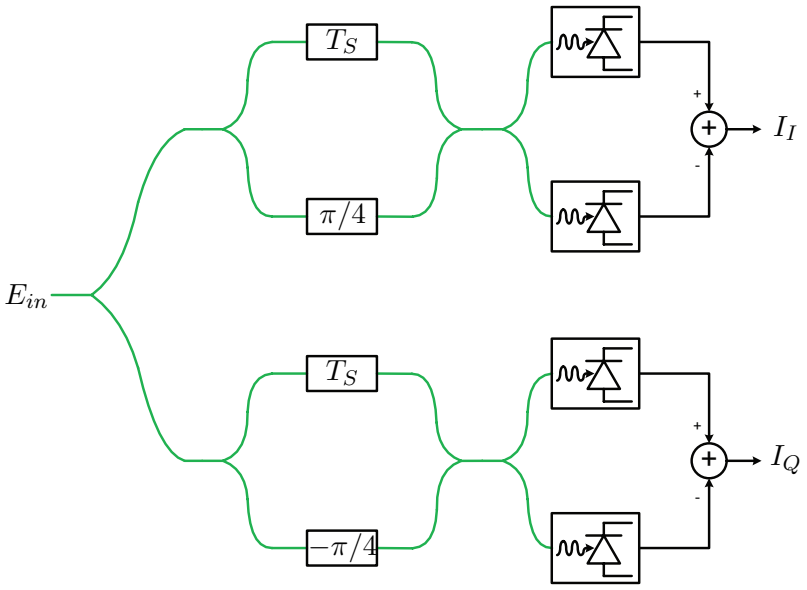

Figure 3.16: Schematic of our DQPSK receiver.

3.4.5 Decision Circuit Model

After receiving the signal we need to perform an analog to digital conversion. This requires two elements, a threshold and a sampling point, as explained in Section 2.4.4.

Both can be optimized by determining the values providing the lowest BER. Note that the optimum threshold current should be zero when we employ balanced detection. In practice one would need to generate a clock at the right symbol rate. In our case the symbol rate is a known parameter and sampling becomes very easy. We neglect any jitter in the sampling point.

The code to implement this is very simple,

```
Nsymbols = length(I)/SamplesPerSymbol;
bit_sequence = zeros(1, Nsymbols);
for i = 1:1:Nsymbols
    if I(SamplesPerSymbol*(i-1)+sampling_index)>threshold
        out(i) = 1;
    else
        out(i) = 0;
    end
```

end

3.4.6 BER Determination

The technique we will apply throughout all this work (and that will be implicitly used every time we provide BERs) is called *Monte Carlo*. It consists in sending N bits and detecting them. The BER will then be given by the ratio of wrongly detected bits over the transmitted ones. To get an accurate result one needs to work with a large number of bits. As a rule of thumb, one needs about $N = 10/\text{BER}$ to have an uncertainty of about some tenths of dB on the OSNR scale [6]. For very low BERs this means that a very high number of bits has to be transmitted.

Since we have a limited number of bits due to the finite seed we use to generate the bit sequence, we will repeat the simulation many times, each time using the same bit stream but adding new instances of the ASE noise[1]. It is now clear why a long seed for the generation of the bit sequence is detrimental for the computational time. If the seed is short, we work on a small number of bits (therefore the time array is short) and then we move to another instance of the same set of bits. Short time arrays are fast to process (especially Fourier transforms are much faster) and require less memory. For the same reason one should also try to limit the number of samples per symbol. For the same N, a simulation with a shorter seed is way faster to perform than one with a longer seed or a higher value of SPS.

Instead of sending a predetermined number of bits, we keep running the simulation until we count as many errors as a preset goal number of errors. As a default, we will set an error threshold of $100 \cdot m$ errors per channel, where $m = \log_2 M$ is the number of currents we have at the output of the receiver, or the number of bits per symbol. Errors are counted on each current signal, and the simulation is stopped when all the currents have produced at least 100 errors. As an example, a DQPSK signal will be detected as a pair of current signals I_I and I_Q. So, we will detect at least 100 errors on each of them before declaring a value for the BER. In the case of OTDM signals, we

[1] Note that, for a more reliable result, one should produce new instances of all the noise components in the system for each run. For example, also the laser phase noise should be simulated at each loop. Most often, we just repeat the simulation of the system from the block adding ASE noise, generating the transmitter only once. This is not totally accurate, but decreases the computational time significantly.

will count the errors only for one channel, assuming that all the channels have similar performance[1].

Note that there is a small issue we need to overcome to be able to determine the BER. The decision circuit will return a bit sequence, but to compare it with the original one, we have to make sure that they are not delayed with respect to each other. Unfortunately, a few blocks can introduce delays, especially electrical filters with complex transfer functions, like the Bessel and Butterworth ones (see Section 3.5.2.2). In practice this is not a problem, since we compensate for the delay while keeping an eye on the BER. In our model, the compensation is done by means of the *cross-correlation*. For two real functions f and g, it is defined as

$$R_{f,g}(t) = f * g(t) = \int_{-\infty}^{\infty} f(\tau)\, g(t-\tau)\, d\tau. \tag{3.54}$$

For two currents in our model it becomes a sum instead of an integral. It should be pretty intuitive that, if a signal is the delayed version of another, their cross-correlation will have a maximum for a t corresponding to the delay.

To determine and compensate for the delay, we thus calculate the cross-correlation between the electrical signal generated from the initial bit sequence, and the photocurrent produced by the receiver. We take the maximum value of the cross-correlation function and we anticipate the photocurrent produced after each cycle of the simulation so to fully compensate for the delay. The code to determine the delay will be

```
[max_xcorr,max_index] = max(xcorr(I,delayed_I));
delay = length(delayed_I)-max_index;
```

While we can anticipate the photocurrent simply by using the following code,

```
delay_compensated_I = circshift(I_in,[1,-delay]);
```

3.4.7 OTD Demultiplexer Model

We have to different models of OTD demultiplexers. One is utilized together with direct detection, the other with coherent detection. Let us start by describing the former, which is very easy. The founding principle is shown in Figure 3.17. We simply create a window function by which we multiply both the polarizations of the electric

[1] Again, this is not always true, but it is a useful assumption when it comes to keeping the computational time as low as possible.

field. If this function is properly aligned with the signal pulses and the width is neither too much nor too little, a nice demultiplexing is achieved. It is advisable not to have a rectangular window, since it would generate abrupt changes in the signal, which in turn correspond to high frequency components in the spectrum.

This is of course far from being a realistic method in its implementation, but the outcome is not far from what one tries to obtain in practice. Since we did not study any demultiplexing techniques for direct detection, doing it this way appeared to be a good idea. This method will be employed only in Section 4.2.3.

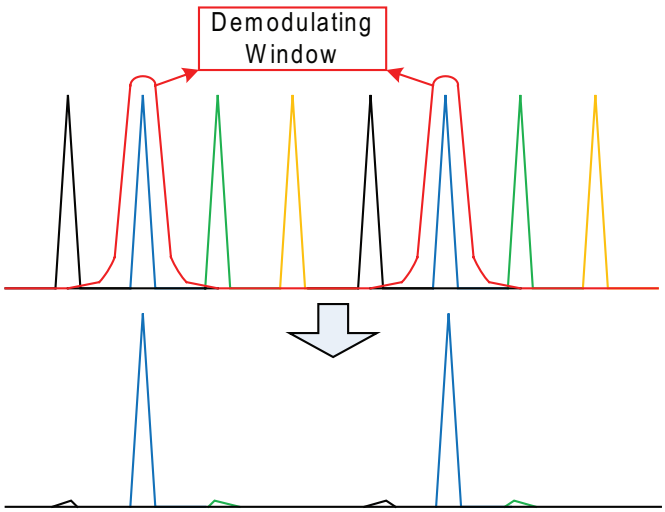

Figure 3.17: Principle behind one of the two demultiplexing techniques implemented in our model.

The second method consists in modeling the schematic of Figure 2.23, as seen in Section 2.4.10. The only difference is that we beat our LO pulses with just one channel, and therefore we only have one front-end. The other three channels are lost. This is acceptable as long as we believe that all the channels behave in the same way and are subject to the same impairments, so that analyzing one is equivalent to analyzing all of them. In general we tried to check that this was verified, but the results we report within this thesis are obtained by monitoring only one channel at a time.

3.5 Frequency Domain Operations

Some crucial blocks in our model work with the signal in the frequency domain. In this section we clarify our implementation of *fast Fourier transform* (FFT) before we move on to describe the filters we use and the way we implemented a model of spectrum analyzer.

3.5.1 Fast Fourier Transform

For simplicity, filtering in our model is carried out in the frequency domain. This is a convenient choice, since the transfer functions of the commonly used filters are well known in the frequency domain, and the filtering is reduced to a simple multiplication in this case (see Section 2.1.4).

It should be clear that we need to efficiently Fourier transform the vector representing our signal. A simple multiplication by the desired frequency response follows, concluding with the inverse Fourier transform that restitutes the filtered signal in the time domain. To perform such operations in as optimized a way as possible we exploit a very popular Matlab® function, `fft`, and its inverse, `ifft`. These are proper ways to transform discrete-time signals, such as ours.

The FFT algorithm is fastest when being fed with vectors of 2^n elements, with n natural. This is guaranteed in our model (see Section 3.1.1). Note that `fft` returns a vector whose elements represent the value of the Fourier transform of the signal at a certain frequency. The first half of the output vector contains the frequencies from 0 to f_{max}, followed by those between $-f_{max}$ and 0. The function `fftshift` allows us to reorder the vector properly. Similarly, `ifftshift` helps us deal with the inverse transform. Figure 3.18 summarizes the described steps.

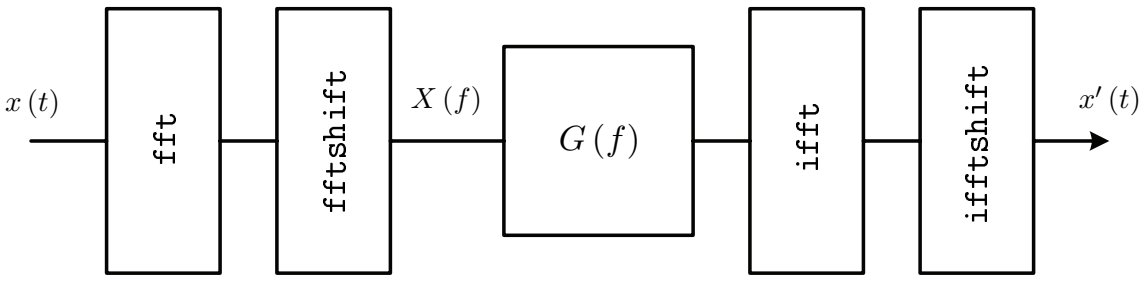

Figure 3.18: Filtering process in our model.

For the sake of completeness we should now remind the reader of the way `fft` and `ifft` work. The equations on which the algorithm is based are, for a vector x of n elements,

$$X(k) = \sum_{l=1}^{n} x(l)\, e^{-\frac{j2\pi}{n}(k-1)(l-1)} \tag{3.55}$$

and

$$x(l) = \frac{1}{n} \sum_{k=1}^{n} X(k)\, e^{\frac{j2\pi}{n}(k-1)(l-1)} \tag{3.56}$$

for discrete fourier transform (DFT) and its inverse respectively. Note that, due to scaling factors, the actual conversions between the discrete signal g and its Fourier transform G are given by the code `G=fft(g)/n` and `g=ifft(G)*n`. In our model n will correspond to the total number of samples.

3.5.2 Filter Models

Filters largely populate our model. We essentially have three main categories of analog filter models. First, we have what we called smoothing filter, with the function of shaping ideal square waves into more realistic signals, characterized by specific rise and fall times. Second, we have electrical filters simulating those that in practice will be used within the electronics surrounding the optical components. Last but not least, we modeled optical filters, which are generally employed before the receiver to suppress some of the out-of-band noise. Digital filtering is performed in the digital coherent receiver. Details are found in [12].

Every time we want to filter a signal we first bring it to the frequency domain,

```
X = fftshift(fft(x));
```

Then we multiply it by the filter frequency response $G(f)$, before transforming the resulting signal back to the time domain,

```
x_filtered = ifft(ifftshift(X.*G));
```

Note that we will often measure the filter bandwidth as normalized over the symbol rate R_S. For electrical filters we will label this normalized bandwidth as $b_e = B_e/R_S$, for the optical ones it will be $b_o = B_e/R_S$, where B_e and B_o are the actual bandwidths expressed in Hz.

3.5.2.1 Smoothing Filter

This filter is used only contextually with the generation of the analog electrical signal from the bit stream. Its function is to shape the otherwise square wave into a smoother function. Specifically, we want to be able to apply wanted rise and fall times.

To make calculations simpler, we decided to use a Gaussian filter. Its frequency response is

$$G(\omega) = e^{-\frac{\omega^2}{2\omega_0^2}}. \tag{3.57}$$

Now, we have to relate ω_0 to the rise time obtained when filtering a square wave with such a filter. When transforming $G(\omega)$ into the time domain, we get

$$g(t) = \frac{\omega_0}{\sqrt{2\pi}} e^{-\frac{\omega^2 t^2}{2}}. \tag{3.58}$$

If we now calculate the convolution between (3.58) and a step function $V \cdot \Theta(t - t_0)$, where Θ stands for the well-known Heaviside (or step) function, so that the step is located at t_0 and has a certain height V, we end up with,

$$V\Theta * g(t) = V\left(1 - \frac{1}{\sqrt{\pi}} \int_{\frac{\omega_0}{\sqrt{2}}(t-t_0)}^{\infty} e^{-t'^2 dt'}\right) = \frac{V}{2}\left[2 - erfc\left(\frac{\omega_0}{\sqrt{2}}(t - t_0)\right)\right], \tag{3.59}$$

where we have recognized the error function $erfc$, whose values are known and tabulated. By finding the values of t such that $V\Theta * g(t)$ equals $0.1V$ and $0.9V$, we can identify the rise time as being given by

$$t_r \approx \frac{\sqrt{2} \cdot 1.82}{\omega_0} \tag{3.60}$$

Given this, the code for the frequency response of the smoothing filter is very simple,

```
omega0 = 1.82*sqrt(2)/tr;
G = exp(-(FrequencyArray.^2)/(2*(omega0/2/pi).^2));
```

3.5.2.2 Electrical Filters

We have three different types of electrical filters, all of them are low-pass filters:

- Gaussian any order,
- Bessel up to the 10^{th} order,

- Butterworth up to the 10^{th} order.

A Gaussian filter of n-th order has a frequency response of the type

$$G(f) = e^{-\frac{f^{2n}}{2f_0^{2n}}}. \tag{3.61}$$

Bessel and Butterworth filters of n-th order have frequency responses in the form

$$G(f) = \frac{c_0}{c_0 + c_1 f + c_2 f^2 + ... + c_n f^n}, \tag{3.62}$$

where $c_0, c_1, ..., c_n$ are known coefficients that can be found in a multitude of sources. They depend on the desired filter bandwidth.

3.5.2.3 Optical Filters

The optical filters are band-pass filters, and as such they have a central frequency f_c different from 0. On top of this, we have to consider that the optical signal has two polarizations, and is represented as a structure in our model. We just have to filter the two polarizations separately. Four types of optical filters are implemented in our model:

- Gaussian any order,
- Matched for a square wave,
- Fabry-Pérot.

The Gaussian filter works exactly like the one discussed in the previous section. The matched filter is by definition the filter that maximizes the SNR in case of AWGN. One could calculate that for a square wave (like in the case of NRZ-OOK) under ideal circumstances. Its frequency response is a sinc(), and it is described by the code

```
G = sinc((FrequencyArray+ReferenceFrequency-fc)*
    SamplesPerSymbol*dT);
```

A Fabry-Pérot filter simulates the behavior of a grating, often used in optical communications to filter the optical signal. Without going into the details of such a device, the code to simulate it is

```
G = 1./(1+1i*2*(FrequencyArray+ReferenceFrequency-fc)/
    bandwidth);
```

3.5.3 Spectrum Analysis

Our model of spectrum analyzer is utterly simple. The spectrum of a signal is nothing else than its power spectral density, as defined in Section 2.1.2. The power spectrum can be obtained by taking the power of the Fourier transform of the signal itself. This is equivalent to calculating the spectral density as described in Section 2.1.2. This is a widely accepted way of determining the power spectrum of a signal, the reasons why these two methods give the same result have not been studied within this work and should be subject of further investigation and understanding.

Notice that in the case of an optical signal we have two polarizations. We calculate the Fourier transform of both and then we sum the squares of their absolute values. For an electrical signal we just Fourier transform the signal and then take the square of its absolute value. Let us show some of the main code for an optical spectrum analyzer,

```
N = length(FrequencyArray)
E_in_f.x = fftshift(fft(E_in.x))/N;
E_in_f.y = fftshift(fft(E_in.y))/N;
power_spectrum = Power(E_in_f);
plot(FrequencyArray,10*log10(power_spectrum));
```

4

Simulations

This chapter contains the results of many simulations run with our model. Of course this is just a small part comprising the most interesting, significant, and sometimes novel results. We tried to avoid reporting results that were already present in other sources (one can find an impressive amount of information about multi-level modulation formats and their performances in [6]) and overwhelming the reader with torrents of plots. We hope we managed to find a good balance.

We will start by validating our model, comparing it to the theory (when possible) and to other models found in the literature, then we will present a study of our PMCW pulse source. We will continue with an analysis of the non-idealities of an IQ modulator, before concluding with simulations of a complete multi-level modulation system employing OTDM, coherent receiver and DSP.

Let us set a few default values here. SPS will be 32 per channel, so a 4-channel OTDM system will have 128 samples per symbol. The PRBS seeds will be 9-bit long for all modulation formats. The reference frequency 193.1 THz, and the rise and fall times of the electrical signals driving the modulators $0.25/R_S$. We will not simulate shot and thermal noise, no non-idealities (linewidth, RIN, timing jitter, etc.) will be present unless otherwise specified. The split step Fourier method we employ is the one in which the step size depends on the relative local error, and the goal error δ_G is set to 0.001. The optical filter will be Gaussian 1^{st} order, the electrical one Bessel 3^{rd} order, with $b_o = 2.5$ and $b_e = 0.75$ respectively (we remind the reader that these normalized bandwidths were defined in Section 3.5.2). These values are found in [6] as averagely good for most modulation formats.

So, if we do not state otherwise, these will be some of the system parameters. By remarking this now, we will shorten the list of parameters to be reported contextually with each simulation. Most often the exact parameters will be reported in the text, while the figure captions will be shortened for readability. The OSNR sensitivities will be determined as defined in Section 2.4.5.

Let us also specify that we will find the abbreviation "B-to-B" in the legend of some figures. That simply means "back-to-back" and refers to a simulation in which we have received the signal just after the transmitter, without fiber.

4.1 Model Validation

During and after the development of this model of optical communication system, we have kept testing the different blocks and units. The reader will surely be happy to know that we do not intend to report these tests here, apart from a few very important ones. First, we test the fiber model comparing it to the theoretical behavior under specific conditions. Second, we compare the performance of our system to references found in literature on the subject. We do this by looking at the BER-OSNR curves produced by our model and those found in several sources.

4.1.1 Fiber Model Testing

We start by testing our model of optical fiber. We do not bother the reader with the testing of fiber losses, which are very straightforward, but start with dispersion then move on to nonlinearities.

4.1.1.1 Second-Order Dispersion Testing

As explained in Section 2.3.3 a pulse broadens while propagating in a fiber (depending on the values of chirp and β_2 there can be an initial shrinkage). Figure 4.1(a) shows the broadening of an unchirped Gaussian pulse 10 ps wide (FWHM) after 3.6 km of propagation over a fiber with $D = 17$ ps/(nm·km) and no higher-order dispersion. Note that the pulse is described by 128 samples, so it looks quite smooth. Of course this is not enough to state that we implemented dispersion correctly. A way to do this is to compare the numerical outcome with a theoretically known one. Let us do so.

The broadening of a Gaussian pulse in a fiber with only second-order dispersion can be quite easily analytically calculated as (see [4])

$$\frac{T(z)}{T_0} = \sqrt{1 + \left(\frac{\beta_2 z}{T_0^2}\right)^2}, \tag{4.1}$$

where T_0 and $T(z)$ are the pulse full widths at 1/e of the peak power at the input of the fiber and after a fiber length of z respectively. In Figure 4.1(b) we show how our numerical results overlap perfectly with the theoretical curve. The parameters are the same as the ones of Figure 4.1(a). We repeated similar simulations with other parameters, always obtaining a perfect match. We do not show these results for brevity. We should have also tested the third-order dispersion, but we could not for reasons of time. As a consequence, higher-order dispersion is never simulated in this thesis.

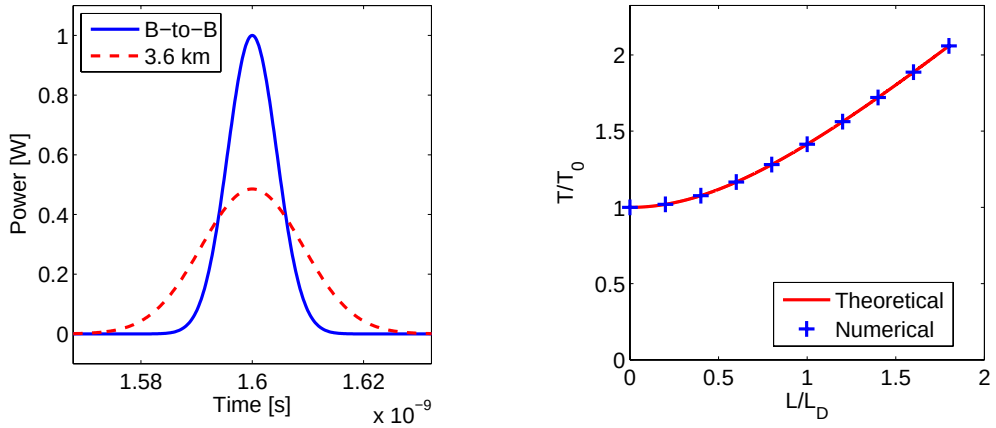

(a) (b)

Figure 4.1: For an unchirped Gaussian pulse, (a) broadening after 3.6 km, (b) relative broadening as a function of distance (normalized over the dispersion length).

4.1.1.2 Nonlinearities Testing

To test the fiber nonlinearities we proceed in two steps. First, we check that a Gaussian pulse undergo a phase shift of -1 rad when propagating over a nonlinear length of fiber. This is verified in our model. Second, we check that nonlinearities and dispersion work together. This is readily done by propagating a first-order soliton (see Section 2.3.4).

We use a fiber with $D = 17$ ps/(nm·km) , no higher-order dispersion and $\gamma = 3$ 1/(W·km) , the pulse is clearly a hyperbolic secant and we set a peak power of 10 mW. 128 samples describe the pulse. Being the soliton of 1^{st} order, the width of the pulse can be calculated from (2.72) by setting $N = 1$. It is about 27 ps. Theoretically, the soliton should be perfectly preserved during propagation. We propagate the pulse over a fiber length of $40L_{nl}$, which is approximately 1300 km, and we repeat the simulation with two different precisions for the split-step Fourier method. In Figure 4.2(a) we have set $\delta_G = 0.1$ and, as a result, the soliton is not properly preserved, with a loss of energy (calculated integrating the power over the entire time window with Simpson's rule) of about 7%. In Figure 4.2(b) we have used a better precision, namely $\delta_G = 0.001$. The computational time is approximately tripled, but the result is very satisfactory, with at first sight a fully preserved soliton and a loss of energy of just 0.1%. We can conclude that our model of fiber nonlinearities is very likely correct.

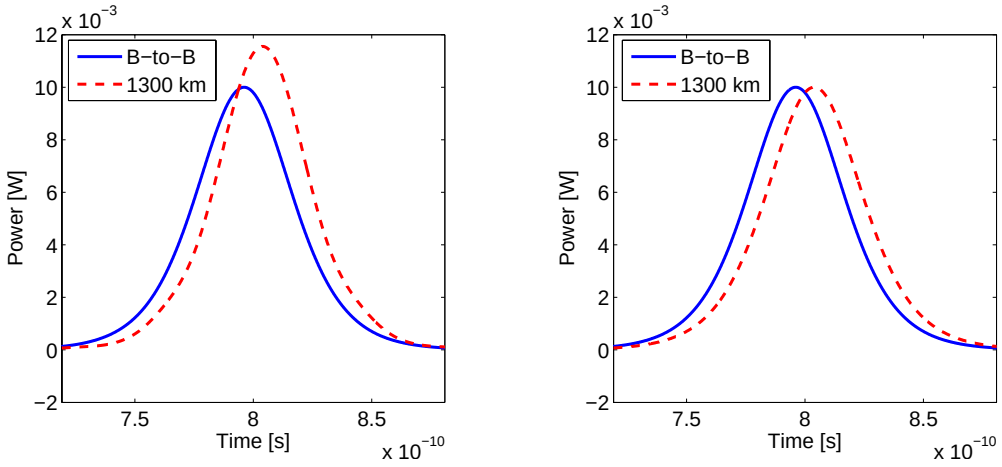

(a) (b)

Figure 4.2: A first order soliton is propagated over nonlinear fiber. We compare the original pulse with the one after 1300 km (note that we have artificially introduced a slight delay to make the pulses more distinguishable). The split step Fourier is carried out with (a) $\delta_G = 0.1$, (b) $\delta_G = 0.001$.

4.1.2 System Performance Comparison

We begin by comparing our numerical results to the ones found in a milestone paper [1]. Here the modulation format is a NRZ-OOK and there is no fiber. Rise and fall times

are 0, so that we have a perfect step function. Curves BER-OSNR are generated for different configurations of optical and electrical filters. OSNR and SNR are of course defined as explained in Sections 2.1.11 and 2.1.12. Specifically, we apply ASE noise only on one polarization, so $p = 1$. The results of this comparison are found in Figure 4.3. Let us discuss them one by one.

The first system configuration consists in a matched optical filter and no electrical filter. This establishes the quantum limit for an NRZ-OOK, since the matched filter by definition optimizes the noise performance of the system. The correspondence is perfect (see Figure 4.3(a)), and this is a very reassuring result. Hitting the quantum limit is indeed great evidence of correctness and consistency for our model.

The curves are also perfectly overlapped (see Figure 4.3(b)) in the case of a first-order Gaussian optical filter and a first-order Gaussian electrical filter with normalized bandwidths of $b_o = 8$ and $b_e = 0.7$ respectively.

We then looked at other two configurations: both feature a Gaussian 1^{st} order with $b_0 = 8$ as optical filter, the first has an RC electrical filter (just another name for a Bessel 1^{st} order) with $b_e = 0.7$ (see Figure 4.3(c)), while the second has a Butterworth 2^{nd} order with $b_e = 0.7$ (see Figure 4.3(d)). In both cases our system shows a slightly (about 1 dB at a BER of 10^{-3}) better receiver sensitivity. The difference is quite small, but still unexplained. From [1], it is not clear how sampling point and threshold current are optimized (if they are at all). A small inaccuracy in the sampling point could lead to the 1-dB penalty we have noticed. Another possible explanation would arise from the fact that the electrical filters employed in these two simulations introduce some slight delay that has to be compensated. Maybe in [1] this was not done.

We followed up with a comparison with [2]. Here the noise is applied on both polarizations, so $p = 2$. The modulations formats employed are NRZ-DBPSK (see Figure 4.4(a)) and NRZ-DQPSK (see Figure 4.4(a)). Rise and fall times are once more zero, no fiber is in between transmitter and receiver and, for both simulations, the optical filter is a Fabry-Pérot with $b_o = 3.2$ and the electrical filter a Bessel 5^{th} order with $b_e = 0.55$. We obtain perfect matches in both cases. This is very comforting, since we have now good agreement with two different sources, moreover we have extended the comparison to other modulation formats and we have applied the noise in both polarizations with nice results.

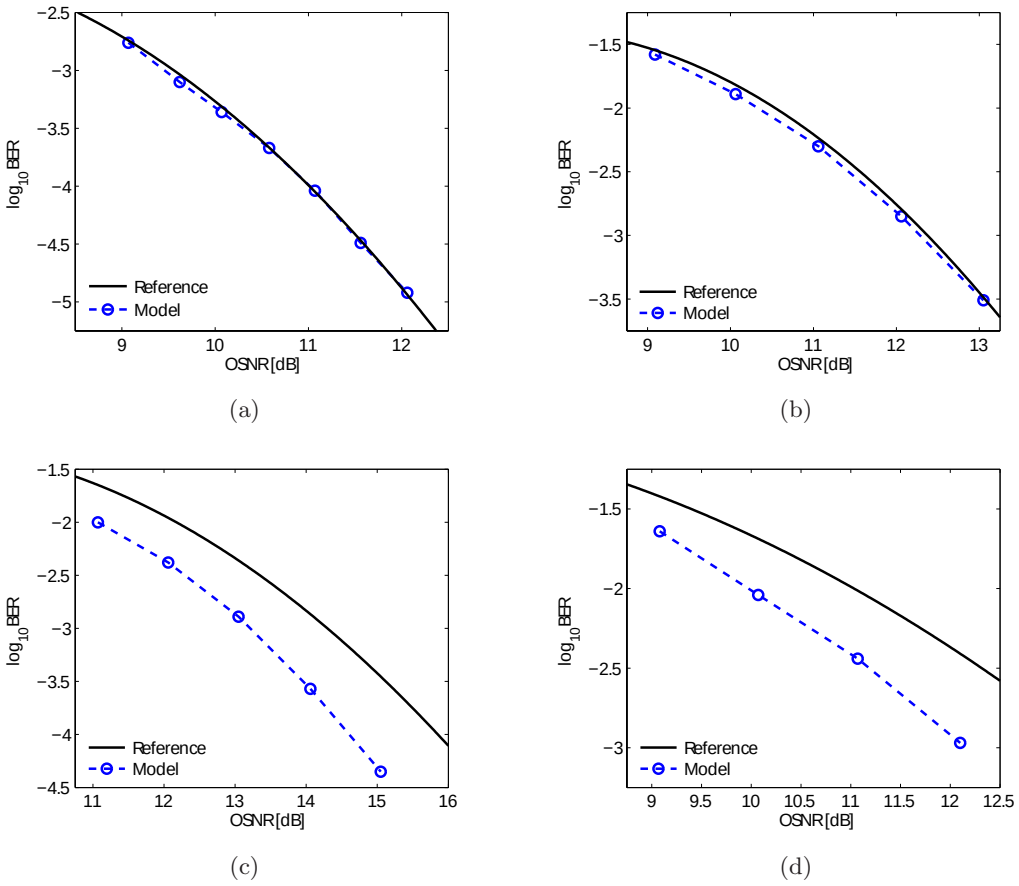

Figure 4.3: BER-OSNR curves of a NRZ-OOK modulation for our model and references provided in [1] for four different filters configurations. (a) Matched optical filter and no electrical filter, (b) Gaussian 1^{st} order for both optical and electrical filters, (c) Gaussian 1^{st} order optical filter and RC (Bessel 1^{st} order) electrical filter, and (d) Gaussian 1^{st} order optical filter and Butterworth 2^{nd} order electrical filter.

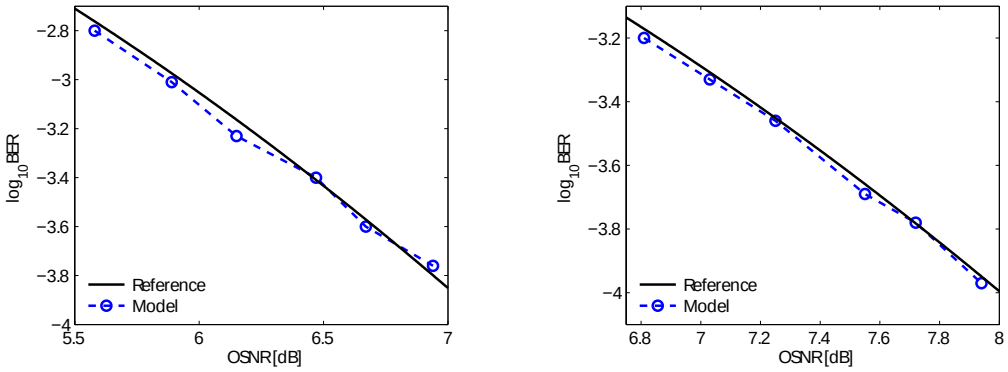

Figure 4.4: BER-OSNR curves for our model and references provided in [2]. (a) NRZ-DBPSK and (b) NRZ-DQPSK.

Finally, we compared our model to the one of [3]. Once more, the modulations format employed are NRZ-DBPSK (see Figure 4.5(a)) and NRZ-DQPSK (see Figure 4.5(b)) and $p = 2$[1]. The filters are a Gaussian 1^{st} order optical with $b_o = 2.2$ and a Butterworth 3^{rd} order electrical with $b_e = 0.7$, rise and fall times of the driving signals $0.44T_S$. We obtained a perfect overlap in the case of DQPSK, but our model presents a penalty of approximately 0.4 dB at a BER of 10^{-3}. This could not be explained, however such a small difference could be due to small details we might have failed to match between the two models.

To conclude, we can state that the comparison has given good results and that we have a perfect match in most cases and a fairly acceptable match in the few others. Note that we have not reported the baud rate of any simulation. This is just because the system in these cases was independent of it, since there was no fiber (dispersion depends on the baud rate) and the filter bandwidths were given as normalized.

4.2 PMCW Pulse Source Investigation

We will hereby study the behavior of the PMCW pulse source. First, we try to get acquainted with the functioning of this module by observing how some pulse parameters like peak power and FWHM depend on the pulse source configuration. Second, we try

[1] Actually, we could note retrieve this piece of information from [3]. However, with noise in both polarizations, we get a perfect overlap for the DQPSK curves, so we assumed this was the case.

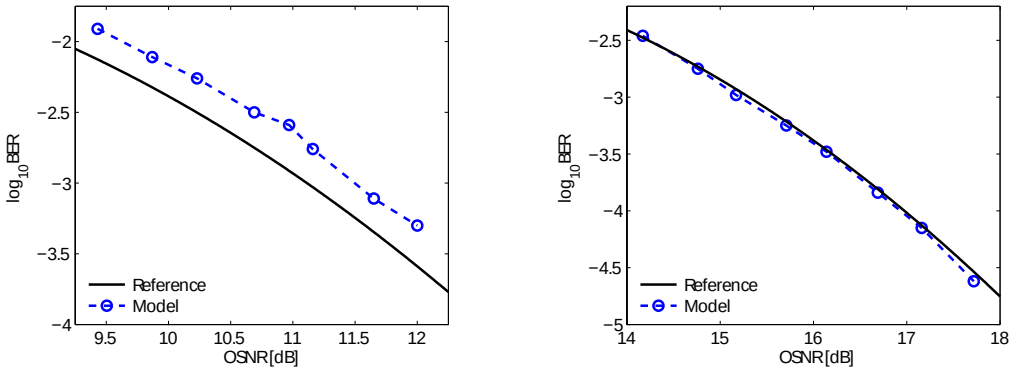

(a) (b)

Figure 4.5: BER-OSNR curves comparison between our model and [3]. (a) DBPSK and (b) DQPSK.

to determine the suitability of this pulse source for an OTDM system, and we determine a possible maximum number of multiplexable channels. Finally, we try to analyze the relation between the power penalty that occurs when we multiplex our pulses with two parameters describing the OTDM cross-talk.

4.2.1 Introductory Study of the Pulse Source Behavior

In this section we will study the behavior of the pulse source described in Sections 2.2.1.5 and 3.2.2.5. To have a nice detail of the pulses, we will set SPS to 2048 and shorten the seed to just 3 bits, since we do not need to determine any BER for now. Moreover, we will assume a standard SMF, for which $D = 17$ ps/(nm·km) and no higher-order dispersion is present.

First, we want to see how the pulses depend on the different parameters. Let us set $R_S = 40$ GBd/s so that the pulses are produced at a frequency of 40 GHz. Additionally, we fix the fiber length to 330 m. We produce pulses for both configurations of our PMCW pulse source, i.e. without and with the MZM as pulse carver just after the laser. We do this for different values of B, setting MI accordingly so that (3.22) be verified. The result is shown in Figure 4.6. As one can notice, for low values of B the pulses are barely formed. By increasing B they become more apparent and start developing side peaks. When we exaggerate the pulses get fragmented and useless for transmission.

We can already draw a simple conclusion by observing the pulses in the case a pulse carver is utilized and in the case it is not. In the latter case, the pulses have an unacceptably low extinction ratio, in most cases comprised between 3 and 7 dB. We will have a chance to see how important it is to have a low ER when operating an OTDM system (see Section 4.2.3).

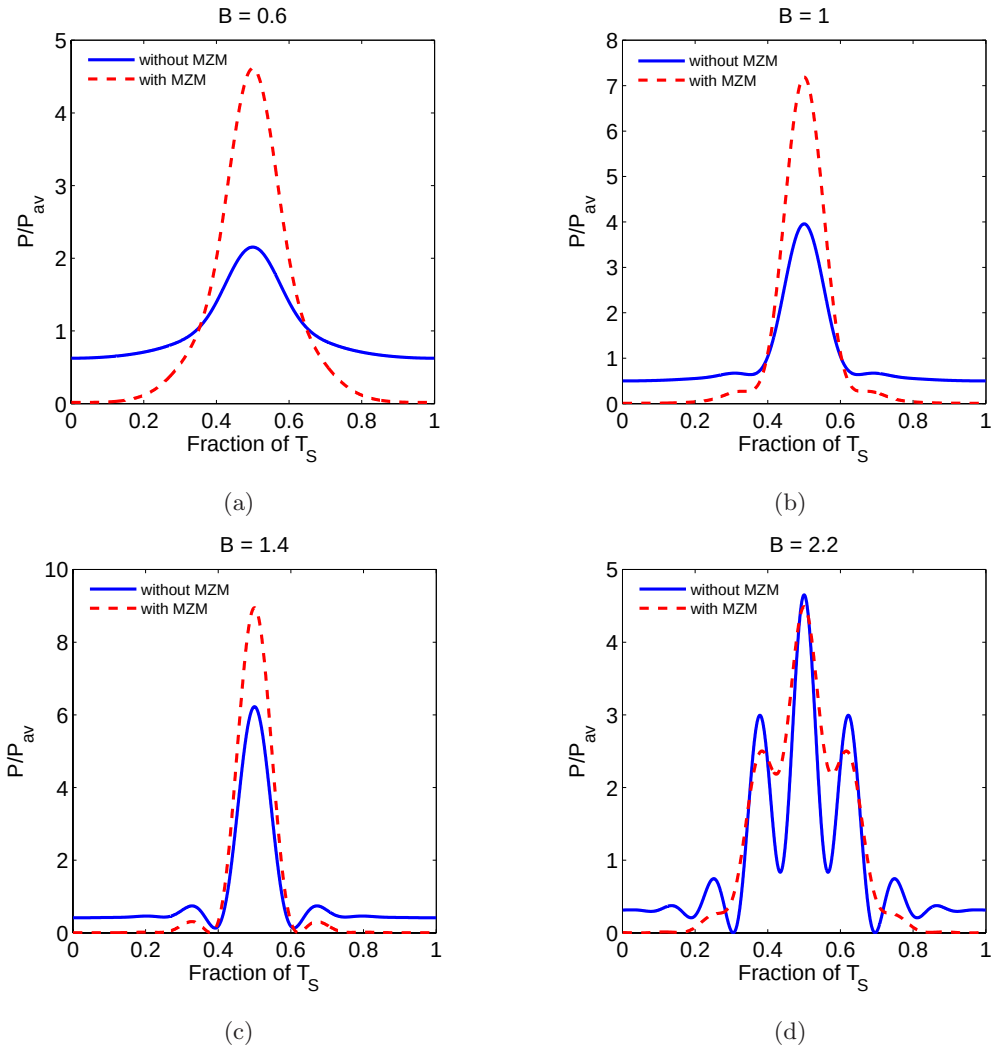

Figure 4.6: Pulses generated at 40 GHz by our PMCW pulse source without and with pulse carver (MZM) for (a) $B = 0.6$, (b) $B = 1$, (c) $B = 1.4$, and (d) $B = 2.2$.

Now, to have a better understanding of the pulse source behavior, we repeat the exact same simulations at a pulse rate of 10 GHz. The outcome can be visualized in

Figure 4.7. As expected, the pulses look fairly different. Interestingly, one may notice how for $B = 1$ the shape of the pulses is very similar to the one obtained for the same B at 40 GHz. This is not a coincidence, when $B = 1$ dispersion and chirp are balanced so that slowly traveling frequencies and fast traveling frequencies meet exactly at the end of the fiber span. For lower values of B the pulse is not fully formed yet, for values above this threshold the fast frequencies overtake the slow ones and the pulse starts breaking up in a multitude of peaks.

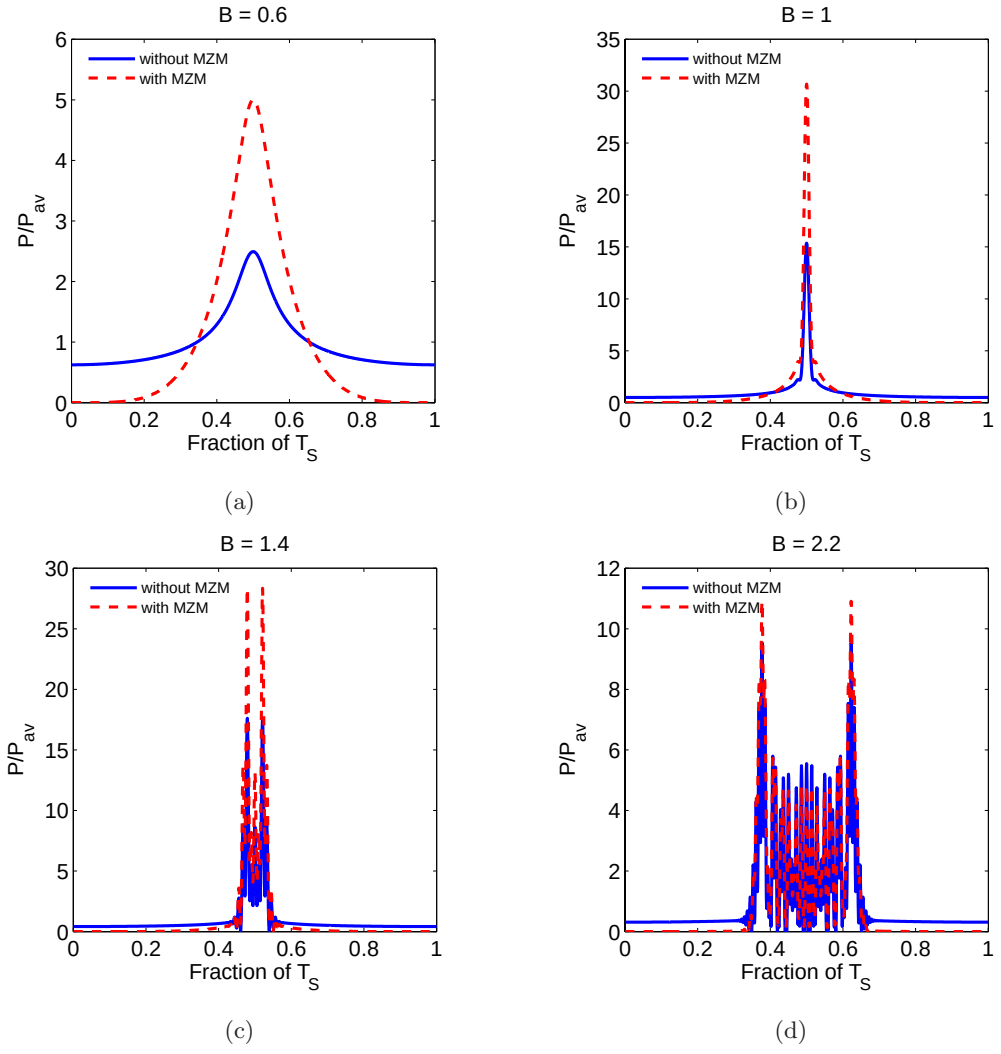

Figure 4.7: Pulses generated at 10 GHz by our PMCW pulse source without and with pulse carver (MZM) for (a) $B = 0.6$, (b) $B = 1$, (c) $B = 1.4$, and (d) $B = 2.2$.

For the given reasons, setting the parameters so to have $B = 1$ is a good starting point when generating pulses with this method. However, this is not the best way of creating pulses for an OTDM transmission. Let us first look at how we could improve our pulses while keeping their shape nice. We generate pulses for a variety of values of MI, and we set the fiber length so that this sort of rough optimal value $B = 1$ be maintained. For each instance of the pulses, we measure the FWHM and the peak, and we do that for both the configuration with MZM and the one without. The pulse rate is 40 GHz for this simulation. In Figure 4.8 one can see the results. It should be noticed how we can both narrow the pulse and increase its peak by having a larger MI. In practice, it is quite difficult to have an MI larger than 3 or 4. V_π is most generally comprised between 3 and 6 V (see Section 2.2.3.1) and amplifiers delivering voltages above 20 V are quite bulky and release a lot of heat. Figure 4.8(b) might suggest that the usage of a pulse carver increases the peak power of the pulses. This is not true, and the red line stays above the blue one because the average power for pulses carved by means of a MZM is lower.

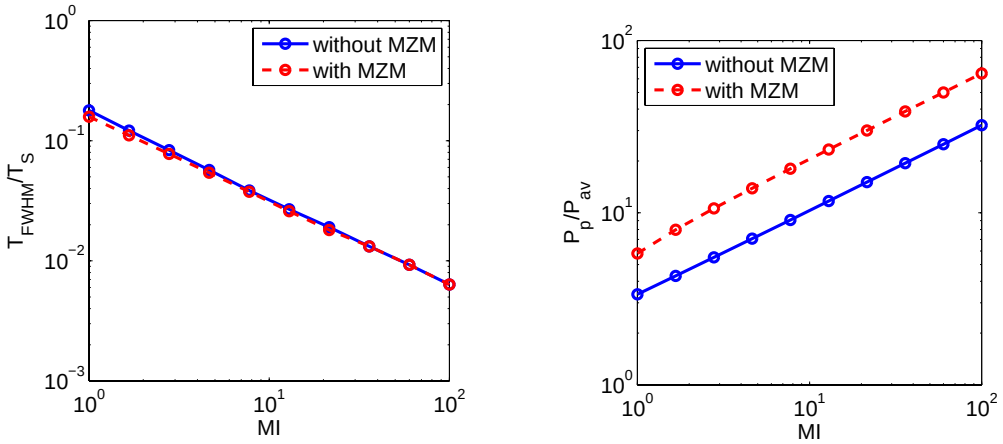

(a) (b)

Figure 4.8: As a function of MI, keeping $B = 1$, and for a PMCW pulse source without and with pulse carver (MZM), (a) pulse FWHM normalized over the symbol slot, and (b) peak power normalized over the average power.

4.2.2 Lower Limit for OTD Multiplexing

For our purposes, a good pulse is a well confined one[1]. A measure of the energy confinement is given by the rms value of a pulse, which was defined in Section 2.1.7. Since our pulse is described by samples (as many as 2048 in this case, which makes the quantization error quite negligible), we substitute the integral of (2.33) with a sum. The code is

```
den = sum(pulse_train(peak_index-SPS/2+1:peak_index+SPS/2));
num = 0;
for k = 1:SPS/2
    num = num+pulse_train(peak_index-k+1)*((k-1)*dt)^2 +
        pulse_train(peak_ind+k)*(k*dt)^2;
end
T_rms = sqrt(num/den);
```

T_{rms} is a very good way of determining the suitability of a pulse for OTDM applications. T_{FWHM} is not reliable in most situations. First, it does not take into account the shape of the pulse. If we have two significant side lobes, they would be very detrimental for the adjacent channels, but they might be lower than half the power and be ignored in the calculation of FWHM. As a consequence, T_{FWHM} is not a very interesting quantity for an OTDM system, while T_{rms} is a very nice one. Let us provide an intuitive explanation. In Figure 4.9(a) we show a pulse generated for $R_S = 40$ GBd/s, $L = 330$ m, $B = 1.4$, and using the pulse carver. It should be very clear how most of the energy (more than 99%) is confined in a time interval of $6T_{rms}$ centered on the peak. In Figure 4.9(b) we do the same but this time with no pulse carver. The pulse FWHM is roughly the same, but the rms value is by far larger, taking into account the very poor ER. Hopefully, one should have now grasped that T_{rms} is a more proper way of measuring a pulse confinement.

We can now determine the value of B that minimizes the rms of the pulses. This is done for a pulse rate of 40 GHz and both the configuration with pulse carver and the one without. We repeat for two fiber lengths, 330 and 1000 m. The results are reported in Figure 4.10. Clearly, the curves change for different fiber lengths, but the optima remain the same, namely $B = 1.4$ and $B = 2$ for the two configurations respectively. This holds true also when we change the pulse repetition rate.

[1] We might use pulses to carry information or as local oscillator, in both cases we would like them to be as confined as possible to limit the cross-talk between our OTDM channels.

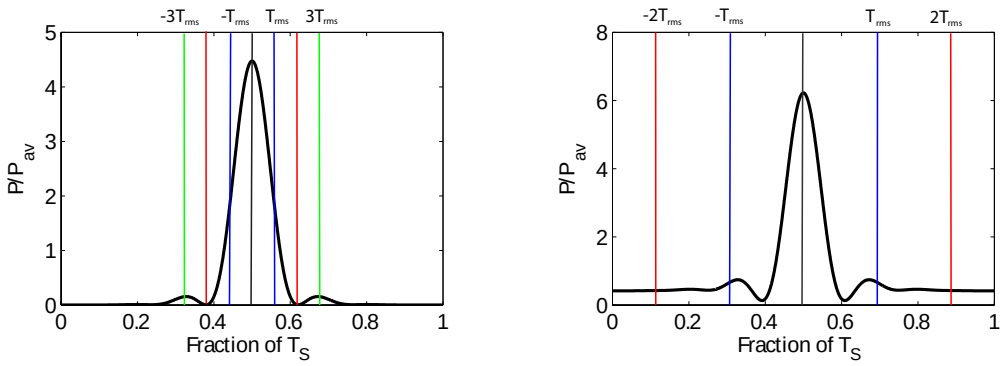

(a) (b)

Figure 4.9: The rms of a pulse is a measure of the energy confinement of a pulse with respect to the peak. Pulse generated with a PMCW pulse source (a) with pulse carver and (b) without pulse carver.

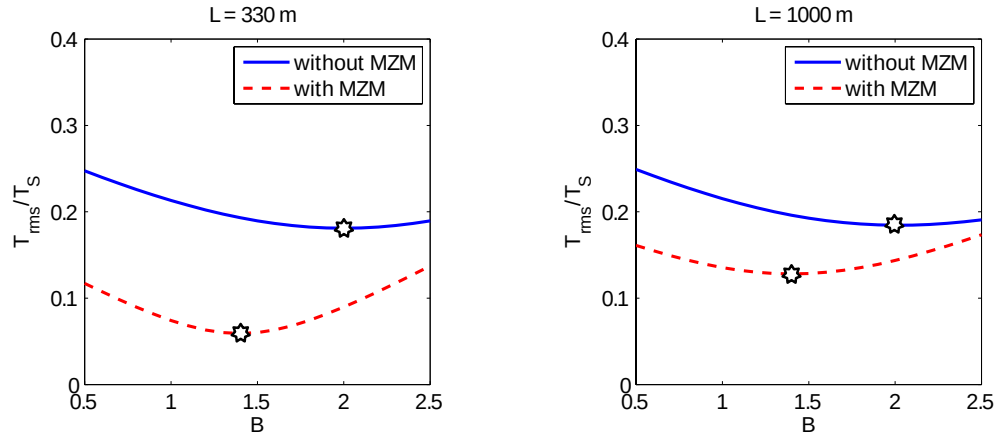

(a) (b)

Figure 4.10: T_{rms}/T_S as a function of B for a fiber length of (a) 330 m and (b) 1000 m.

After this last finding it would be interesting to see how the rms of the pulse depends on MI while keeping B at the optimal values of 1.4 for the configuration with the pulse carver and 2 for the one without. This is shown in Figure 4.11 for a pulse rate of 40 GHz. Unfortunately, it looks like we cannot confine the pulse below a certain level, no matter how large an MI we can get. This sets a lower limit to the number of channels we can multiplex together. The minimum T_{rms} for the red dotted curve of Figure 4.11 is $0.044 \cdot T_S$. If we want less than 1% energy falling into neighboring channels, than the maximum number of channels we can multiplex is given by

$$N_{max} = \frac{T_S}{6 \cdot T_{rms}^{min}} \approx 3.8. \tag{4.2}$$

Consequently, we cannot multiplex more than 3 channels. If the constraint is set to $4 \cdot T_{rms}$, than we get

$$N_{max} = \frac{T_S}{4 \cdot T_{rms}^{min}} \approx 5.7, \tag{4.3}$$

and the energy spilling into the neighboring channels is at most 5%[1].

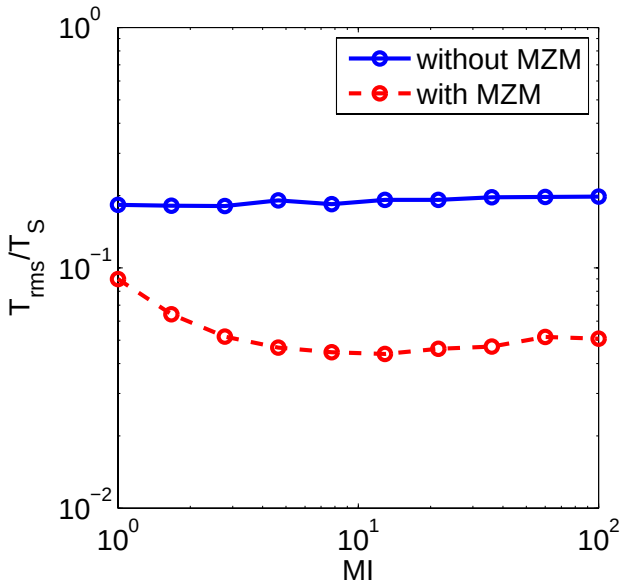

Figure 4.11: T_{rms}/T_S as a function of MI and keeping $B = 1.4$ for the configuration with the MZM and $B = 2$ for the one without.

To conclude this section, we generate 40 GHz pulses for a grid of values of MI and L. SPS is reduced to 256 to speed up the simulation. From now on we will only work

[1] This can be estimated by actually measuring this energy by integration for various pulse shapes.

with the pulse carver, since we have sufficiently shown how fundamental it is for being able to use this pulse source within an OTDM system. The pulse carver will have an ER of 15 dB, which is a realistic value as one can find out by browsing through some manufacturers' websites. We produce a contour plot where the color depends on the rms value of the pulses. As one should notice right away, the lowest values follow the line corresponding to $B = 1.4$, which is in accordance with what we have found out so far.

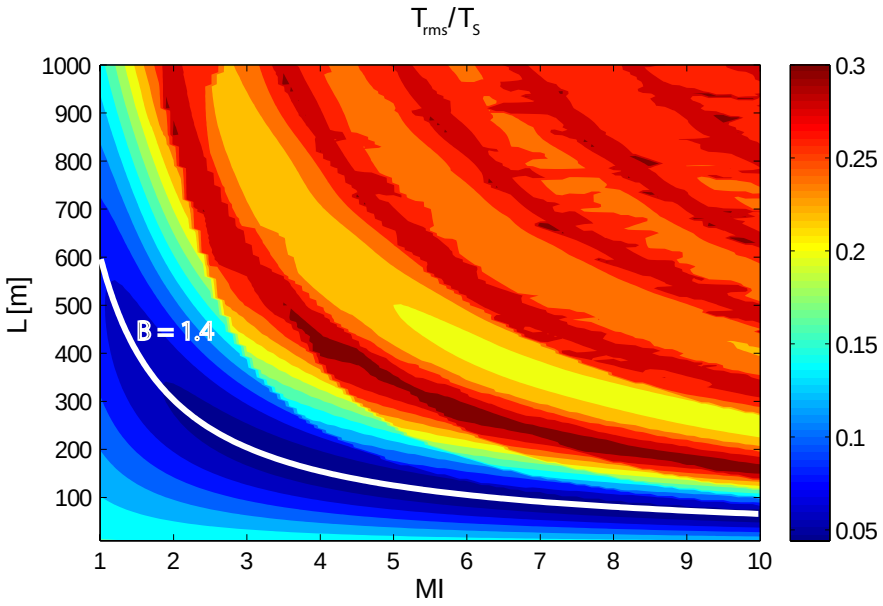

Figure 4.12: Contour plot of T_{rms}/T_S as a function of MI and L.

4.2.3 OTD Multiplexing Penalty

In this section, we would like to test the way cross-talk impairs an OTDM system in which our PMCW pulse source is used. Cross-talk will generate a penalty, and we would like to test how different pulse parameters are related to this penalty. Let us first introduce two different ways of measuring cross-talk in an OTDM system. The first one is called *pulse tail extinction ratio* (PTER), and consists in measuring the ratio between the pulse peak and the highest point in the adjacent channel slot (see Figure 4.13, blue arrow, and refer to [36]). It is generally expressed in dB. The second way of assessing cross-talk is by measuring the energy that a pulse "spills" in the adjacent

channel. For simplicity, we will define this quantity E_{spill}. Note that we define it as the energy in only one of the two adjacent OTDM slots (see Figure 4.13, red area).

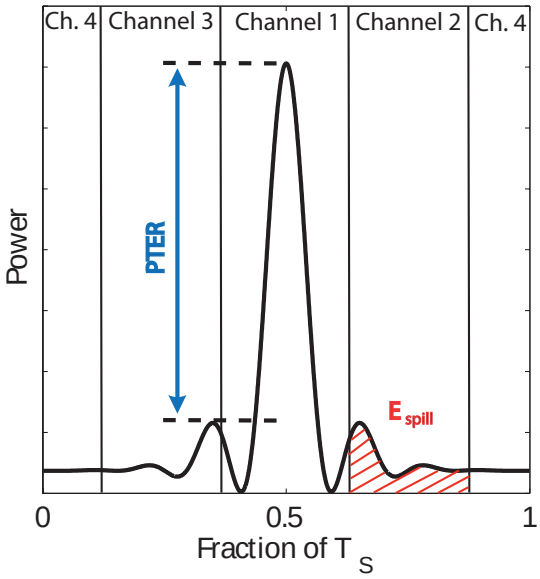

Figure 4.13: Definitions of PTER and energy spill for an OTDM signal with 4 channels.

Clearly, not all the points are actually suitable for employment in an OTDM system. The goal is to select a set of pulses on which to calculate the power penalty as a function of PTER and E_{spill}. In general, we would want to use pulses with a central dominant peak, and quite low side peaks. It is difficult to be quantitative in this discrimination. Surely one wants to have an evident peak in the middle. In the case we use this pulse source as LO, we want to make the signal beat in correspondence of the peak to improve the sensitivity and the quality of the demultiplexing (see Sections 2.4.8 and 2.4.10). If the signal carries information, we will have to optimize the sampling point on one of the peaks. More peaks mean that more energy is wasted in points we will not detect. Let us remark that this is a purely qualitative discussion, and that only an actual BER test within a complete system could give us an answer. For now, we will discard the pulses with double main peaks (symmetric peaks form around the middle of the symbol slot for some combinations of parameters) and the ones with a rms value larger than $1/8T_S$, since they do not allow for multiplexing even two channels with the rule stating that a channel occupies $4 \cdot T_{rms}$. Consequently, the contour plot results a bit trimmed.

The result is shown in Figure 4.14. The white thick line delimits the area in which we select our pulses (one for each point of a grid with an MI step of 0.2 and an L step of 20 m),

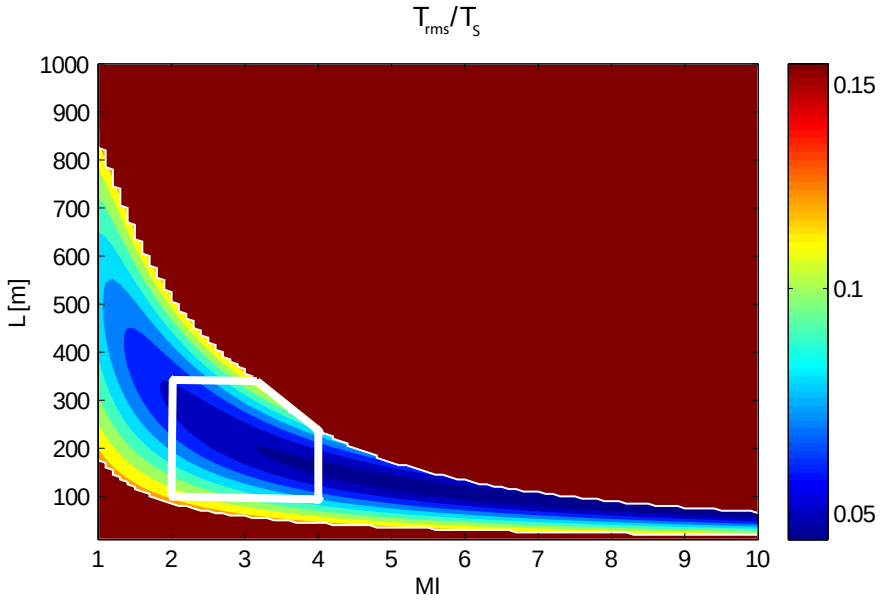

Figure 4.14: Contour plot of T_{rms}/T_S as a function of MI and L, where we have limited ourselves to pulses suitable for OTDM systems (according to the qualitative analysis explained in the text) and bordered the area in which we select the pulses to simulate.

Our intention is now to asses the back-to-back power penalty deriving from the cross-talk do to the multiplexing of these pulses in an OTDM system. We do this with an RZ-OOK, the seed is a 7-bit one, SPS goes back to a value of 128, the rise time for the electrical signal is set to $0.25 * T_S$, the base rate is 40 GBd/s, and the ASE noise is imposed only in one polarization. We simulate pulses within the bordered area in Figure 4.14, and then we first transmit the pulse stand alone, assessing the OSNR corresponding to a BER of 10^{-3}. Afterwards, we perform an OTDM multiplexing of four channels using the multiplexer described in Section 3.2.5, we demultiplex one channel with the demultiplexer described in Section 3.4.7, we add the noise[1], and we receive. The OSNR sensitivity at 10^{-3} is determined and a penalty results from the

[1]Since the OSNR depends on the average power, demultiplexing prior to imposing the noise is necessary to then compare the sensitivities obtained with a single channel and the OTDM system in a meaningful way.

difference between the two sensitivities. As a result, we will have a power penalty for each point in the grid. For each pulse we also measure PTER and E_{spill}.

As a term of comparison, we do the same as above for a ML laser emitting ideal Gaussian pulses with duty cycles from 0.12 to 0.23. In Figure 4.15(a) one can notice how the power penalty grows for smaller PTERs (very much expected), but also how dispersed the points are. This means that measuring the PTER of a pulse is not necessarily a good way of assessing the impact of cross-talk. The points are all around the curve relative to the Gaussian pulses, which is much smoother.

In Figure 4.15(b) we have the same but for E_{spill}/E_{tot}, where E_{tot} is the total energy of the pulse. In this case there is less agreement between the curve relative to the Gaussian pulses and the green dots. On the other hand, the points obtained by means of our PMCW pulse source are a bit less dispersed than before.

We conclude that neither PTER nor E_{spill} are very reliable ways of assessing the impact of cross-talk. We would probably prefer using the PTER since it is definitely easier to determine from a pulse train.

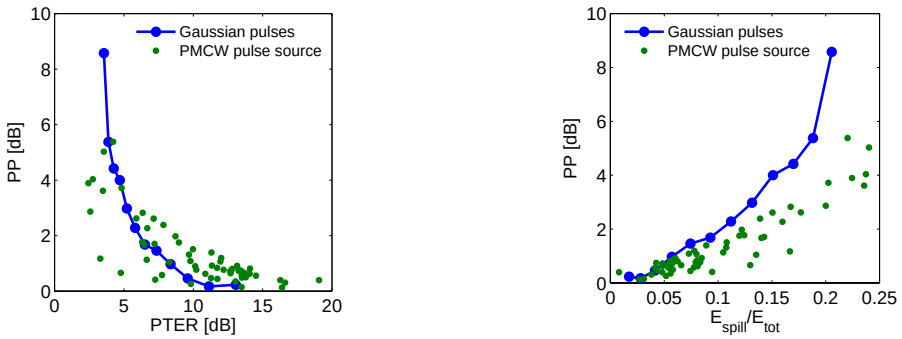

(a) (b)

Figure 4.15: Power penalty deriving from multiplexing 4 OTDM OOK channels as a function of (a) PTER and (b) E_{spill}. The green dots are for pulses obtained by means of our PMCW pulse source and the blue ones are for Gaussian pulses.

4.3 IQ Modulator Non-Idealities

In this section the goal is to look at the effect of some of the non-idealities that can affect an IQ modulator (see Section 3.2.4.3) and assess their impact both qualitatively and

quantitatively. To our knowledge this has not been done before. We believe this would be very interesting, since IQ modulators are employed in both QPSK and 16QAM modulations.

Of course, one needs to study a specific case. We decided to consider an NRZ-DQPSK signal with direct detection. We will observe the signal in three different ways: the constellation after modulation, the optical power after modulation, and the photocurrent after detection. We will set all the other system parameters to their ideal value, and we will perform a back-to-back detection. Apart from the calculations of power penalties, all simulations will be performed without optical and electrical filters. This is done to highlight the effects of the studied non-idealities.

We take into account three non-idealities:

- The power split ratio r at the input of the interferometric structure,
- The bandwidth limitation of the phase modulators within the MZMs,
- A possible delay between V_I and V_Q.

Note that we modeled many other non-idealities, as described in Section 3.2.4.3, but they are in our opinion either very unlikely to be noticeable (for example, we would not expect a significant delay between the electrical signals driving the two arms of a MZM, since the paths are optimized during the manufacturing process), or related to the three we mentioned above (for instance, we have many power split ratios in an IQ modulator, but we will study only one of them).

Our analysis will be repeated for each of the three non-idealities listed above, and divided into two parts. First, we will carry out a qualitative observation of their impact on the signal, both transmitted and received. The objective here is to understand the behavior of the transmitter and possibly to help recognize the source of some often seen deformations of the signal. Second, we will determine the power penalty associated to their presence, to give a measure of how impairing they can be for a multi-level modulation system. For the first category of simulations, we will have as many as 512 samples per symbol, to have totally smooth signals. The seed will be a 7-bit one, so to have a sufficiently long sequence of symbols and cover quite a few combinations. When not differently stated, rise and fall times will be $0.25T_S$. For the BER determination we apply differential encoding so that direct detection be possible, we decrease SPS to 64,

and we reintroduce optical and electrical filters with standard values as stated at the beginning of this chapter. The rest of the parameters will also be set to their default values.

Before we begin, we just want to show how a clean and ideal signal looks like, so that we will be able to make comparisons later on. Let us start by the constellation (see Figure 4.16). The four symbols will always be at $\pi/4$, $3\pi/4$, $-3\pi/4$, and $-\pi/4$ because we set the initial phase of the laser to 0 for simplicity, and we work at f_{ref}, so that there is no linear phase shift due to a $f_0 - f_{ref} \neq 0$. The red points correspond to sampling the signal at half the symbol slot, the black lines are traces of the movements of the signal over the complex plane, between one sampling point and the following one. They are as one would expect: straight lines between points, since the electrical signals are perfectly synchronized. Note that all values are normalized over the highest value taken by the signal.

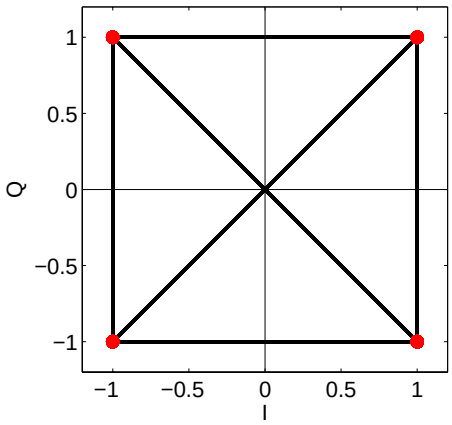

Figure 4.16: For a QPSK signal, constellation after modulation.

To understand Figures 4.17(a) and 4.17(b), one needs to know the concept of *eye diagram*. The eye diagram of a signal is what one obtains by overlapping the signal with a periodicity equal to a finite number of symbol slots. For example, we plot the first four symbol slots, and then we plot the following four on top of the previous ones, and so on. This is what we do with the time representation of optical power and of photocurrent. Their shapes should not surprise the reader if the functioning of MZMs has been understood. All values are given in arbitrary units, since we care about the deformations, not the actual values.

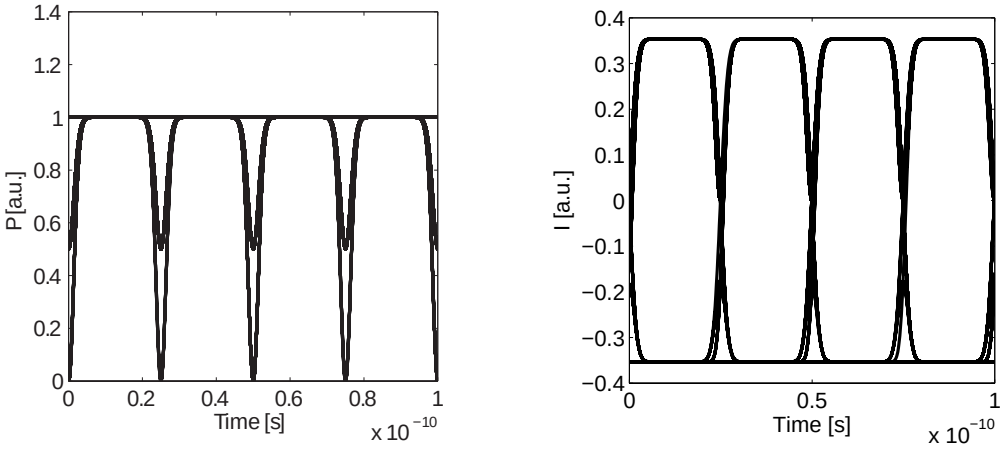

(a) (b)

Figure 4.17: For a QPSK signal (a) optical power eye diagram after modulation and (b) photocurrent eye diagram.

4.3.1 Power Split Ratio

The power split ratio r is here defined as the ratio between the power measured at the input of the Q-arm and the one at the input of the I-arm. In figure 4.18 we observe what happens to the constellation when we move r from its ideal value of 1/2, specifically it is set to 0.55 and 0.65. As expected, the quadrature component of the signal becomes more intense, so that the square formed by the four symbols on the constellation gets squeezed. Note that the modulation span on the Q arm increases, but the points preserve a normalized amplitude of 1 only because we operate the normalization with the maximum value of the electric field. Potentially, this could turn into a power penalty, since the distance on the constellation between any two points is not optimized anymore. This is not so easy to forecast when employing direct detection, we will have to look at the BER performance in a while.

In Figure 4.19 we visualize the optical power eye diagram. There is no real effect on the high level, which is still 1 (normalized value), as expected since no power is lost, just split differently between the two branches. The only noticeable difference with respect to the ideal signal is that we have a splitting of the trace during the transition (as clearly marked by the blue circle).

Figure 4.20 allows us to have a better grasp of the impact of r on the system

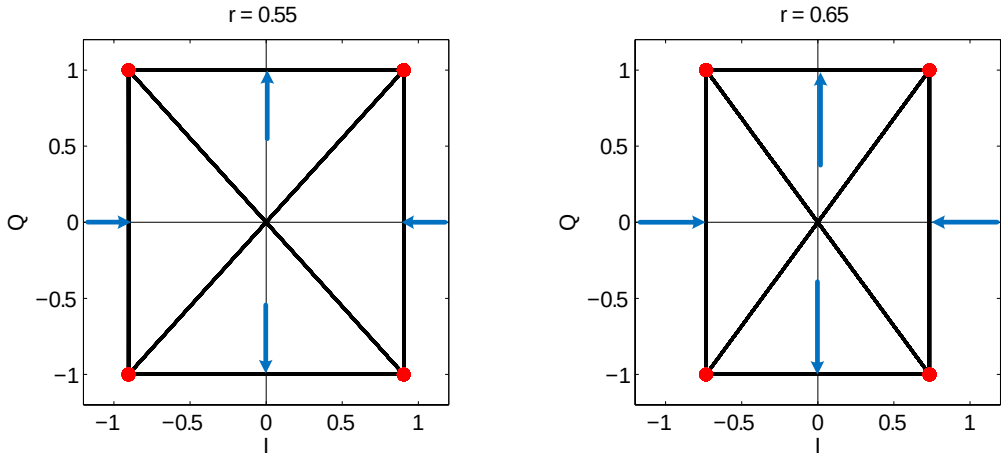

(a) (b)

Figure 4.18: Constellation for a QPSK modulation carried out with an IQ modulator with input power split ratios of (a) 0.55 and (b) 0.65.

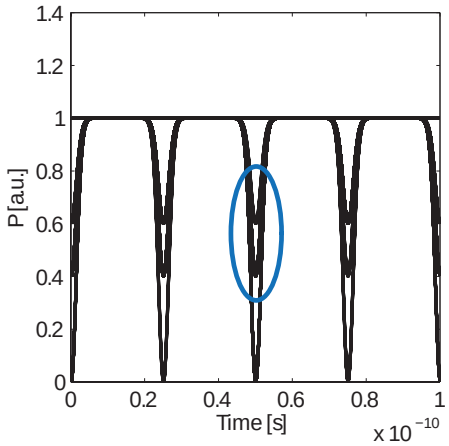

Figure 4.19: Eye diagram of the optical power for a QPSK signal generated by means of an IQ modulator with input power split ratio of 0.6.

performance. As a consequence of the imbalance between the branches of the IQ modulator, the photocurrent plateaus are split into three levels. This causes the eye to close, making the impact of ASE noise more important. It has to be noted that, on the other hand, the highest current is actually increased, which means that noise will be less detrimental when imposed on symbols characterized by the highest current.

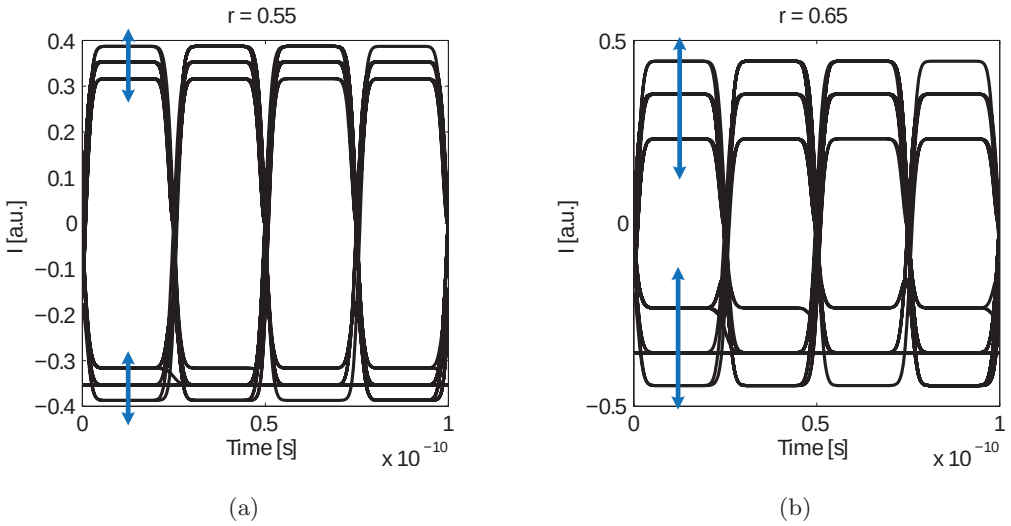

(a) (b)

Figure 4.20: Eye diagram of the photocurrent for a QPSK modulation carried out with an IQ modulator with input power split ratio of (a) 0.55 and (b) 0.65.

Let us conclude this brief analysis of the IQ modulator input power split ratio by showing the power penalty related to this non-ideality in the case of an NRZ-DQPSK format. From Figure 4.21 one can notice how the penalty is very low (lower than 1 dB) for $0.4 < r < 0.6$, while it becomes more noticeable (even though not tremendously high) for larger deviations from 1/2. In practice, we would not expect a commercially available device to have such a poor balancing, so we conclude that the input power split ratio should not be a main impairment within a high-order modulation system.

4.3.2 Delay Between V_I and V_Q

In practice, two driving voltages has to be provided to an IQ modulator, V_I and V_Q. They drive the MZMs of in-phase branch and quadrature branch respectively. Ideally,

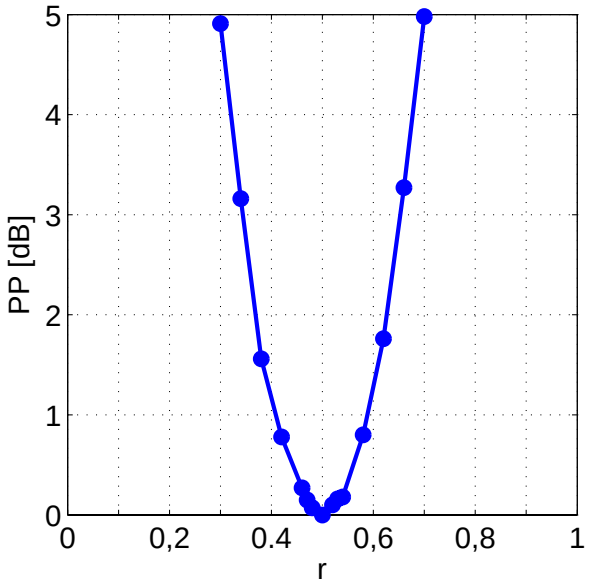

Figure 4.21: Power penalty as a function of the IQ modulator input power split ratio for a DQPSK signal.

they should modulate contemporaneously[1], but there might be a delay comparable to T_S, especially when the baud rate is in the order of the tens of GBd/s.

Here we simulate a delay by means of the Matlab® function `circshift`. The delay will be of course expressed by a finite number of samples, since we have a finite resolution for the time axis. To be more general, we define the delay as

$$\Delta T = \frac{\text{Delay expressed in number of samples}}{\text{SPS}}, \tag{4.4}$$

where a positive delay means that V_Q is delayed with respect to V_I. Note that some of the delays we discuss below are values approximated to the hundredths.

In Figure 4.22 we observe the consequence of a delay between the driving voltages on the constellation. Since one of the two MZMs starts imposing the modulation of a symbol while the other is still waiting on the previous symbol, the trace between two symbols on the constellation is curved.

In this case, things are probably clearer when looking at the eye diagrams (see Figure 4.23). A QPSK signal presents a plateau between two transitions, and one would

[1] If we assume the delays introduced by the paths of I-branch and Q-branch to be identical, which should be the case for a well manufactured device.

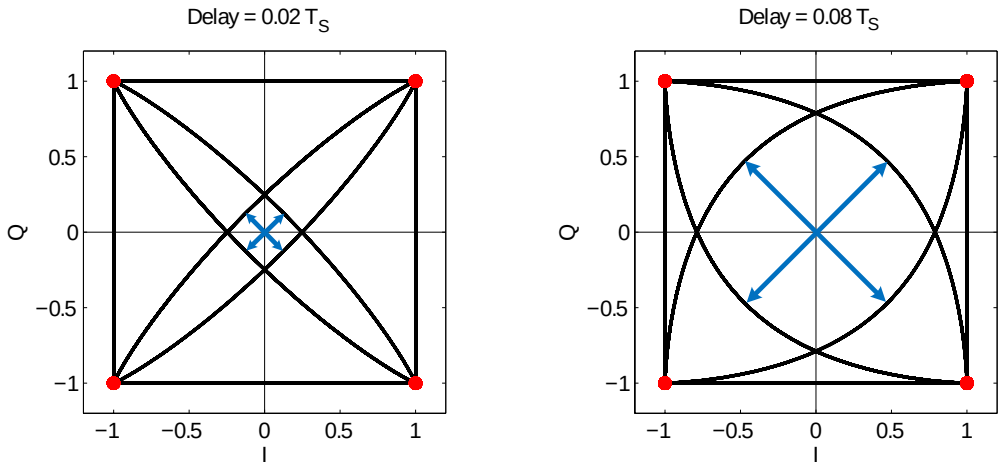

(a) (b)

Figure 4.22: Constellation for a QPSK modulation carried out with an IQ modulator with a delay between V_I and V_Q of (a) $0.2T_S$ and (b) $0.08T_S$.

generally try to sample somewhere in the middle of this plateau. When we introduce a delay between the modulating signals, the flat portion of the signal is reduced, since it takes more time before both drivers have produced the desired modulation for a specific symbol. Consequently, one has less margin when sampling. This means that we will have a penalty, and that this penalty will probably grow to infinity if the delay gets close to the actual symbol duration.

We show this in Figure 4.24. The penalty grows constantly for increasing values of the delay, and one can notice how it peaks abruptly when ΔT is about half of the symbol slot. As one could expect, having a larger rise time for the modulating signals is detrimental. For low delays this is not noticeable, but then the penalty is higher for longer values of t_r. This makes sense if we think that the signal will not be fully modulated until after the rising front is completed. If the delay plus rise and fall times makes up for the whole symbol slot we can foresee a large penalty, since it will not be possible to find a clean sampling point.

4.3.3 Bandwidth Limitation

In Section 2.2.3.1 we have shown how a phase modulator is limited in bandwidth. A rapid search on the internet for the most well known manufacturers would reveal

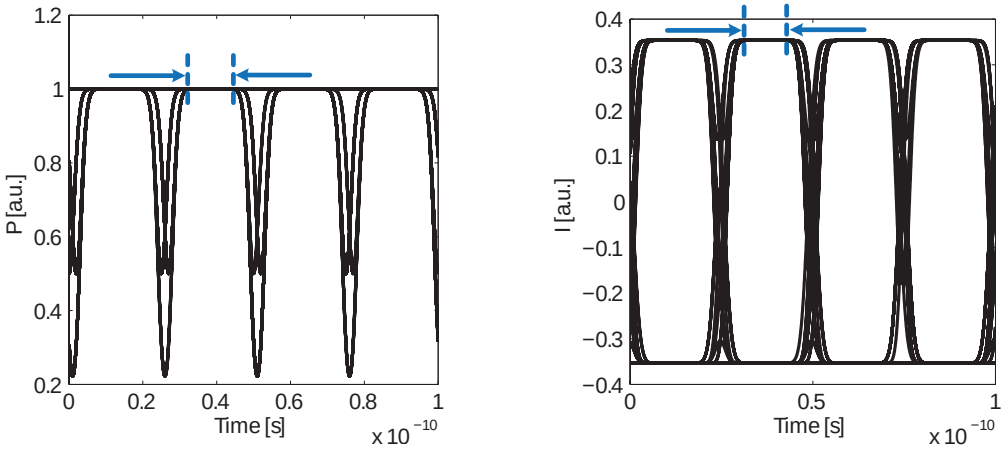

(a) (b)

Figure 4.23: For a QPSK signal, eye diagrams of (a) the optical power and (b) the photocurrent, for a delay between V_I and V_Q within the IQ modulator of $0.08T_S$.

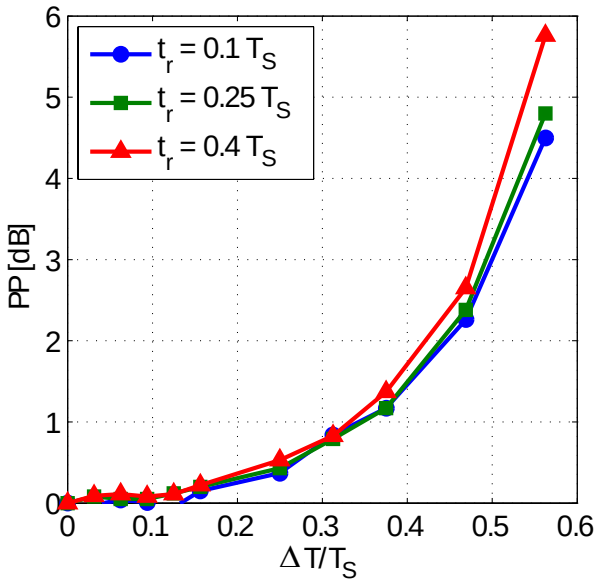

Figure 4.24: For three different values of the rise time of the driving voltages, power penalty as a function of the delay between V_I and V_Q within the IQ modulator for a DQPSK signal.

that today's devices have bandwidths up to 40 GHz. Most devices will probably be less performing, and this makes it very interesting to study how such a limitation can impair an optical communication system. Of course, this bandwidth limitation can be directly related to the whole IQ modulator where as many as four PMs are dynamically driven. We assume that all of them have the same bandwidth, and we label this $b_{IQ} = B_{IQ}/R_S$, where B_{IQ} is the 3-dB bandwidth in Hz and b_{IQ} the normalized one.

In this case, it will be easier to first look at the eye diagrams (see Figure 4.25). If one has the concept of bandwidth limitation clear in mind, then it should be no problem to understand what happens here. The driving signals are limited in the transition from high to low and vice versa[1]. This turns into a disappearance of the flat plateau into a smoother curve (for sufficiently narrow bandwidths). Once more, the margin for a good sampling point is reduced, and the photocurrent eye opening is reduced as well for bandwidths narrower than roughly $R_S/2$.

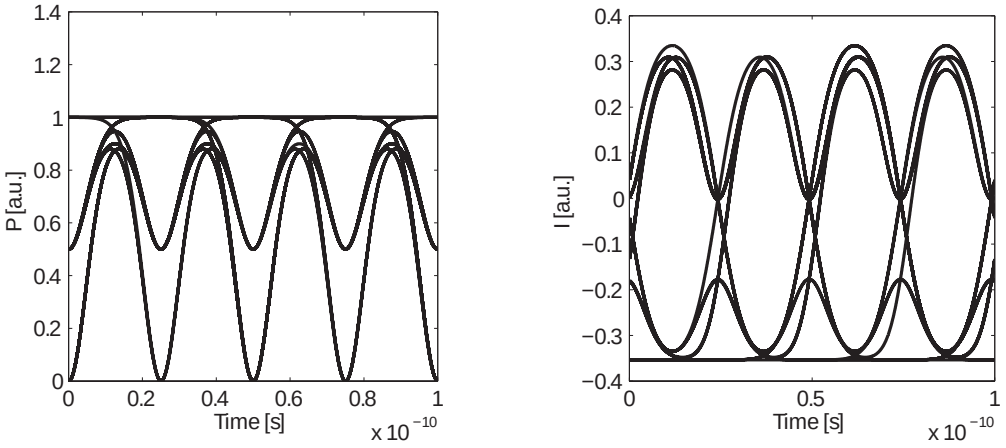

(a) (b)

Figure 4.25: For a QPSK signal, eye diagrams of (a) the optical power and (b) the photocurrent, for an IQ modulator bandwidth of $0.4R_S$.

Let us now look at this on the constellation, which is in this case a bit less intuitive. As long as the bandwidth is large enough so that the signal maintains a flat trend in

[1]Clearly, it was already limited by a finite rise time. The rise time is indeed an expression of a bandwidth limitation, even though in our case it is representative of a realistic electrical signal, while the bandwidth limitation we are discussing here has completely different origins, as explained in Section 2.2.3.1.

the middle of the symbol slot, the optimum sampling will produce the same old four symbols. When the bandwidth is narrower than half the baud rate, the signal is so distorted that the sampled points on the constellation start spreading. As a prediction, one would therefore expect a limited penalty for bandwidths larger than $R_S/2$, and then a much faster increase in penalty, since the eye starts closing.

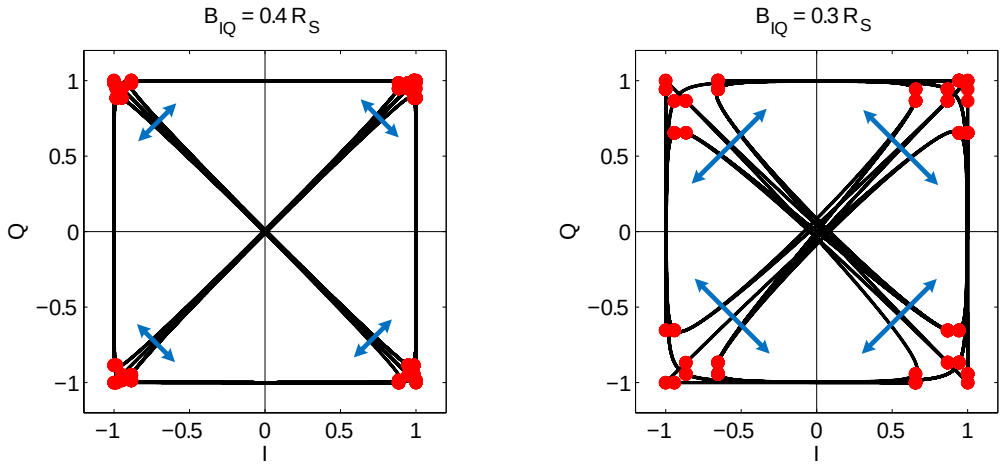

(a) (b)

Figure 4.26: Constellation for a QPSK modulation carried out with an IQ modulator with a bandwidth limitation of (a) $0.4R_S$ and (b) $0.3R_S$.

The power penalty curve exposed in Figure 4.27 is definitely a very interesting result. As we have partially predicted above from mere observation, the impact of a bandwidth limitation of the IQ modulator on the system becomes extremely fierce for values of b_{IQ} larger than about 0.5. This appears to hold true more or less independently of the filter we use to model this bandwidth limitation.

Let us try to give an intuitive (and hopefully convincing) explanation. If $b_{IQ} = 0.5$, ideally a sinusoidal modulating voltage at a frequency equal to half the symbol rate should be perfectly applied to the optical signal. The transitions observed in QPSK signals (see any of the eye diagrams presented so far) would take exactly all of the symbol slot, and the photocurrent would reach its maximum precisely in the middle of it. This would give us an optimum sampling point, even though more difficult to catch, being the flat top of the photocurrent eye diagram degenerated into a single point. Therefore a relatively small power penalty. If we now decrease the bandwidth even further, the optical signal will not be fully modulated anymore, and the photocurrent will

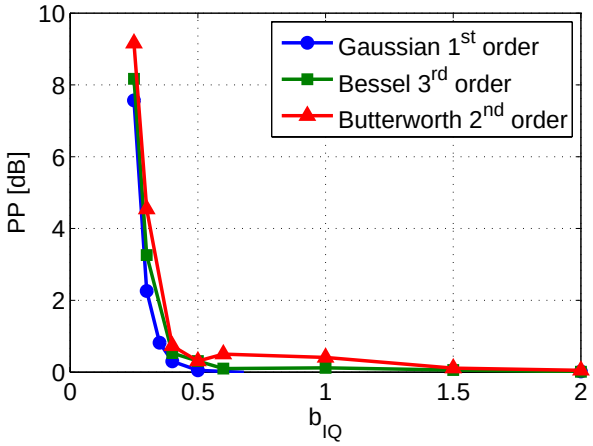

Figure 4.27: Power penalty as a function of the normalized bandwidth of the IQ modulator for a DQPSK signal. The three curves indicate three different filters used to model this bandwidth limitation.

start experiencing a closing of eye. This induces significant penalty, and the maximum and minimum currents will get closer to each other for even smaller bandwidths. We exemplify this reasoning by showing the photocurrent eye diagrams for three values of the IQ modulator bandwidth in Figure 4.28.

4.4 Split-Step Fourier Methods Comparison

This is a very short section devoted to a brief comparison of the three methods for the determination of the step size within the split-step Fourier algorithm described in Section 3.3.3.

The comparison we report here is obtained by propagating a 2^{nd} order soliton described by 1024 samples, and with peak power 35.2 mW and FWHM 4 ps through 500 km of fiber with $D = 0.078$ ps/(nm·km) and $\gamma = 2.2$ 1/(W·km) . These parameters satisfy (2.72) for $N = 2$. According to [35] solitons of order higher than 1 are good tests for the split-step Fourier method because they periodically regain their initial shape and undergo a lot of variations in the peak power.

We first simulate at a constant step length of 10 cm obtaining what we will consider an accurate reference solution. Then we apply the three methods described in Section 3.3.3 setting different values for step length, ϕ_{nl}^{max}, and δ_G. The result is shown in

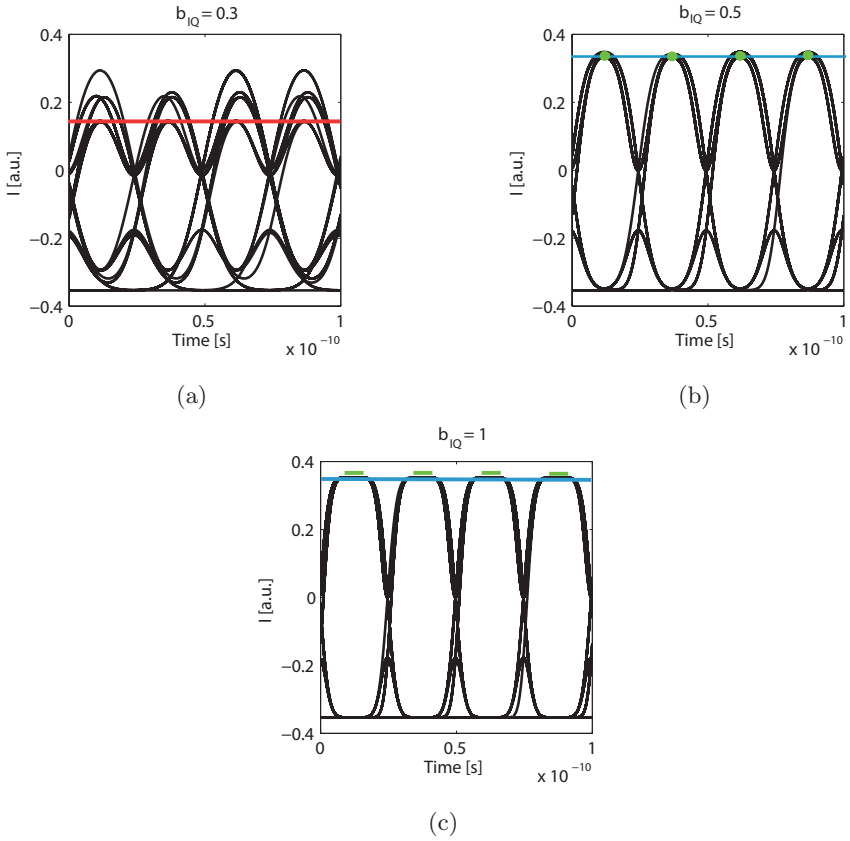

(a) (b) (c)

Figure 4.28: For a QPSK modulation, photocurrent eye diagrams for IQ modulator bandwidth (a) $b_{IQ} = 0.3$, (b) $b_{IQ} = 0.5$, and (c) $b_{IQ} = 1$.

Figure 4.29. It is very clear how, for global relative errors lower than 10^{-3}, the method determining the step size according to the local relative error is the fastest, requiring the fewest FFTs. We are aware of the fact that this is not an absolute proof that this method works better, since this test should be repeated on a number of different system configurations. Moreover, one should make a careful assessment of whether or not the reference solution can actually be considered reliable or if an even shorter step size would be necessary. However, this result is in agreement with [35], where also other simulations seem to advise for the use of the method calculating the step length basing on the local relative error. This is the method we will use to simulate nonlinearities in this thesis.

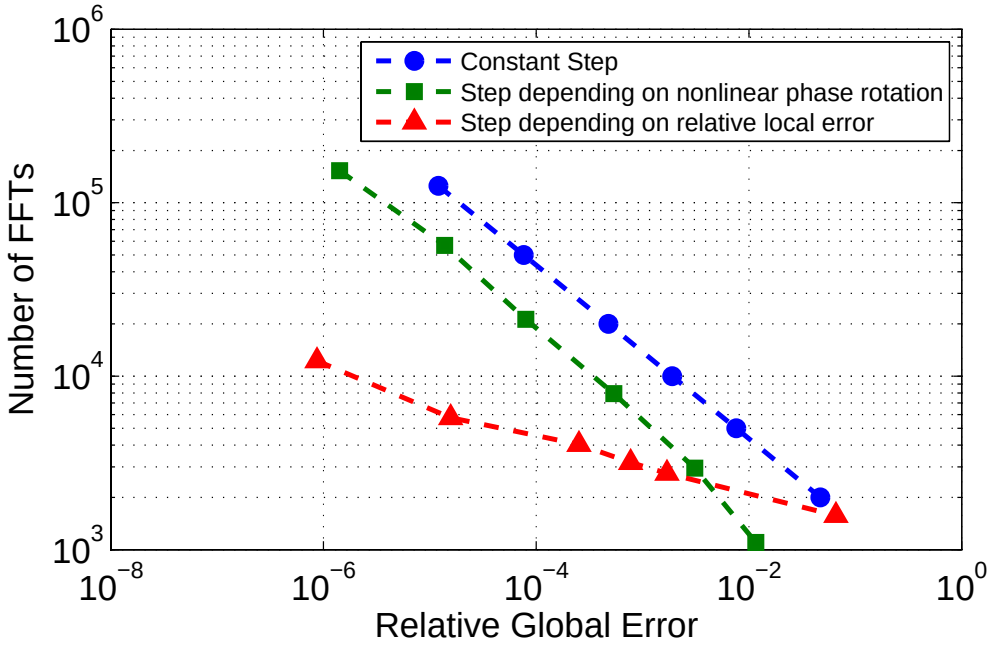

Figure 4.29: Number of FFTs as a function of the global relative error for a nonlinear fiber simulated with three different methods for determining the step size.

4.5 Complete System with Coherent Detection and DSP

We conclude this chapter of numerical simulations with a study of DQPSK and 16QAM with coherent receiver and DSP. This is the system Francesco Patarnello and I studied and modeled during this project. Of course, I would once more recommend the reading

of [12] together with this thesis to have a complete understanding of the way we model all the components, especially the DSP about which we have not written at all.

Specifically, we will show results concerning NRZ-DQPSK, NRZ-16QAM, OTDM DQPSK (4 channels), and OTDM 16QAM (4 channels). The symbol rate is 40 GBd/s. Generally one prefers comparing different modulation formats for the same bit rate. This implies decreasing the symbol rate for higher modulation orders. In this case we have carried out a comparison for the same baud rate but different bit rates, which could be useful if one wanted to upgrade a system keeping existing electronics. SPS is set to 32 for the NRZ simulations and to 128 for the OTDM ones (since narrow pulses need more points to be properly modeled). All the parameters are set to the default (ideal) values unless specified below. The BER measurements are carried out as explained in Section 3.4.6.

Let us here introduce the system. In Figure 4.30 we have the transmitter. For the NRZ formats we use a CW laser, for the NRZ ones a mode-locked one with duty cycle 0.1. The bit sequences are PRBSs generated from seeds of 9 bits, encoding and modulation are performed as described in Section 3.2.6. The driving voltages have rise and fall times of $0.25T_S$. The multiplexing is carried out by recombining the same modulated pulse train according to what explained in Section 3.2.5. Notice that we also perform PolMux in all the simulations. This is of no interest here, since we do not introduce any polarization-related impairment and numerically the two polarizations are perfectly separated. Using PolMux just doubles the bit rate with no drawbacks. We decided to employ it because it is useful for results of [12]. A reader of this thesis might ignore it. Note that the polarization multiplexing is carried out by means of a simple coupler. This is realistic only in our numerical model, in which we have separate vectors for x and y polarizations. In practice one would need a polarization beam combiner (see Section 2.2.5).

Figure 4.31 shows a schematic of our optical channel. We have a certain length of standard SMF, with $D = 17$ ps/(nm·km) and no higher order dispersion. There will be no losses and no Kerr effect apart from the simulations of Section 4.5.6. A DCF with $D_{DCF} = -100$ ps/(nm·km) and no Kerr effect fully compensates for dispersion in Section 4.5.6. At the end of the link we impose ASE according to specific values of OSNR. This is done according to the standard defined in Section 2.1.11 and with $p = 2$.

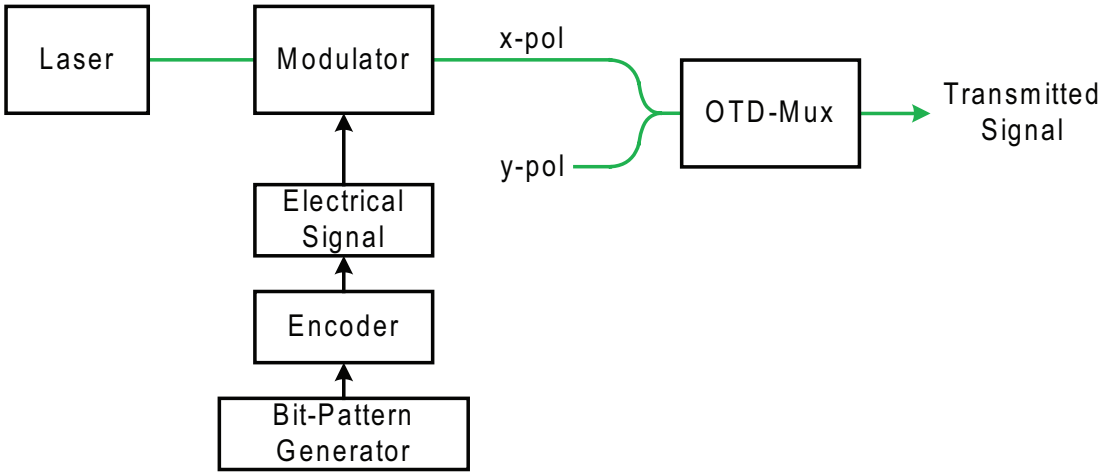

Figure 4.30: Block diagram of the transmitter utilized for the simulations of this section.

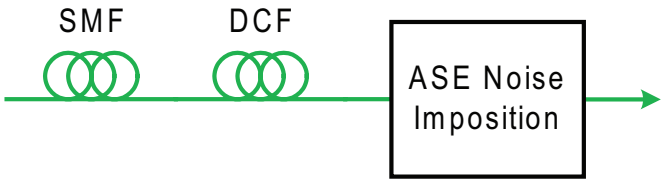

Figure 4.31: Optical channel as we set it for the simulations of this section.

At the receiver (see Figure 4.32) the signal travels through a Gaussian 1^{st} order optical filter. The bandwidth of the filter for all the four modulation formats is optimized in the following section, and the optimal values we obtain are the ones we utilize for all the other simulations. The LO is a CW laser for the NRZ formats, whereas for the OTDM systems it becomes a PMCW pulse source with MI = 3 and $L = 210$m of SMF with the same parameters as the one used for the channel. The demultiplexing is carried out by beating the signal with the LO as explained in Section 3.4.7. The chosen channel goes through a coherent receiver front-end as explained in Section 2.4.8.1 and [12]. This consists of a 90° optical hybrid, photodiodes, and Bessel 3^{rd} order electrical filters whose bandwidths are also optimized in the next section. Neither shot nor thermal noises are simulated. Analog-to-digital conversion is performed at a sample rate of 80 GHz (2 samples for each symbol slot). A DSP stage follows. Here we just perform digital phase estimation and correction. The models of our ADCs and DSP are explained in [12].

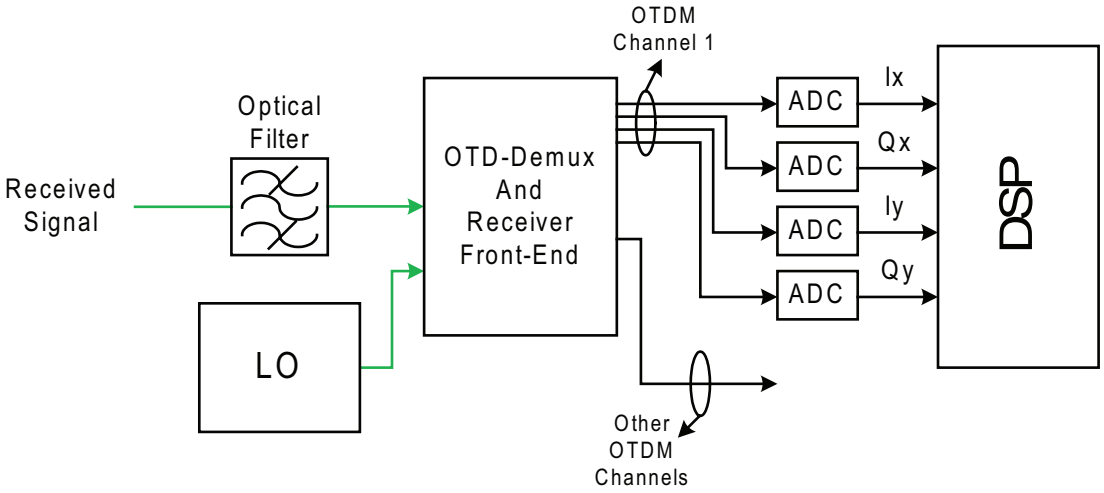

Figure 4.32: Block diagram of the receiver utilized for the simulations of this section.

4.5.1 Filters Optimization

Before starting studying the tolerance of the different modulation formats to a few impairments, we determine the optimum bandwidths for optical and electrical filters. To do this we measure the BER for a grid of pairs b_o and b_e for a fixed OSNR. To keep the computational time acceptable, we use values of OSNR for which the BERs are in

the order of $10^{-2.5}$. For NRZ-DQPSK we measured the BER at 15 dB of OSNR, for NRZ-16QAM 22 dB, for OTDM DQPSK 21 dB, and for OTDM 16QAM 28 dB. The optima are shown in Table 4.1. The resulting contour plots are instead visualized in Figure 4.33.

Table 4.1: Optimum values of optical filter (Gaussian 1^{st} order) and electrical filter (Bessel 3^{rd} order) for the four modulation formats studied in this section.

Modulation Format	b_o	b_e
NRZ-DQPSK	2.2	0.6
NRZ-16QAM	2.2	0.7
4-Ch. OTDM DQPSK	4	3.7
4-Ch. OTDM 16QAM	5	3.4

4.5.2 BER-OSNR Curves for Back-to-Back with no Impairments

The first step to determine any power penalty is to measure a reference sensitivity. We do this by simulating all four systems in absence of impairments and back-to-back. We obtain the curves shown in Figure 4.34. As expected, the increased complexity and bit rate of NRZ-16QAM with respect to NRZ-DQPSK are counterbalanced by a poorer receiver sensitivity, meaning that we need a higher OSNR to achieve the same BER. The same holds true for the OTDM versions. It is instead not very meaningful to compare the sensitivities of NRZ-DQPSK and OTDM DQPSK, since the OSNR is calculated on the average power. This means that an OTDM channel will get much more noise for the same OSNR, since the average power is roughly four times higher than the one of a single channel. Things are even less comparable if we consider that an NRZ format presents almost constant power, while RZ formats are characterized by pulses. The OSNR sensitivities we determined at 10^{-3} are shown in Table 4.2.

4.5.3 Linewidth Tolerances

The power penalty as a function of the transmitter laser is illustrated in Figure 4.35. Note that the linewidth of the LO is zero. We can notice how DQPSK is very resilient to this impairment when compared to 16QAM. This is due to the fact that the constellation points of a square 16QAM are not equally spaced in phase, and therefore the

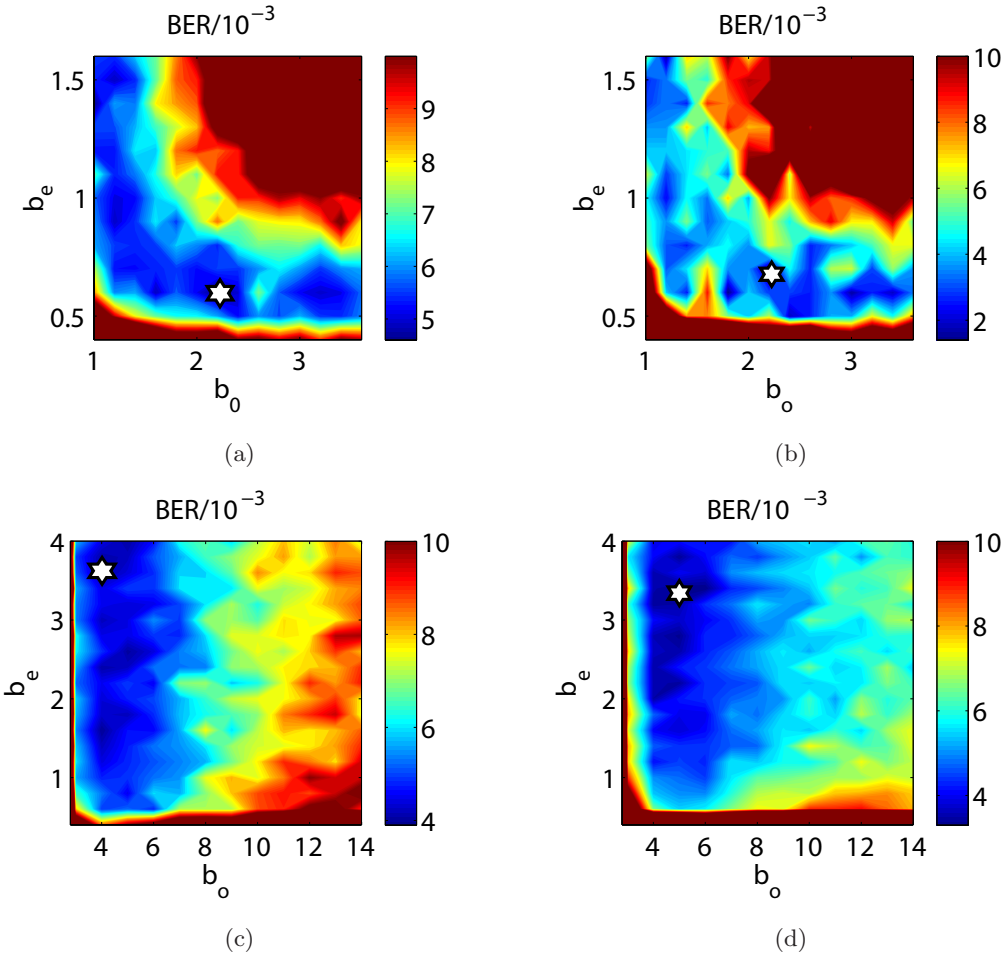

Figure 4.33: Optimal receiver filter bandwidths for (a) NRZ-DQPSK, (b) NRZ-16QAM, (c) OTDM (4 channels) DQPSK, and (d) OTDM (4 channels) 16QAM. The optical filters used are Gaussian 1^{st} order and the electrical ones Bessel 3^{rd} order. The small white stars indicate the optima.

Table 4.2: OSNR sensitivities at 10^{-3} for the four modulation formats studied in this section.

Modulation Format	OSNR at 10^{-3} [dB]
NRZ-DQPSK	16
NRZ-16QAM	23.3
4-Ch. OTDM DQPSK	22.9
4-Ch. OTDM 16QAM	28.9

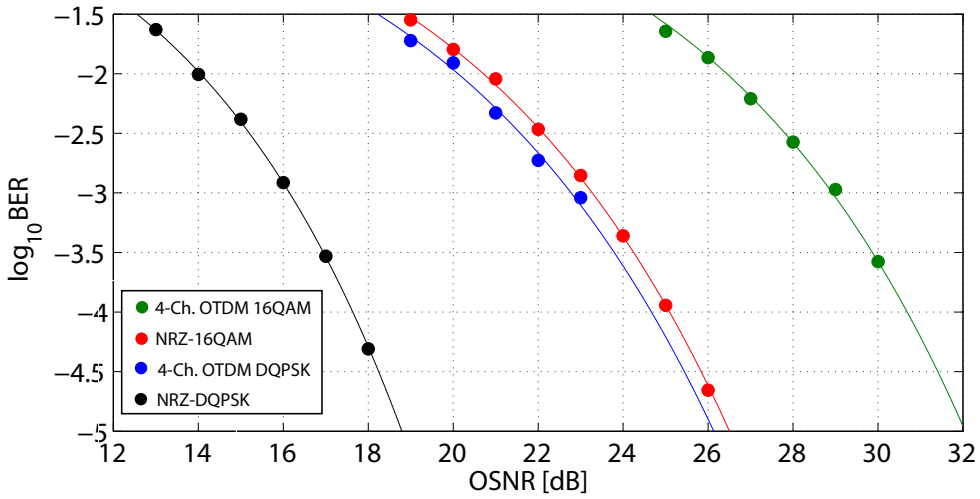

Figure 4.34: For NRZ-DQPSK, NRZ-16QAM, 4-channel OTDM DQPSK, and 4-channel OTDM 16QAM, back-to-back BER-OSNR curves with all the system parameters set to the ideal values.

technique for the carrier phase recovery explained in [12] and used for DQPSK has to be modified and delivers poorer performance.

In general, both DQPSK formats experience almost no penalty up to a few MHz of linewidth, which is a fairly large value in practice. 16QAM, both NRZ and OTDM, still shows an acceptable robustness to the linewidth. At a few hundreds of kHz we have up to 3 dB penalty. One should remember that the linewidth of the LO is zero in these simulations. Generally what matters is the sum of the two linewidths, and in this case the requirements on the lasers become more stringent. Note that our curves for the NRZ formats are in agreement with [6].

4.5.4 Chromatic Dispersion Tolerances

Here we transmit our signal over SMF and we measure the power penalty deriving from chromatic dispersion. The NRZ formats show a much better robustness to uncompensated dispersion, since they are not pulsed. The pulses of the OTDM signals tend to broaden very fast, having large spectra, and this makes them overlap and interfere with each other, increasing the BER. This can be solved compensating for dispersion by means of a DCF or digitally in the DSP. Of course it is not always possible to fully

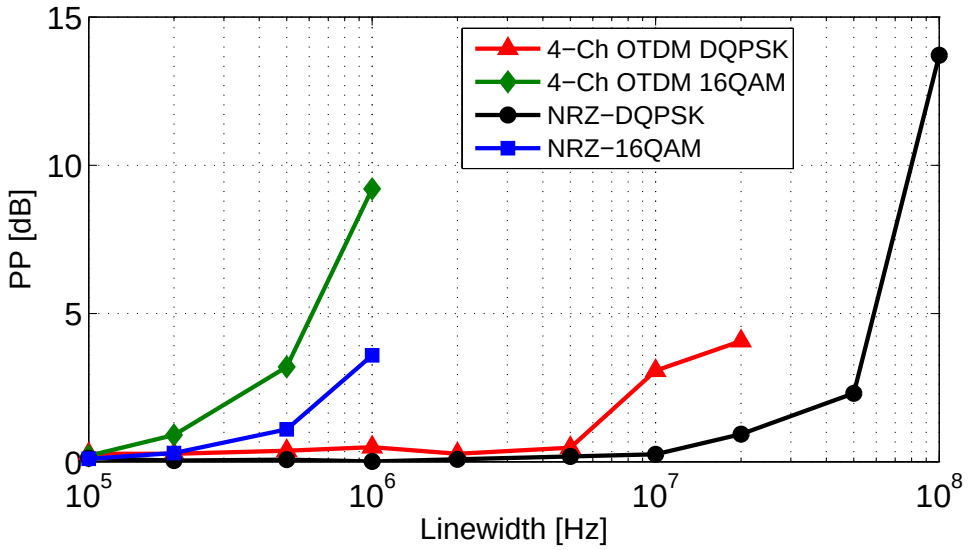

Figure 4.35: For NRZ-DQPSK, NRZ-16QAM, 4-channel OTDM DQPSK, and 4-channel OTDM 16QAM, power penalty as a function of the transmitter ML laser linewidth when the LO laser linewidth is zero.

compensate for a fiber link. This could be due to incomplete information about the link, or changes of the link itself over time. It is interesting to see that, as in most cases, DQPSK is more robust than 16QAM at the same symbol rate.

4.5.5 IQ Modulator Bandwidth Tolerances

In Figure 4.37 we have the power penalty as a function of the IQ modulator normalized bandwidth. We have discussed this non-ideality in detail in Section 4.3.3, so we do not need to devote a lot of effort here. It is nice to see how our findings still hold true for 16QAM and OTDM systems with coherent receiver and DSP. A normalized bandwidth larger than half the symbol rate is indeed necessary to have very low penalty.

It is interesting how, once more, 16QAM is less robust than DQPSK. The OTDM version of both formats is also a bit more impaired than the NRZ one. Unexplained is the slightly negative penalty observed in the OTDM DQPSK for normalized bandwidths larger than 0.6. We tend to believe this is not physical and we are trying to investigate for bugs in the simulation. Hopefully an update of this work will solve the doubt.

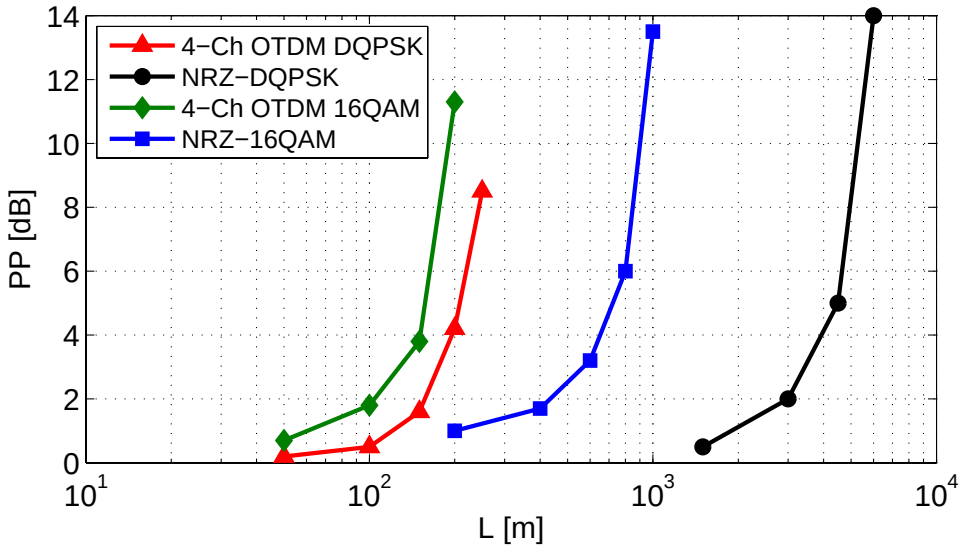

Figure 4.36: For NRZ-DQPSK, NRZ-16QAM, 4-channel OTDM DQPSK, and 4-channel OTDM 16QAM, power penalty as a function of fiber length for a fiber with $D = 17$ ps/(nm·km) , no higher order dispersion and no kerr effect.

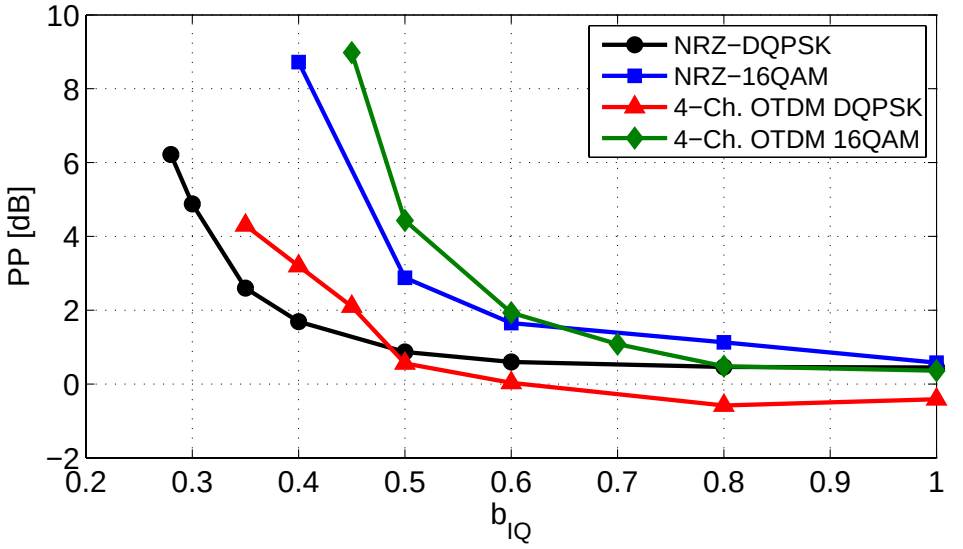

Figure 4.37: For NRZ-DQPSK, NRZ-16QAM, 4-channel OTDM DQPSK, and 4-channel OTDM 16QAM, power penalty as a function of the IQ modulators normalized bandwidth.

4.5.6 Fiber Nonlinearities Tolerances

We assess the tolerance of the system to fiber nonlinearities (see Figure 4.38). In this case the power levels will be considered for only one polarization, since our model of nonlinearities processes the two polarizations separately (see Section 3.3.3). The fiber parameters were given at the beginning of this section, let us just say that we use a 40-km SMF span and we compensate with a 6.8-km DCF span. The DCF does not have any nonlinear Kerr effect. By increasing the average power at the fiber input we increase the impact of the nonlinearities.

For the NRZ formats, 16QAM is more impaired than DQPSK. This is due to SPM, that introduces a phase shift depending on the signal power (see Section 2.3.4). 16QAM signals are characterized by different power levels, so the outer symbols on the constellation rotate faster than the inner ones. This does not happen for DQPSK formats, whose symbols all have the same intensity. The OTDM version of 16QAM has roughly the same trend as the NRZ one if we divide the average power by the number of channels, which is what we did in the figure.

Unfortunately we could not obtain meaningful results for OTDM DQPSK. We will update this plot after we have understood what went wrong.

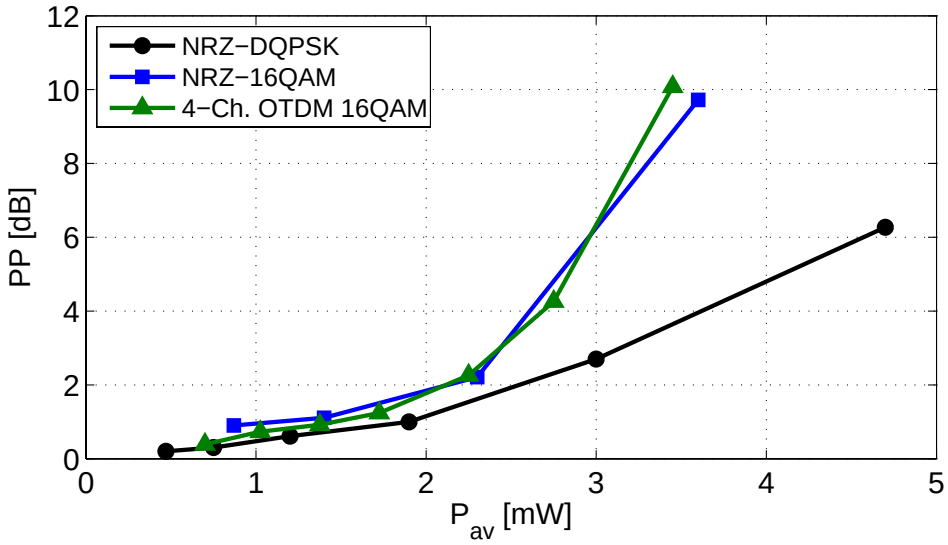

Figure 4.38: For NRZ-DQPSK, NRZ-16QAM, 4-channel OTDM DQPSK, and 4-channel OTDM 16QAM, power penalty as a function of the average signal power at the input of 40 km of SMF with $D = 17$ ps/(nm·km) , no higher-order dispersion, and $\gamma = 1.3$ 1/(W·km) . Dispersion is then fully compensated in a DCF which does not feature nonlinearities. For the 4-channel OTDM 16QAM modulation, the x-axis represents the average power divided by 4.

5

Laboratory Experience

After so much modeling, we had the opportunity of experiencing some laboratory work. We were shouldered in this by Christophe Peucheret, Michael Galili, and Darko Zibar, and it was great pleasure and fun to work with them. We owe them a large part of the successes obtained and displayed in this chapter. So, once more, thank you.

The core objective of this activity was to build a functioning OTDM system with multi-level modulation, coherent receiver, a PMCW pulse source as LO, clock recovery, and finally DSP. This was something never tried before at DTU and, in this very specific fashion[1] never seen in literature, to our knowledge. The optimum goal was to achieve a bit rate on single fiber of 160 Gb/s and then being able to successfully demodulate in back-to-back. We managed to transmit an 8-channel OTDM QPSK at a baud rate of 10 GBd/s, resulting in 160 Gb/s on a single fiber, and to demodulate it with a coherent receiver. The LO was created with the PMCW pulse source largely discussed in this thesis, and the electrical clock retrieved from the received signal by means of a clock recovery based on an electro-absorption modulator (EAM). Digital samples were saved and processed with the software described by Francesco Patarnello in [12]. Even though we did not have the time to perform a BER measurement, we will show how the demodulation can be considered almost completely successful.

On top of this, we also carried out a few measurements. These consisted in measuring the timing jitter of a few pulsed sources of interest for our main experiment. To do this one detects the optical pulse train with a photodiode, and looks at the spectrum

[1] We have not found any records of experiments with such an implementation of LO between the many about multi-level modulation with coherent receiver and DSP.

of the photocurrent on a spectrum analyzer. The larger the timing jitter, the wider the peak of the spectrum. We also measured the optical linewidth of a CW source according to the typical method consisting in splitting the signal, delaying one of the two instances of a sufficiently large amount so to make sure that the coherency is lost, recombining, and then detecting [37]. The optical linewidth can finally be determined on the spectrum analyzer. We are not reporting all the details of these measurements for reasons of time.

5.1 Experiment Overview

Let us start by introducing the system as a whole (see Figure 5.1), before we look into the single parts. We planned on generating an RZ optical signal, starting from a BPSK modulation and possibly going to a more ambitious QPSK one. This signal is to be OTD multiplexed up to eight channels. After transmission (we worked in back-to-back, so just a few tens of meters of fiber), the signal is to be amplified before 10 m of DCF compensate for the dispersion accumulated. The output of the DCF becomes the first input of a coherent receiver.

The other half of the signal is sent to the clock recovery circuit, which, if properly locked, produces an electrical clock at the pulse rate. This clock drives our LO, which is implemented as a PMCW pulse source. The output of the LO is also an input to the receiver, and is to be amplified to a sufficient power by means of an EDFA.

A coherent receiver front-end combines signal and LO and samples at a sampling frequency of 40 GHz. Note that the pulse repetition frequency is 9.953 GHz. This will turn into a serious problem, since the sampling rate is not a multiple of the pulse rate. We will discuss the way we solved this issue in Section 5.2. The digital samples saved this way are then processed in Matlab®.

Let us specify that, for simplicity and readability, we will indicate the points where we monitored the signal with black dots and the monitoring equipment in blue. In practice, one has to split the signal and generally attenuate it, but here this will not be shown to avoid overcrowding the block diagrams. Note that, as in the rest of this thesis, the optical line will be green and the electrical one black, when both present in the same figure.

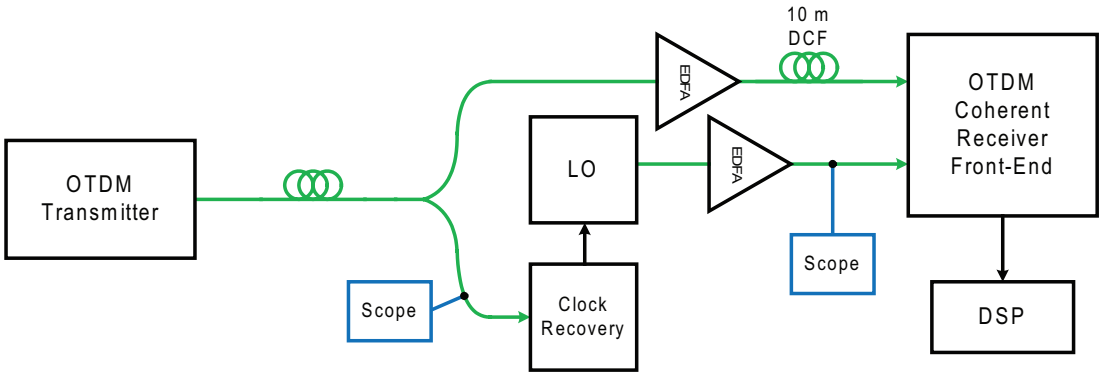

Figure 5.1: Block diagram of the complete setup.

5.1.1 OTDM QPSK Transmitter

A schematic of the transmitter is found in Figure 5.2. The optical source for the transmitter is a mode-locked external cavity ERGO laser, pulsating at a frequency of 9.953 GHz and emitting light at a wavelength of 1542 nm. The pulses are quite narrow, about 2-3 ps. The laser output is split and one branch is devoted to extracting a clock for the modulation, while the signal on the other branch will be actually modulated.

To extract a clock at 9.953 GHz, we proceed as follows. First, the pulsed optical signal is delayed of the desired amount, then attenuated before being detected by a photodiode with a bandwidth of 12.5 GHz. By means of the tunable attenuator, we keep the average input power to the photodiode below 0 dBm, which is where the photodiode starts saturating. The delay line is necessary to make sure that we impose the modulation exactly on top of (or close to) the pulses. The photodiode is followed by a narrow bandwidth amplifier, which filters at roughly 10 GHz, so that the component at 9.953 is preserved and all the surrounding of the spectrum is filtered out. The output should be a nice sinusoidal signal. We did not check this, since this method had been used before and proved to work fine. The so-produced signal is then sent to the first bit-pattern generator as a clock. This generator in turn sends a halved version of the clock (roughly 5 GHz) to a second bit pattern generator and through a tunable delay. Let us explain this in a moment. To be mentioned that the bit sequences produced by the pattern generators were periodic with a period of $2^7 - 1$ bits.

Looking at the other branch, the signal passes through a polarization controller (PC), necessary because the MZM that comes after is polarization sensitive. The

average optical power entering the MZM is about -2 dBm. The MZM is driven in push-pull, so to apply a chirp-free phase modulation. It is driven by the first bit-pattern generator and connected to a power supply for the DC component of the driving voltage. Both PC and DC driving voltage have to be optimized and tuned while looking at the signal on the scope to maximize the output power. A phase modulator follows. It is supposed to apply a further phase modulation to achieve QPSK. This modulation should be at 9.953 GHz, so the second bit-pattern generator has to internally double the received clock (about 5 GHz). The tunable delay line is needed to synchronize the two modulations. The red part of Figure 5.2 can be by-passed so that only BPSK is applied to the signal.

Let us discuss how we optimized the modulation. For BPSK this is quite easy. We observe the waveform on the scope and tune the delay until the pulses are severely distorted. This corresponds to having the pulses on top of the transitions of the modulating signal, so that they are almost suppressed (this should be clear by looking at the MZM transfer function in Figure 2.14(a)). Once we have determined this point, we apply 50 ps of delay, so that the pulses are in the middle of the modulation slot and fully benefit from the modulation. Optimizing the second phase modulation to achieve QPSK was far more difficult, since it has no apparent influence on the wave form. To do this, we sent the pulses to an interferometric structure typical of a DQPSK direct detection receiver (see Section 3.4.4.3) and we observed the eye diagram until it looked reasonably close to the ideally expected one. In doing this we had two degrees of freedom: one was the PM driving voltage span[1], the other the delay applied between the two bit-pattern generators.

The modulated signal travels through an EDFA and is amplified from -12.7 to 13.9 dBm. We then need another polarization controller, since the OTD multiplexer is sensitive to polarization. This is implemented as shown in Figure 5.3. The signal is split and one arm is tunably delayed and attenuated, so that the pulses are combined doubling the bit rate. Other two stages follow, so that we can achieve the equivalent of eight channels. By optimizing the attenuations in each stage, we can equalize the powers of each channel. It is also possible to by-pass any stages, so to multiplex to only two channels, four channels, or not multiplex at all.

[1] V_π had been characterized at 1 GHz, so we did not exactly know which driving voltage we needed to achieve a phase shift of π.

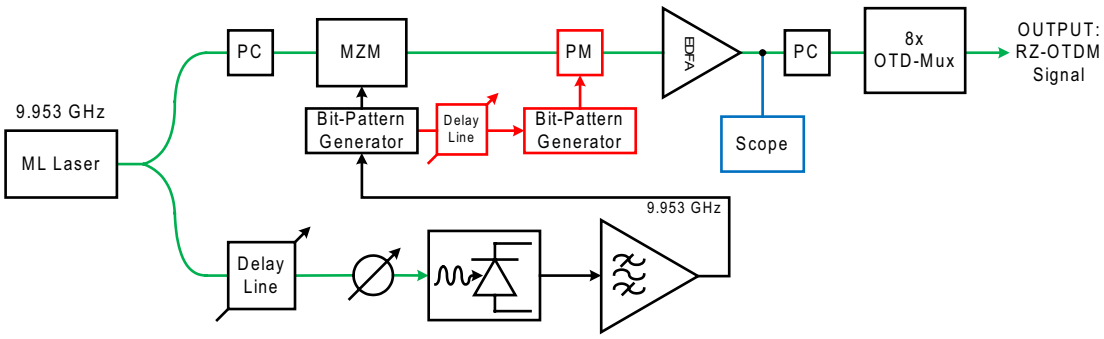

Figure 5.2: Schematic of our OTDM QPSK transmitter.

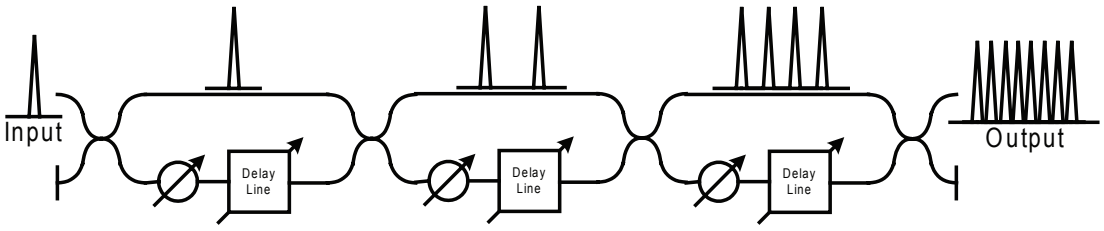

Figure 5.3: The structure of the OTD multiplexer utilized for our experiment.

Before we move forward to the description of the other parts of the system, we want to show how our signal looked like. To do so, we received it by means of an optical sampling scope with an enormous bandwidth of roughly 700 GHz. We needed a large bandwidth to visualize our pulses, since they were quite narrow (we wrote before that the ERGO laser we employed produces pulses as narrow as 2 or 3 ps), too narrow for any photodiode we had. In Figure 5.4 one can observe the pulses for a QPSK modulation as detected at the output of the EDFA we used before the receiver (see Figure 5.1).

5.1.2 PMCW LO

We have amply discussed this way of generating pulses in Sections 2.2.1.5, 3.2.2.5, and 4.2. We should therefore be able to go through this section quite smoothly and quickly. Let us start by showing the schematic of our practical implementation in Figure 5.5. Since the functioning of this scheme is supposed to be clear by now, we will move to the description of the way we optimized it.

The input of our LO is any electrical oscillator. To tune the system, we have used a signal generator at 10 GHz, but in the final system the input was instead the recovered clock, as shown in Figure 5.1. The optimization strongly depends on the frequency of

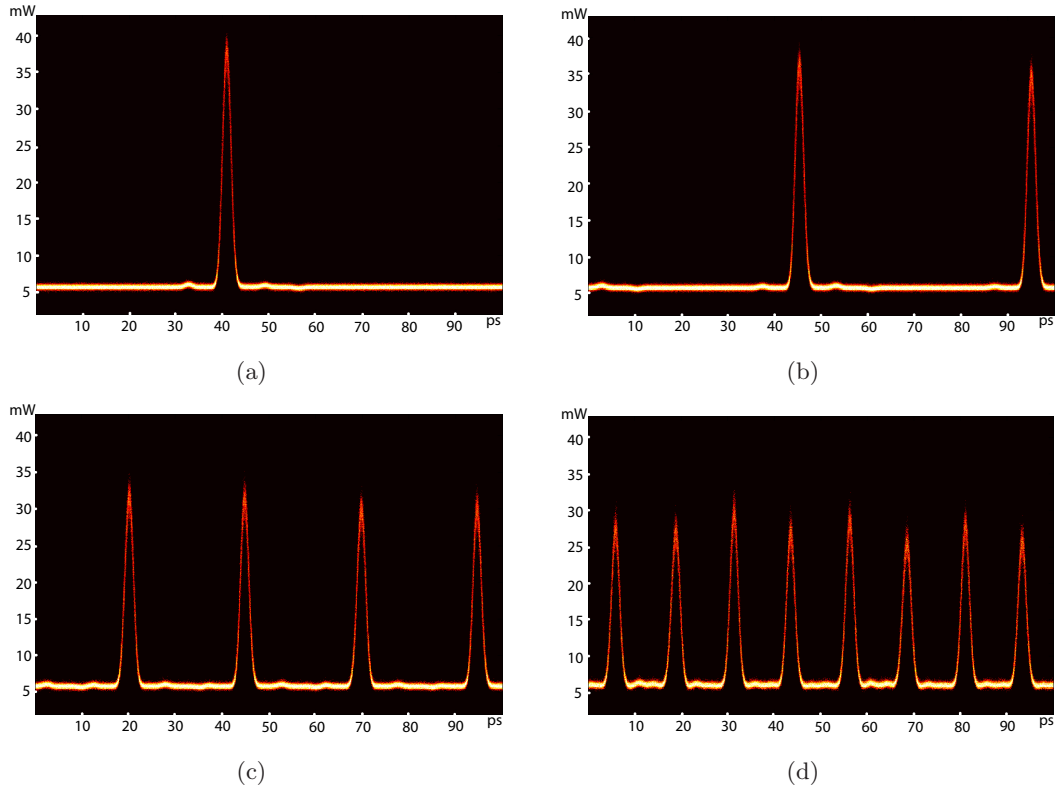

Figure 5.4: RZ signal for a QPSK modulation and (a) no multiplexing, (b) 2x multiplexing, (c) 4x multiplexing, and (d) 8x multiplexing.

the input oscillator, so this setup would not be useful for other baud rates and it would need modifications, as explained in Section 4.2.

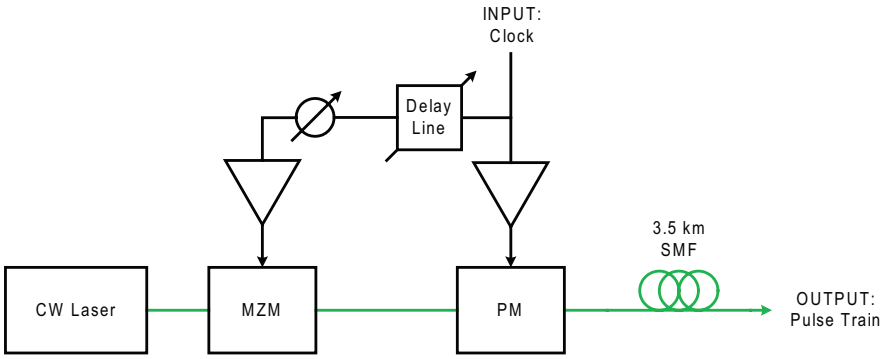

Figure 5.5: Schematic od our PMCW LO.

The CW laser is an external cavity tunable laser, and the emitted light propagates through a MZM used as 50% pulse carver. The DC bias has to be tuned until the output of the MZM is satisfactory. This is the very first operation in building the optical line. The MZM has to be driven with the right peak-to-peak voltage. The driver is actually an amplifier, and to feed it with the right voltage we proceed as follows. We attenuate the input voltage and check the supposedly 50% pulses. If the input voltage is too much, the amplifier saturates and the pulses are flat on the top, if it is too little, the ER is worsened. By attempts, we find out that the best voltage at the input of the amplifier is about 150 mV peak-to-peak. The 50% pulses we obtained are shown in Figure 5.6 as we saw them on the scope when detected with a photodiode with a bandwidth of 70 GHz. They actually resulted to be 40% pulses (i.e. the duty cycle is 0.4). This is acceptable, considering we did not have a very fine resolution in the applied attenuation, so the optimization was quite coarse.

The second operation we performed was to characterize the amplifier that would have driven the PM. From Section 4.2 we know that, in most cases, the higher MI, the narrower the pulses we can obtain. The result of the characterization is shown in Figure 5.7(a). One can clearly notice linear regime and saturation of the amplifier. We decide to operate the amplifier so to have 15.8 V peak-to-peak as output, which is almost as much as we can get without jeopardizing the device health. We determined that this is achieved when, with the present setup, the input sinusoidal voltage is roughly 1.76 V peak-to-peak.

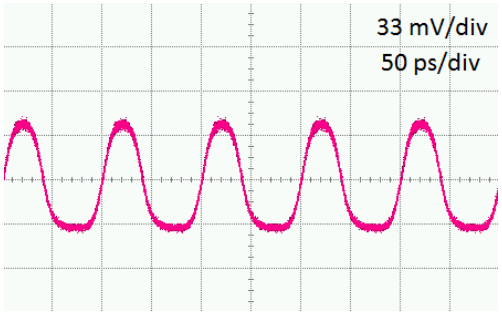

Figure 5.6: Output of the MZM used as 50% pulse carver within the LO setup.

The following step was to decide the fiber length. To do this we relied on a simulation as the ones discussed in Section 4.2. We set a symbol rate of 10 GBd/s and an ER for the MZM of 15 dB. The FWHM for a grid of combinations of MI and L is shown in Figure 5.7(b). Unfortunately, we did not know V_π for the PM in question. Knowing that it was supposed to be around 6 V, we assumed a range of values of MI from 2.4 to 2.8. We were also constrained by a limited granularity in the choice of the fiber length. 3.5 km resulted to be the best choice among the available fiber spans. From the simulation, the pulse width was expected to be between 8 and 10 ps.

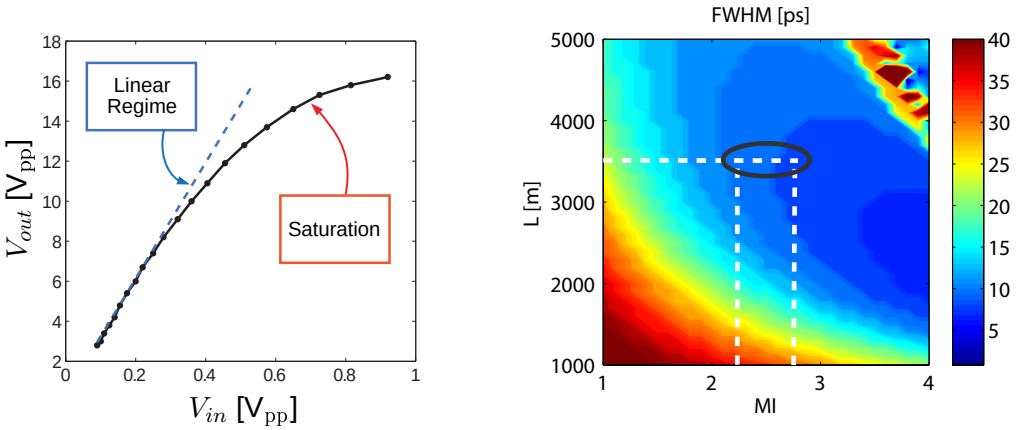

(a) (b)

Figure 5.7: (a) Characterization of the amplifier driving the PM within our PMCW LO. (b) Numerical FWHM in ps as a function of MI and fiber length for our PMCW LO.

The last step in setting up the LO was to optimize the delay so that the phase modulation be applied on top of the pulses, and not in between them. This was fairly

easy to do while looking at the scope. The process is shown in Figure 5.8. When the delay is optimum, the peak power is maximized.

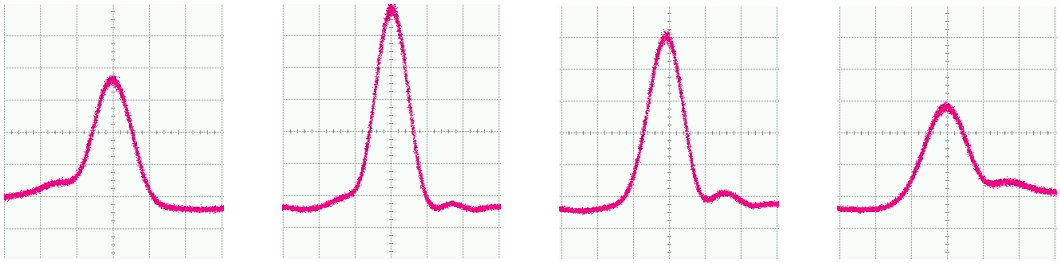

(a) (b) (c) (d)

Figure 5.8: The output of our LO for different values of the delay between the electrical signals driving pulse carver and PM.

The optimum pulses result about 9 ps wide, as predicted by the numerical simulations of Figure 5.7(b). One can see how they look like in Figure 5.9, when detected by the already mentioned optical sampling scope.

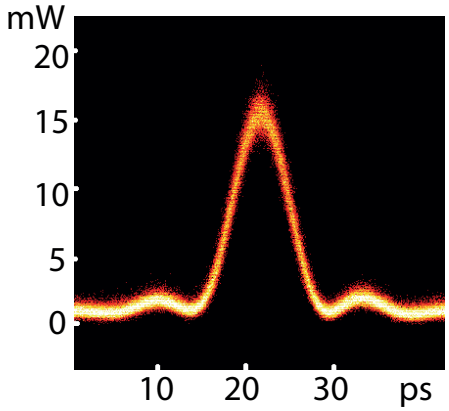

Figure 5.9: LO pulses as detected by the optical sampling scope.

5.1.3 EAM-Based Clock Recovery

The clock recovery was installed and optimized by Michael Galili. This system is not trivial to understand and we will not pretend to master the theory behind it. We will limit ourselves to providing the description of the setup and some naive explanations.

The schematic of the clock recovery circuit is presented in Figure 5.10. It is based on an electro-optical feedback loop. The optical signal is attenuated to about 1-2 dBm

and then propagated through an electro-absorber modulator, which is simply a device whose absorption coefficient depends on the applied voltage. Tuning the input power can help achieve locking. When the clock was unstable we generally tried to increase the optical power a bit. The EAM output is detected by a photodiode with a bandwidth of approximately 100 MHz. The resulting photocurrent is low-pass filtered to extract the offset frequency between the data signal and the VCO driving the EAM. The EAM basically acts as a mixer between the VCO clock and the base-frequency of the OTDM signal. When the clock recovery is locked the output from the photodiode is DC. The bandwidth of the loop filter is about 200kHz. The loop filter subtracts a tunable DC level from the photodiode output. This was the other means by which we managed to lock to the right frequency. The output of the EAM depends on the phase and frequency error between the 2 GHz clock (VCO) and the base rate frequency of the OTDM signal. This error signal is used to drive the VCO to correct the error in phase and frequency. The frequency of the VCO output is then multiplied by five. The signal is then amplified before being doubled in frequency, amplified, and finally doubled in frequency again. Along the line we therefore have clocks at different frequencies: roughly 10, 20, and 40 GHz. The 40 GHz clock is amplified and then slightly attenuated so to obtain a peak-to-peak voltage of about 5 V. This signal drives the EAM, thus closing the feedback loop.

If we tune the circuit sufficiently well, the feedback will stabilize and the electro-absorption modulation be in phase with the VCO clock. The recovered clock at 9.953 GHz will be our output. We will attenuate it of 9 dB to obtain 1.8 V peak-to-peak, which is the required voltage for our LO, as described in the previous section.

5.1.4 Coherent Receiver

The theory provided in Chapter 2 might not be enough to thoroughly understand how the receiver of Figure 5.11 works. This part of the setup was studied in detail by Francesco Patarnello in [12]. Nonetheless, we will hereby describe how things work, without giving all the details of some of the steps.

Our coherent receiver (see Section 2.4.8.1) has two inputs, one is the LO and the other the received OTDM signal. We attenuate both of them to 0 dBm and 1 dBm respectively, in the safe zone according to the receiver front-end specifications. A polarization beam splitter takes only one of the signal polarizations. We also need

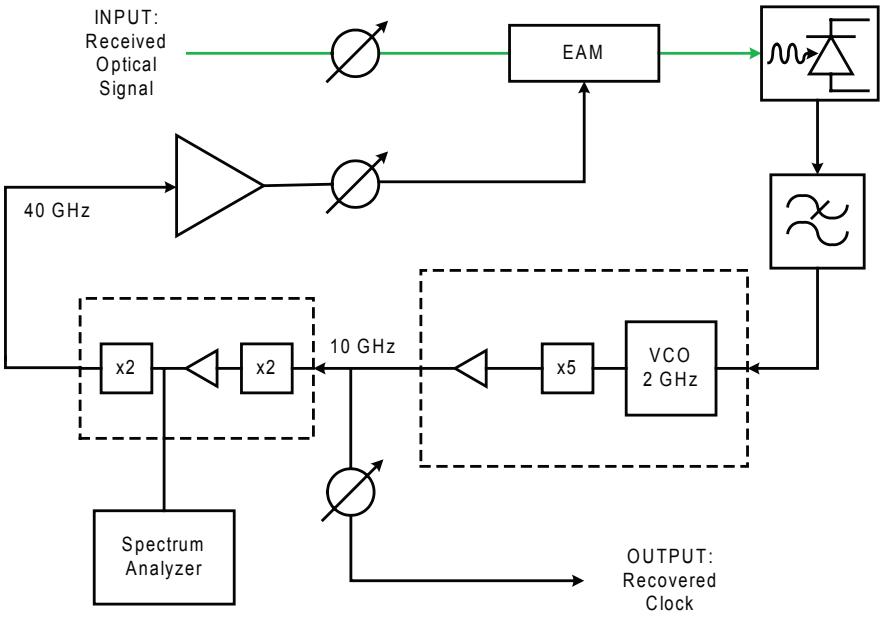

Figure 5.10: Schematic of the clock recovery employed in this experiment.

polarization controllers. The one on the signal branch aims at maximizing the signal power in the polarization allowed by the polarization beam splitter, the other is tuned to maximize the beating between LO and signal by making sure that they have the same polarization. The beating taking place within it is indeed clearly maximized when signal and LO have the same polarization. Within the optical hybrid we also demultiplex one channel, simply by tuning the delay of the LO until it overlaps with one channel. As explained in Section 2.4.10, this magnifies that channel power and extinguishes the others.

The outputs of the optical hybrid are detected in the balanced way by photodiodes with a bandwidth of about 7.5 GHz (still good enough for our signal which, at this point, is a 10 Gb/s one). The resulting currents, which correspond to the in-phase and quadrature components of the modulated field after beating with the LO, are analog-to-digital converted at a sampling frequency of 40 GHz, which means roughly four times faster that the signal. This is quite acceptable and allows to have at least a sample quite close to the pulse peak, especially after that the pulses have been smeared out because of the bandwidth limitation of the photodiodes. The digital signals are shown on an oscilloscope which allows for optimization and saving of the samples destined to processing.

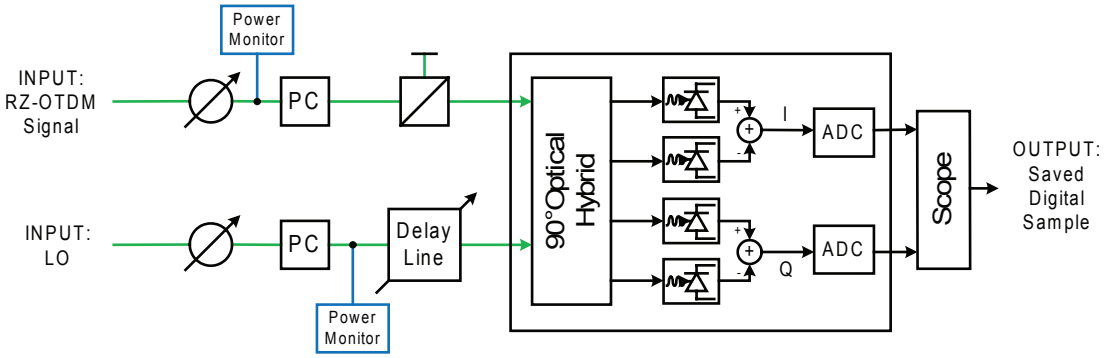

Figure 5.11: Schematic of our receiver front end.

The first step was to make sure that the LO wavelength (tunable) was as close as possible to the one of the mode-locked laser used for the information signal. This was done by first coupling both signal and LO into a spectrum analyzer and making sure that their spectra be centered on the same frequency. This is shown in Figure 5.12, where the smooth hill is the spectrum of the modulated signal. The peaks on top of the hill belong to the LO. This was only a coarse tuning. The following step was to observe the spectrum of the digital signal, which is the beating of optical signal and LO, and slightly change the tunable laser wavelength trying to minimize the frequency offset (i.e. the frequency difference between the two optical sources), distinguishable as a frequency component arising at a frequency equal to the offset itself. Then we tuned the delay until the power measured on the scope was maximum. This meant that our LO pulses were overlapping with one of the channels. A tuning of the polarizations followed, again aimed at maximizing the power of the beating of LO and signal.

5.1.5 DSP

The samples we save with the scope are then processed off-line by means of the code described in [12]. It would be here too ambitious to explain exactly how this works. Let us just give some guidelines.

First the digital signal is decimated, meaning that we take just one of the four sets of samples provided by the scope. We then determine the best sample, defined as the one whose samples have the highest average power.

We follow up with two steps in our digital recovery. The frequency offset estimation takes care of assessing the frequency difference between LO and signal and correcting it.

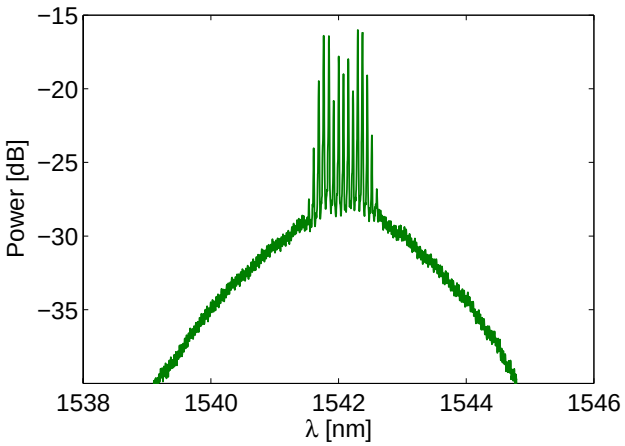

Figure 5.12: Spectrum of signal and LO coupled together in the same fiber.

A carrier phase estimation is carried out afterwards, resulting in the correction of the phase difference between LO and signal. Both steps work with the decimated signal.

At this point we can demodulate the signal and look at constellation and eye diagram. Unfortunately, we did not have the time to attempt a BER measurement.

5.2 Results

To reach the tentative goal of transmitting and demodulating at 160 Gb/s, we first tried simplified versions of the system. One of the first attempts was done with an RZ-BPSK signal and the pulsed LO discussed above. We could not demodulate the signal, while the demodulation worked perfectly when we subsequently tried with a CW LO. As previously announced, the problem was identified in the fact that the ADCs at the receiver front-end sampled at a frequency of 40 GHz, which is not a multiple of the pulse repetition rate of 9.953 GHz. Because of this lack of synchronization, the sampling points drifted over the symbol slot, and the demodulation resulted impossible (see Figure 5.13(a)). Unfortunately, we could neither apply an external clock to the ADCs, nor tune their sampling frequency, nor tune the pulse rate of the ML laser.

We solved the problem in the digital domain by interpolating the existing samples with a factor of $10/(10-9.953) \approx 213$, and then decimating back to the original 4 samples per symbol by selecting a sample every 214 for each of the four sets of samples. This corresponds to reducing the sampling rate to $4 \cdot 9.953\text{GHz} = 39.812\text{GHz}$. The

result was astonishing for improvement from an almost shapeless cloud of samples to a nicely separated pair of BPSK symbols on the constellation, as one can see from Figure 5.13(b).

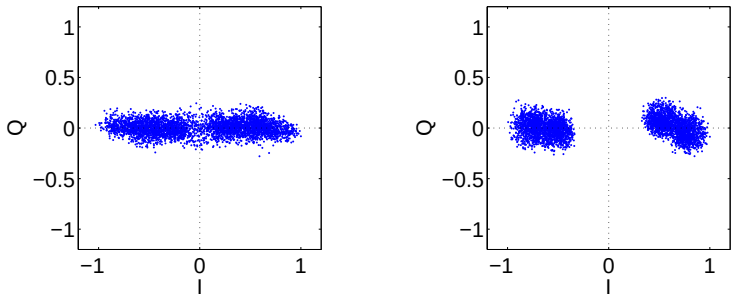

Figure 5.13: Constellations of the demodulated RZ-BPSK signal with pulsed LO (a) before and (b) after applying the sampling frequency adjustment described in the text.

Without bothering the reader with the many other minor obstacles that our heroes had to overcome to finalize the experiment, which mostly consisted in optimizing different stages, we hereby show the demodulated signal for 8-channel OTDM both BPSK and QPSK. The former yields a bit rate of 80 Gb/s, the latter 160 Gb/s. Looking at Figure 5.14, one clearly sees how most of the channels are very cleanly demodulated, with only channels 3 and 4 a bit less polished. Figure 5.14 shows instead the results for our QPSK signal. The result is still quite satisfactory, even though in general the points on the constellation are much less concentrated and well separated. In particular, channels 3 and 5 are definitely not acceptably demodulated.

To conclude this section, we show how the DSP block in charge of the frequency offset estimation plays a major role in improving the demodulation. In Figure 5.16 one observes the constellation of the recovered signal with and without the aid of the frequency offset estimation block, for both 8-channel OTDM BPSK and QPSK signals.

5.3 Conclusions and Future Potential

An important step we would like to perform is to measure some BERs. This could not be done for lack of time, but it would probably be not too difficult to perform. We would just need to know the exact sequence of bits (the bit pattern generator allows for

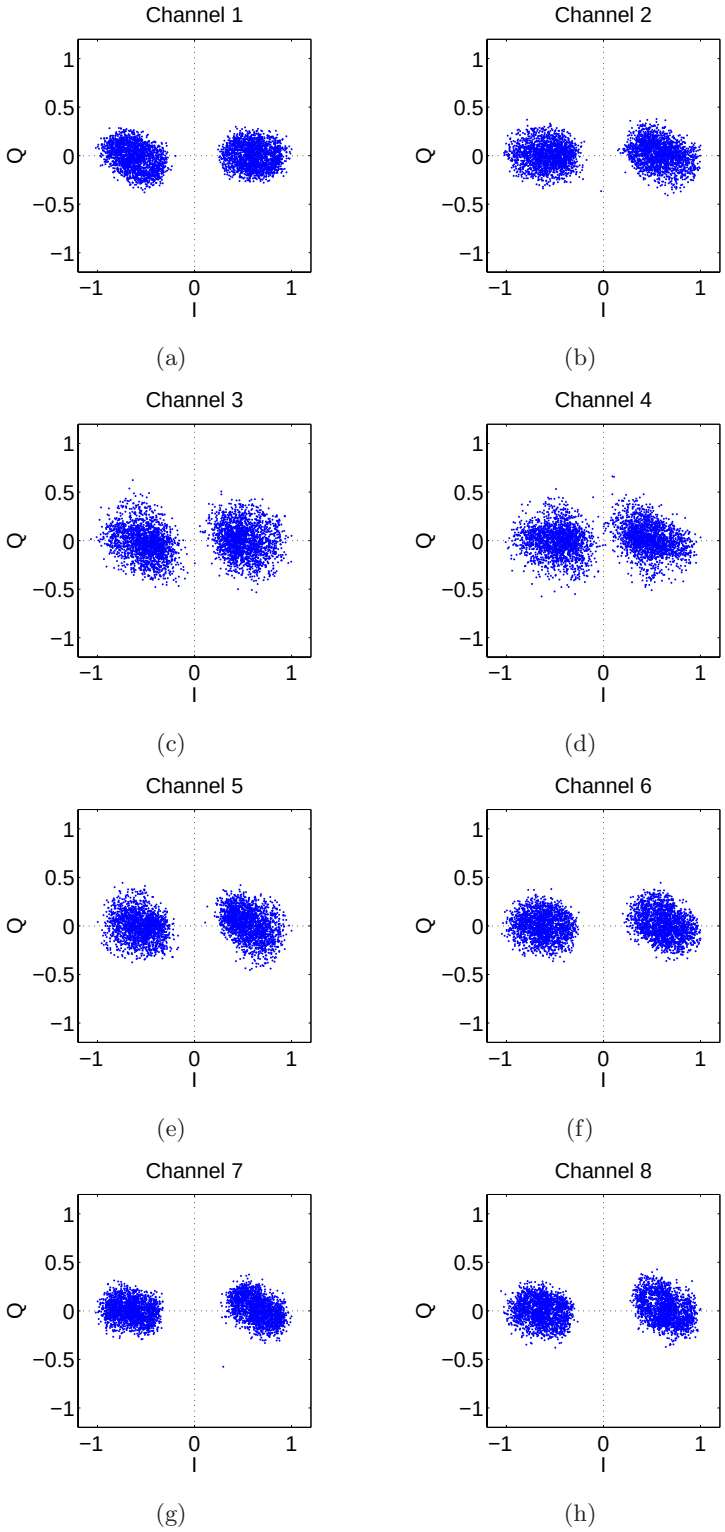

(a) (b) (c) (d) (e) (f) (g) (h)

Figure 5.14: Constellations of the demodulated OTDM (8 channels) BPSK.

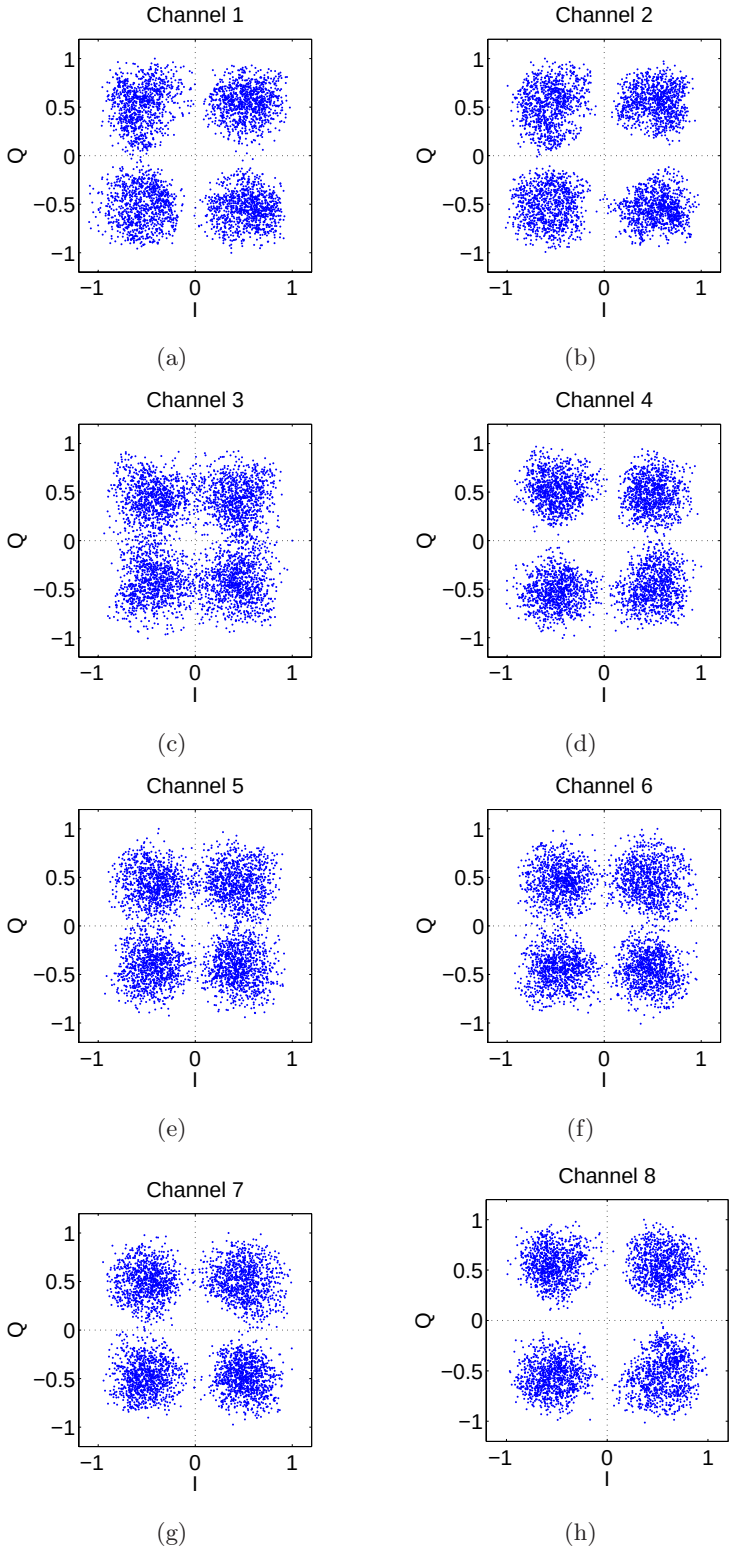

(a) (b) (c) (d) (e) (f) (g) (h)

Figure 5.15: Constellations of the demodulated OTDM (8 channels) QPSK.

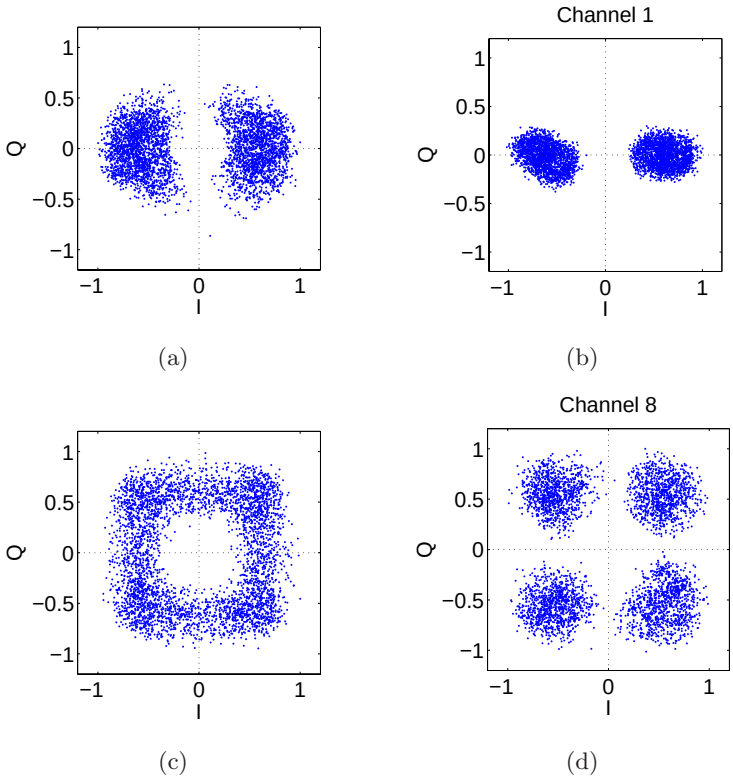

Figure 5.16: Constellations of the demodulated signal for (a) 8-channel OTDM BPSK without frequency offset estimation, (b) 8-channel OTDM BPSK with frequency offset estimation, (c) 8-channel OTDM QPSK without frequency offset estimation, and (d) 8-channel OTDM QPSK with frequency offset estimation.

personalized sequences) and apply a starting sequence so to recognize the beginning of the information stream. The comparison and consequent error counting could be done off-line in Matlab®. Nonetheless, observing the demodulated signal constellations, one can gauge how well the system is performing. By experience with numerical simulations, we think that most channels would present BERs lower than 10^{-3}.

We do believe there is still quite a lot of margin for improvement, especially considering that the QPSK modulation was not totally satisfactory. By employing an IQ modulator we think that the modulation would be more precise, with better timing and exact driving voltages. This would largely help, since we could not achieve any sort of demodulation before optimizing the QPSK modulation as described in Section 5.1.1, and still the resulting eye diagram visualized by means of the optical sampling scope was not perfect.

On top of this, we might try to double the bit rate to 320 Gb/s by adding another multiplexing stage. This would be easy to do since the pulses are definitely narrow enough (see Figure 5.4(d)). We would have to narrow the LO pulses though. This could be done by increasing MI and changing the fiber length accordingly. Even though we pushed the electrical amplifier to the limit to deliver 15.8 V, we estimated V_π of the PM we utilized to phase modulate the signal to be around 3.5 V. By using that instead, we could have MI ≈ 4.5 and in turn pulses with a FWHM around 5 ps, which should do for our purpose of multiplexing 16 channels.

Other paths are probably not practical, since increasing the baud rate would require to buy a new ML laser. Trying a 16QAM would necessitate two IQ modulators and in general this would make the requirements on coherence of signal and LO and frequency offset much more stringent (see Section 4.5.3 and [12]).

6

Conclusions

We conclude this thesis by recapping the main findings and identifying the potential paths to follow for future work.

We have developed a fairly complete model of an optical communication system, comprising transmitters, fiber link, and receivers. This required a great shared effort, but the outcome was worth the pain. Still a lot of work can be done to improve the detail of our model, introducing new aspects and simulating a more realistic behavior of some components. A more thorough testing is needed, and some blocks could be computationally optimized.

We proved we can compare our results to some of the top literature in this field, and we produced results on our own. Specifically, we carried out a study of the impairments related to the IQ modulator non-idealities which shed light on some issues that so far had not been attentively addressed, to our knowledge. Especially interesting is the requirement on the phase modulators bandwidth we have set. We proved how, for both NRZ and OTDM versions of DQPSK and 16QAM, a 3-dB bandwidth of at least $0.5R_S$ is needed in order to have low power penalty (below 4 dB).

Another novel analysis focused on the so-baptized PMCW pulse source. This method for the generation of pulses proved of great interest for its simplicity and flexibility. We can in fact generate pulses narrower than 5% of the symbol slot at any symbol rate, provided that we can have an electrical oscillator at that symbol rate. This has a chance of being cheaper than buying a ML laser, and it is likely more robust if carefully implemented. We also built such a pulse source in practice, and the measurements agreed with the numerical simulations.

To conclude our work, we also spent time in the laboratory, building an ambitious optical communication system. At a baud rate of 10 GBd/s, we employed QPSK and 8-channel OTDM for a final bit rate over single carrier and single fiber of 160 Gb/s. This was done by means of coherent detection and off-line digital processing to demodulate the signal. The clock driving our PMCW LO was recovered from the transmitted signal by means of a EAM-based clock recovery. To our knowledge, only once such a system has been demonstrated before and as recently as 2010 [7]. We believe that our system has large room for improvement, both on transmitter and receiver side.

This has been a magnificent experience, and I am profoundly grateful to every person I worked with during this year. I learnt a lot, and I became a better engineer, but also a better human being, I believe. Thank you, reader, for spending your time with this thesis, I hope it has been, if not cozy and nice as I wished you in the introduction, at least interesting.

References

[1] E. Forestieri, "Evaluating the error probability in lightwave systems with chromatic dispersion, arbitrary pulse shape and pre- and postdetection filtering," *Journal of Lightwave Technology*, vol. 18, November 2000. xi, 120, 121, 122

[2] J. Wang and J. M. Kahn, "Impact of chromatic and polarization-mode dispersions on dpsk systems using interferometric demodulation and direct detection," *Journal of Lightwave Technology*, vol. 22, February 2004. xi, 121, 123

[3] M. Serbay, *Multilevel Modulation Formats for Optical Communication Systems Based on Direct Detection*. PhD thesis, Christian-Albrechts-Universitat zu Kiel, 2007. xi, 123, 124

[4] G. P. Agrawal, *Fiber-Optic Communication Systems*. Wiley Series in Microwave and Optical Engineering, John Wiley and Sons, third ed., 2000. xvii, 4, 16, 21, 39, 51, 52, 53, 55, 56, 57, 58, 61, 63, 105, 106, 119

[5] S. N. Knudsen, M. Ø. Pedersen, and L. Gruner-Nielsen, "Optimisation of dispersion compensating fibres for cabled long-haul applications," *Electronics Letters*, vol. 36, December 2000. xvii, 53

[6] M. Seimetz, *High-Order Modulation for Optical Fiber Transmission - Transmitters, Receivers, System Performance*. Springer Series in Optical Sciences 143, John Wiley and Sons, 2009. 1, 2, 4, 26, 36, 42, 65, 72, 73, 109, 117, 153

[7] C. Schmidt-Langhorst, R. Ludwig, L. Molle, D.-D. Groß, R. Freund, and C. Schubert, "Terabit/s single-carrier transmission systems based on coherent time-division demultiplexing," in *OSA/OFC/NFOEC*, 2010. 3, 178

[8] J. K. Fischer, R. Ludwig, L. Molle, C. Schmidt-Langhorst, A. Galperin, T. Richter, C. C. Leonhardt, A. Matiss, and C. Schubert, "High-speed digital coherent receiver with parallel optical sampling," 2010. 3

[9] C. Zhang, Y. Mori, M. Usui, K. Igarashi, K. Katoh, and K. Kikuchi, "Straight-line 1,073-km transmission of 640-gbit/s dual-polarization qpsk signals on a single carrier," in *35th European Conference on Optical Communication*, 2009. 3

[10] A. H. Gnauck, G. Charlet, P. Tran, P. J. Winzer, C. R. Doerr, J. C. Centanni, E. C. Burrows, T. Kawanishi, T. Sakamoto, and K. Higuma, "25.6-tb/s wdm transmission of

polarization-multiplexed rz-dqpsk signals," *Journal of Lightwave Technology*, vol. 26, no. 1, pp. 79–84, 2008. 3

[11] H. C. H. Mulvad, M. Galili, L. K. Oxenlwe, H. Hu, A. T. Clausen, J. B. Jensen, C. Peucheret, and P. Jeppesen, "Demonstration of 5.1 tbit/s data capacity on a single-wavelength channel," *Optics Express*, vol. 18, Jenuary 2010. 3

[12] F. Patarnello, "Sampling digital coherent receiver for demultiplexing and processing of otdm signals employing high-order modulation," Master's thesis, Danmarks Tekniske Universitet, July 2010. 3, 24, 26, 28, 47, 62, 63, 64, 65, 67, 69, 70, 104, 106, 107, 113, 148, 150, 153, 159, 168, 170, 176

[13] M. Pauer, P. J. Winzer, and W. R. Leeb, "Bit error probability reduction in direct detection optical receivers using rz coding," *Journal of Lightwave Technology*, vol. 19, September 2001. 21

[14] T. Mizuochi, "Recent progress in forward error correction and its interplay with transmission impairments," *IEEE Journal of Selected Topics in Quantum Electronics*, vol. 12, July/August 2006. 25

[15] R. J. Essiambre, G. Kramer, G. J. Foschini, and P. J. Winzer, "High spectral efficiency modulation for high capacity transmission," in *Digest of the IEEE/LEOS Summer Topical Meetings*, pp. 113–114, 2008. 27

[16] L. A. Coldren and W. Corzine, *Diode Lasers and Photonic Integrated Circuits*. Wiley Series in Microwave and Optical Engineering, John Wiley and Sons, 1995. 31, 33

[17] J. T. Verdeyen, *Laser Electronics*. Prentice Hall, third ed., 1995. 31, 32, 49, 50

[18] P. Meystre and M. Sargent, *Elements of Quantum Optics*. Springer, fourth ed., 2007. 35

[19] D. A. B. Miller, *Course Notes for EE243 - Semiconductor Optoelectronic Devices*. Stanford University, 2004. 35, 50, 57

[20] C. W. Pitt, "Mode-locking." Lecture notes collected at University College of London, 1994. 37

[21] H. A. Haus, "Mode-locking of lasers," *IEEE Journal on Selected Topics in Quantum Electronics*, vol. 6, November/December 2000. 38

[22] T. Kobayashi, H. Yao, K. Amano, Y. Fukushima, A. Morimoto, and T. Sueta, "Optical pulse compression using high-frequency electrooptic phase modulation," *IEEE Journal of Quantum Electronics*, vol. 24, February 1988. 39, 40

[23] C. Peucheret, "Elements of electromagnetic theory, anisotropic media, and light modulation by the linear electro-optic effect." Notes collected at Danmarks Tekniske Universitet. 42, 43

[24] G. P. Agrawal, *Nonlinear Fiber Optics*. Academic Press, third ed., 2001. 49, 53, 54, 55, 99, 101

[25] Y. Painchaud, M. Poulin, M. Morin, and M. Tetu, "Performance of balanced detection in a coherent receiver," *Optics Express*, vol. 17, March 2009. 62

[26] F. J. MacWilliams and N. J. A. Sloane, "Pseudo-random sequences and arrays," *Proceedings of the IEEE*, vol. 64, December 1976. 72

[27] D. Zibar, *High-Speed Clock Recovery and Demodulation Using Short Pulse Sources and Phase-Locked Loop Techniques*. PhD thesis, Danmarks Tekniske Universitet, May 2007. 77

[28] G. Einarsson, *Principles of Lightwave Communication*. John Wiley and Sons, 1996. 79

[29] M. Sundelin, *Detection of Optical DPSK*. PhD thesis, Royal Institute of Technology, Stockholm, December 1995. 79, 80

[30] C. J. Rasmussen, *Transmission Analysis in WDM Networks*. PhD thesis, Danmarks Tekniske Universitet, September 1999. 81

[31] A. Hajimiri and T. H. Lee, "A general theory of phase noise in electrical oscillators," *IEEE Journal of Solid-State Circuits*, vol. 33, February 1998. 83

[32] P. Xing, "Polarization and prbs preserving fibre based multiplexer," Master's thesis, Danmarks Tekniske Universitet, October 2002. 89

[33] N. Kikuchi, "Intersymbol interference suppression technique for optical binary and multilevel signal generation," *Journal of Lightwave Technology*, vol. 25, no. 8, pp. 2060–2068. 91

[34] T. Tokle, *Optimized Dispersion Management and Modulation Formats for High Speed Optical Communication Systems*. PhD thesis, Danmarks Tekniske Universitet, September 2004. 94

[35] O. V. Sinkin, R. Holzlhner, J. Zweck, and C. R. Menyuk, "Optimization of the split-step fourier method in modeling optical-fiber communications systems," *Journal of Lightwave Technology*, vol. 21, Jenuary 2003. 101, 103, 145, 147

[36] K. S. Jepsen, H. N. Poulsen, A. T. Clausen, A. Buxens, and K. E. Stubkjaer, "Investigation of cascadability of add-drop multiplexers in otdm systems," in *ECOC - Madrid*, 20-24 September 1998. 131

[37] D. Derickson, *Fiber Optic - Test and Measurement*. Prentice-Hall, 1998. 160

Declaration

I herewith declare that I have produced this paper in conformity with the rules of both Danmarks Tekniske Universitet and Università degli Studi di Padova, and without the aid of any prohibited third parties. Notions retrieved from other sources have been clearly identified as such, and the exact sources specified. This thesis has not been previously presented in similar form to any other examination board.

The thesis work was conducted from August 2009 to July 2010 under the supervision of Christophe Peucheret, Michael Galili, and Hans Christian Hansen Mulvad.

Copenhagen, 7 July 2010